2018

Myelin and glial pathology in aging and congnitive decline: evidence for faulty myelin clearance in the rhesus monkey

BOSTON UNIVERSITY

SCHOOL OF MEDICINE

Dissertation

MYELIN AND GLIAL PATHOLOGY IN AGING AND COGNITIVE DECLINE: EVIDENCE FOR FAULTY MYELIN CLEARANCE IN THE RHESUS MONKEY

by

ELI TOWNSEND-SHOBIN

B.A., Connecticut College, 2010

Submitted in partial fulfillment of the

requirements for the degree of

Doctor of Philosophy

2018

Approved by

First Reader _____

Douglas L Rosene, Ph.D.
Professor of Anatomy and Neurobiology

Second Reader _____

Maria Medalla, Ph.D.
Assistant Professor of Anatomy and Neurobiology

ACKNOWLEDGMENTS

This dissertation and the work within was made possible by my adviser, Doug Rosene. Thank you for the encouragement over the years and always allowing me to pursue my own experimental ideas, no matter how misguided they may have been. To all my lab mates, I could not have asked for a better group of people to spend time with and collaborate with while pursuing my PhD. I hope to receive all future invitations to J J Foleys.

Shelley Russek and Sandra Grasso: you accepted me into this program and were here for me every step of the way. I could not have made it to where I was without your guidance and the Graduate Program for Neuroscience. The support and critiques my committee have offered over the years have been essential towards the success of this project. In particular, Tsuneya Ikezu for chairing the committee and always providing insight into neuroimmunology, Carmela Abraham and Cidi Chen for opening their lab to me and teaching me biochemical assays, Maya Medalla for helping me try some of my crazier experimental ideas and keeping them grounded, and Adam Bero for being a great mentor, collaborator and friend.

Outside of the lab, my cohort, Mariel, Dante, and Nat: thank you for taking this journey with me and being great friends along the way. I'm so proud of how far we've come. To my family for piquing my interest in science and giving me every opportunity to succeed. Finally, the wonderful Samantha Calderazzo, who was always there to help me through my scientific woes, my best friend, and a great mother to our dog, Tabitha.

MYELIN AND GLIAL PATHOLOGY IN AGING AND COGNITIVE DECLINE: EVIDENCE FOR FAULTY MYELIN CLEARANCE IN THE RHESUS MONKEY

ELI TOWNSEND-SHOBIN

Boston University School of Medicine, 2018

Major Professor: Douglas L. Rosene, Ph.D., Professor of Anatomy and Neurobiology

ABSTRACT

Aging is associated with a loss of cognitive function related to learning, memory, and executive function with varying severity. Although there is no age-related loss of neurons in healthy aging, myelin damage accumulates and is associated with cognitive decline. The brain's resident macrophages, microglia, are responsible for clearing damaged myelin and promoting subsequent oligodendrocyte-mediated remyelination. To test the hypothesis that age-related dysfunction of microglial phagocytosis and oligodendrocyte remyelination capacity contributes to myelin pathology and cognitive impairment. To test this, rhesus monkeys from across the lifespan (7-30 years of age) were tested in three specific aims. 1) To characterize gene expression of myelin basic protein (MBP) in the brain and clearance of MBP to the cerebrospinal fluid (CSF) in relation to age-related myelin pathology. The density of myelinated axons visualized using label-free spectral confocal reflectance imaging did not correlate with age, but was significantly lower in aged animals with cognitive impairment. Next, *MBP* gene expression was measured using qPCR in the dorsal prefrontal cortex along with quantification of MBP protein levels in the CSF using ELISA. Age-dependent increases of *MBP* gene expression in the brain and MBP protein levels in the CSF were observed. Interestingly, MBP levels in the CSF were lower

in animals with cognitive impairment. 2) To test the hypothesis that microglia would become increasingly primed for phagocytosis with age-related myelin pathology. The number of microglia immunostained with galectin-3, a marker for phagocytic activation, was quantified in the frontal white matter and increases in both aging and cognitive decline were detected. 3) To evaluate the hypothesis that lipofuscin, an age-related accumulation indicative of autophagic dysfunction, would accumulate and impair glial cells of the white matter in aged animals. Lipofuscin accumulation was increased with age in the frontal white matter and the size of lipofuscin clusters was associated with cognitive impairment. Lipofuscin was found primarily in microglia and oligodendrocytes, but not in astrocytes. These data suggest that lipofuscin burden in microglia and oligodendrocytes inhibits their homeostatic functions resulting in improper myelin clearance and turnover, leading to a devastating feed-forward cycle of myelin damage that contributes to age-related cognitive impairment.

TABLE OF CONTENTS

LIST OF FIGURES

LIST OF ABBREVIATIONS

AD ..... Alzheimer's disease

APP ..... amyloid precursor protein

CC ..... corpus callosum

CE ..... Cavalieri estimator

CGB ..... cingulum bundle

CII ..... cognitive impairment index

CLC ..... Co-localization coefficient

CSF ..... cerebrospinal fluid

CSST ..... category set shifting task

Ct ..... cycle threshold

DNMS ..... delayed non-match to sample

DRST ..... delayed recognition span task

DTI ..... diffusion tensor imaging

EAE ..... experimental autoimmune encephalomyelitis

EM ..... electron microscopy

FA ..... fractional anisotropy

FWM ..... frontal white matter

Gal-3 ..... galectin 3

GFAP ..... glial fibrillary acidic protein

ISF ..... interstitial fluid

MBP ..... myelin basic protein

mOligos.....mature oligodendrocytes

NCA.....normal cognitive impairment

NFH.....neurofilament H

OPC.....oligodendrocyte precursor cell

PCC.....Pearson's correlation coefficient

PDGFRA.....platelet derived growth factor α

qPCR.....quantitative polymerase chain reaction

RNAseq.....RNA sequencing

ROI.....region of interest

ROS.....reactive oxygen species

RT.....reverse transcriptase

SCoRe.....spectral confocal reflectance

TBS.....tris buffered saline

CHAPTER 1: INTRODUCTION

Age-related cognitive decline is known to occur both in health and disease, particularly in the domains of memory, processing speed, and executive function (Brayne et al. 1995; Cullum et al. 2000; Salthouse 2010; Singh-Manoux et al. 2012). While Alzheimer's disease (AD) is the devastating age-related dementia most often associated with cognitive decline, for those who escape AD, aging is accompanied by noticeable, but less severe cognitive impairment that affects individuals at different rates (Fjell and Walhovd 2010). Age-related cognitive decline is known to occur both in health and disease, particularly in the domains of memory, processing speed, and executive function (Brayne et al. 1995; Cullum et al. 2000; Salthouse 2010; Singh-Manoux et al. 2012). While Alzheimer's disease (AD) is the devastating age-related dementia most often associated with cognitive decline, for those who escape AD, aging is accompanied by noticeable, but less severe cognitive impairment that affects individuals at different rates (Fjell and Walhovd 2010). Rather than cell loss, the cognitive decline of normal aging comes with a distinct white matter pathology, accompanied by loss of synaptic connections, that is most severe in the frontal regions (Salat et al. 2004; Abe et al. 2008; Fjell et al. 2009). Although the cause of the white matter pathology is poorly understood, it has been linked to deficits in myelin – the insulating sheath on axonal fibers that enhances conduction of signals across interconnected brain areas. The brain’s immune system may play a role by failing to clear damaged myelin debris or even by directly damaging white matter. In this review, we will present the evidence of a connection between the aging of the neuroimmune system and the pathologies of normal aging and normal cognitive aging (NCA). We hope to demonstrate

that although great strides have been made in our understanding of normal cognitive aging, a greater focus on neuroimmunology of the white matter may elucidate the cause of the underlying pathology. In this review, we will present the evidence of a connection between the aging of the neuroimmune system and the pathologies of normal aging and normal cognitive aging (NCA). We hope to demonstrate that although great strides have been made in our understanding of normal cognitive aging, a greater focus on neuroimmunology of the white matter may elucidate the cause of the underlying pathology.

Pathology of Alzheimer's disease – neuronal loss and the hippocampus

Although aging is the greatest predictor of AD (Alzheimer's Association 2013; Guerreiro et al. 2015), the symptoms and pathology of aging and AD must be separated to be fully understood. Most commonly, AD affects the cognitive domains of short-term memory and executive function and is characterized by the slow, progressive loss of function over time (McKhann et al. 2011). The well-documented pathology that defines AD centers on neurodegeneration starting in the hippocampal formation in the medial temporal lobe. Preceding clinical symptoms by a decade, and potentially causing the neuronal loss, is the accumulation of amyloid beta plaques (Aβ plaques) and intracellular neurofibrillary tangles of phosphorylated tau (pTau) (Ringman et al. 2008; Bateman et al. 2012). Eventually this degeneration spreads beyond the hippocampal formation to other brain regions causing multi-domain cognitive dysfunctions (see Masters et al. 2015).

Pathology of normal cognitive aging – white matter and myelin

Unlike the neurodegeneration of AD, a consistent finding of healthy aging and NCA is that neurons are not lost with age in humans (Terry et al. 1987; Freeman et al. 2008).

However, non-neurodegenerative aging is still associated with a decrease in cognitive function, particularly in the domains of memory, processing speed, and executive function (Brayne et al. 1995; Cullum et al. 2000; Salthouse 2010; Singh-Manoux et al. 2012). Despite a lack of neuronal loss, MRI studies have determined that gray matter volume appears to decline slowly with age beginning in early adulthood (Courchesne et al. 2000; Good et al. 2001; Storsve et al. 2014). White matter, however, does not begin to show alterations until late middle-age (40-60 years old) at which point volume begins to decrease (Albert 1993; Guttmann et al. 1998; Jernigan and Gamst 2005; Fjell and Walhovd 2010). In addition to volumetric loss, researchers have also identified white matter hyperintensities, age-related lesions that can be visualized with MRI and correlate with cognitive decline (De Groot et al. 2000; de Leeuw et al. 2001; Prins and Scheltens 2015). With diffusion tensor imaging (DTI) fractional anisotropy (FA) to measure what is thought to be myelin integrity (Moseley 2002; Sullivan and Pfefferbaum 2006), decreases with age (Charlton et al. 2006; Voineskos et al. 2012; Teipel et al. 2014). Unlike AD, where disease progression seems to begin in the temporal lobe, age-related loss of both gray and white matter volume begin in the frontal lobe (Salat et al. 2004; Abe et al. 2008; Fjell et al. 2009). The regional volume differences between normal aging and AD brains make for a useful diagnostic parameter to distinguish AD from NCA (Head et al. 2005; Raji et al. 2009; Fjell et al. 2010).

In contrast to non-invasive MRI studies of the human brain, postmortem studies of the aging human brain are difficult as preservation of tissue for histological or molecular studies is often confounded by post-mortem delay in tissue harvest. In addition, while

donations from elderly subjects with and without AD are often available, obtaining healthy younger adults brains is very difficult. Nevertheless, the studies that have been done largely corroborate the volumetric studies with MRI. Age-related loss of gray matter volume is thought to reflect neuronal shrinkage (Terry et al. 1987) and decreases in dendritic arborization (Anderson and Rutledge 1996; Jacobs et al. 1997; Esiri 2007). In the white matter, histological and electron microscopic studies have estimated an age-related myelinated fiber decrease by 27% to 45% (Tang et al. 1997; Marner et al. 2003).

For the reasons mentioned previously, researchers attempting to understand the cellular and molecular basis of aging have often turned to animal models. Similar to humans, the rhesus monkey develops cognitive decline with age but does not have neurodegenerative AD pathology (Sloane et al. 1997; Peters et al. 1998; Peters and Rosene 2003). MRI data from rhesus monkeys, similar to human, have shown an age-related decrease in white matter volume with little gray matter loss (Wisco et al. 2008). Additionally, myelin integrity, assessed by DTI, also decreases with age in the monkey (Makris et al. 2007). Our lab has used rhesus monkey animal model to find ultrastructural evidence of age-related myelin fiber loss and myelin damage in the cingulum bundle and corpus callosum (Bowley et al. 2010), the anterior commissure (Sandell and Peters 2003), fornix (Peters et al. 2010), the optic nerve (Sandell and Peters 2002) and the visual cortex (Peters et al. 2000). Importantly, we have also shown that the age-related myelin damage is also correlated with decreased cognitive performance (Bowley et al. 2010).

Based on the literature, it is clear that Alzheimer's disease and normal cognitive aging are distinct pathologies and should be treated as such, rather than a continuum of the same

spectrum. White matter pathology caused by myelin damage is likely the main culprit of cognitive decline in normal aging, but little is known as to why myelination becomes faulty with age. We suggest two potential glial mechanisms that may underlie myelin damage: oligodendrocytes and microglia. Oligodendrocytes, as the cell responsible for creating and maintaining the myelin sheath, may have age-related defects in the ability to produce, maintain myelin or remyelinate after damage (Shields et al. 1999; Ruckh et al. 2012). Alternatively, age-related microglial dysfunction may lead to the inability of these resident macrophages of the brain to clear debris, leaving damaged myelin byproducts to linger (Safaiyan et al. 2016). For the remainder of this review, we will focus on microglia and the brain's immune system to show what is known and unknown about microglia and how they may be involved in myelin damage. We present evidence from the literature that suggest that microglia are at the center of a delicate balance surrounding normal myelination. Understanding the age-related functional alterations in microglia may be the key to understanding the causes of myelin pathology and normal cognitive aging.

Microglia and aging

Neuroimmunology has been at the forefront of aging and AD research. But we argue that, like general aging research, neuroimmunologists have limited their attention to neuronal loss, particularly in the hippocampus, in neurodegenerative disease, and largely ignored normal cognitive aging. In the previous sections, we noted that both dendritic atrophy and spine loss as well as myelin damage are likely the major contributors to normal cognitive aging in humans and monkeys. Both the processes of spine pruning and remyelination are known to involve the brain's immune system and resident macrophage

known as microglia. Microglia are yolk-sac derived myeloid cells originally thought to be only responsible for phagocytosis and the innate immune response in the brain (Alliot et al. 1999; Ginhoux et al. 2010). However, recent research has shed light on microglial functions outside of their immune duties.

Two decades ago, microglia were thought to be "resting" or "quiescent" when not "activated" for inflammation. While these terms still linger, researchers have made a concerted effort to move into more functionally relevant terminology. First, microglia are now known to not be "resting", but actively surveilling the environment (Nimmerjahn et al. 2005). In gray matter, microglia are responsible for sculpting and pruning synapses (Stevens et al. 2007; Schafer et al. 2012), a function that continues throughout life (Stephan et al. 2012; Parkhurst et al. 2013). Although we do not know the role of microglia synaptic pruning in disease, there is an upregulation of complement and concurrent synaptic loss in age-related dementia that implicates microglia (Chung et al. 2015).

Aging can cause microglia to become dystrophic and potentially senescent (Streit et al. 2004). Immune challenge in old mice can cause a shift in microglia to an inflammatory morphology and an M1/pro-inflammatory phenotype (Godbout et al. 2005). Additionally, microglia isolated from old mice have a higher expression of both M1 and M2/anti-inflammatory cytokines and an altered M2 response to challenge with lipopolysaccharide (Sierra et al. 2007). While the traditional inflammatory dichotomy of M1/M2 microglia has been useful for understanding the basics of inflammatory processes, the most recent advances in neuroimmunology have demonstrated that the M1/M2 binary is too simplistic to truly represent microglia functions and responses (Ransohoff 2016). Using RNA

sequencing (RNAseq), researchers have discovered that microglia responses are often unconstrained by traditional schema, and “M1” or “M2” associated proteins can actually be expressed together (Kim et al. 2016) and gene expression can demonstrate transcriptional signatures of differing disease states (Holtman et al. 2015). Therefore, moving beyond the M1/M2 dichotomy is imperative in determining how microglial function is changing with age.

Recent studies using RNAseq have identified a microglial signature distinct from peripheral macrophages which identifies key transcriptional differences between the two cell types. This includes finding a microglial ‘sensome’ comprised of transcripts that mark microglial surveillance (Hickman et al. 2013; Butovsky et al. 2014). While Hickman et al (2013) found an age-related shift towards transcripts involved in neuroprotection and repair, others have reported an increase in phagocytic, lysosomal and antigen-presentation transcripts. Unsurprisingly, aging caused significant differences in microglia transcription profiles in different regions of the brain (Grabert et al. 2016).

A major constraint to RNAseq that has limited our understanding of the human microglial transcriptome and age-related changes is the requirement of fresh, unfixed tissue to isolate microglia. Studies investigating human microglia transcriptomes have taken brain tissue biopsied during surgery, generally from the cortex, or taken from donors immediately post mortem. In both scenarios, acquiring healthy, "normal" tissue is rare, given the requirements. From the data that have been gathered, microglial profiles of mice and humans diverge with age, as human microglia have altered transcripts related to neurodegenerative diseases and are distinct from the gene expression changes seen in the

aging mouse (Galatro et al. 2017; Gosselin et al. 2017). In aging, human microglia have changes to transcripts involved in cell adhesion, axonal guidance, and the sensome that are distinct from the transcriptional changes seen in the aging mouse (Galatro et al. 2017).

Although the presented data offer compelling evidence for microglial alterations in aging, there are some major confounds to understanding the state of microglia in the aging brain. First, microglial cultures have provided a great deal of data, but microglia are extremely context/environment dependent and quickly lose their transcriptional signature in culture (Gosselin et al. 2017). Second, human microglial studies are only able to use tissue from cases where disease is present justifying the cortical brain biopsy. Third, the only other source of tissue is from post mortem studies. This makes it difficult to be confident that the results reflect non-diseased human microglia, especially in human aging where neurodegenerative disease is frequently present. Finally, none of the human studies are able to address the transcriptional profiles of microglia in the white matter.

Microglia in the white matter

Thus far, our knowledge of aging microglia has come almost exclusively from the gray matter of human and mouse brains. As an entire mouse brain consists of 90% gray matter (Zhang and Sejnowski 2000), it allows comparison to human cortical gray matter studies of microglia, but limits what can be known about the major pathology of aging, white matter damage. This is a major deficit in our knowledge for myelin pathology for several reasons. First, microglia are necessary for oligodendrocyte differentiation and maturation (Miron et al. 2013) and for remyelination (Lampron et al. 2015). Furthermore, age-related myelin damage impairs microglial phagocytic function in the mouse (Safaiyan et al. 2016).

It is therefore very likely that microglia play an important non-immune role in the white matter, likely in the homeostatic maintenance of myelin.

Interestingly, aging is associated with an increase in inflammation particularly in the white matter (Hart et al. 2012; Raj et al. 2017; Shobin et al. 2017). Our lab, using the rhesus monkey model of normal aging, has shown that phagocytic priming increases in microglia with age but only in the white matter (Shobin et al. 2017). The observation that there are similar upregulations of genes related to innate immunity in both the AD brain and the 'healthy' aged brain (Cribbs et al. 2012) suggests that neuroinflammation is a feature of aging that occurs independent of neurodegeneration. Nevertheless, studies of neuroinflammation and aging have primarily focused on the gray matter even though white matter damage is a major feature of normal aging pathology. In PubMed, a search for the terms "microglia" and "aging" yields 1763 results. Adding in the term "neuron" reduces this to 771, but adding in "myelin" brings up only 72 articles (as of February, 10, 2018).

White matter microglial research is still in its very early stages and an abundance of foundational questions are left to be answered. What roles do microglia in the white matter play outside of their jobs as immune cells? We have reports that these cells are involved in remyelination and oligodendrocyte differentiation (Miron et al. 2013; Lampron et al. 2015), but the extent of this is unknown. With very limited knowledge of white matter microglia, we assume that all microglia are equal, but with such a strong tie to environment (Gosselin et al. 2017) it would not be surprising to find that microglia in the gray matter and white matter function differently. Finally, is inflammation in the white matter a cause of white matter dysfunction, resulting from problematic white matter microglia, or is it

merely a response to age-related deterioration of myelin and/or myelinating oligodendrocytes?

Microglia in normal cognitive aging and AD

Streit et al (2005) hypothesized that dystrophic or senescent microglia seen in humans are functionally impaired and may be contribute to normal cognitive aging but few studies have specifically examined microglia in relation to cognitive aging. As an example of microglia dysfunction with age, peripheral immune challenge in older mice causes both increased microglial inflammation and cognitive decline but the same effects do not occur when young mice are challenged (Barrientos et al. 2006). High levels of IL-1β, a pro-inflammatory cytokine produced by microglia, can impair memory and synaptic plasticity (see Patterson 2015). Hypomethylation of the IL-1β gene increases with age and can cause an increase in IL-1β production that correlates with cognitive impairment (Cho et al. 2015). We have reported that white matter microglial inflammation and phagocytic priming correlate with cognitive impairment in aging monkeys (Sloane et al. 1999; Shobin et al. 2017). In humans, cortical inflammatory microglia measured with positron emission tomography correlated with mini-mental state examination scores in AD patients (Edison et al. 2008). Finally, a plethora of studies have reported that antioxidants can counter the pro-inflammatory processes of microglia and reduce age-related cognitive impairment (Cotman et al. 2002; Crichton et al. 2013; Chaudhari et al. 2014; Huhn et al. 2015; Natrajan et al. 2015; Yuan et al. 2016).

Common ground in normal cognitive aging and AD

Although this review has made a point of distinguishing aging, normal cognitive aging, and AD, the pathologies of AD and normal cognitive aging may actually share some similarities. In AD, the hallmarks of plaque and tangle accumulation stem from inappropriate cleavage of amyloid precursor protein (APP) that eventually results in neurodegeneration. Although normal cognitive aging does not have the same neurodegeneration, the white matter has an accumulation of damaged myelin. In both cases, microglia are known to respond, but are unable to phagocytose the aggregated amyloid β and resolve the problem (AD: Hickman et al. 2008; Njie et al. 2012; Krabbe et al. 2013; Aging: Safaiyan et al. 2016). Additionally, gene expression of aging and AD revealed similar changes to innate immunity (Cribbs et al. 2012).

Conclusions

The traditional focus of aging research on neurodegenerative diseases like AD and the associated loss of gray matter neurons has left changes in white matter under studied. Here we propose that not only should white matter be a major focus of brain aging studies but it may be a critical factor in normal cognitive aging for those who escape AD. In addition, in the search for the mechanism of white matter pathology, normal and aberrant neuroimmune functions in the brain may be a part of the pathogenic process.

We propose that white matter microglia dysfunction drives myelin damage in aging and cognitive impairment. In the healthy brain, myelin turnover is dealt with quickly, allowing for remyelination and limited appearance of myelin damage. We hypothesize that the increased presence of myelin debris with age is indicative of faulty clearance

mechanisms due to phagocytic impairment of microglia. As microglia become less efficient in phagocytosing myelin, the debris on the myelin sheath or interstitial fluid lingers, impairing remyelination. Without resolution, microglia remain chronically inflamed, leading to a devastating feed-forward cycle of more myelin damage and more inflammation. In this mechanism, microglia are certainly at fault, but there are still many gaps left to consider. As such, understanding the complex interplay of microglia and myelin may be a key to comprehending our normal aging and provide novel insights to uncover new therapies for neurodegenerative dementias.

In this dissertation, we will experimentally address some of the questions surrounding age-related changes to the white matter and related neuroimmune cells. We will test the overall hypothesis that impairments in the clearance of myelin debris in aging is associated with cognitive decline. Specifically, we will look to evaluate age-related myelin changes at the bright field level, assess related gene expression changes, and determine the efficacy of myelin clearance into the cerebrospinal fluid. Next we will determine changes to microglial phagocytic activation in the white matter throughout aging and cognitive impairment. Finally, we will show that lipofuscin accumulation in the white matter may be involved in the age-related myelin pathology and normal cognitive aging.

CHAPTER 2: MYELIN DYSFUNCTION

Introduction

Although original findings suggested a loss of neurons was responsible for mild cognitive impairment, it is now accepted that there is no neuronal loss with aging in humans (Haug et al. 1984; Terry et al. 1987, Freeman et al. 2008) or in monkeys (e.g. Peters et al. 1998; Merrill et al. 2000). Similarly, quantitative MRI studies have shown that although gray matter cortical thickness is reduced (Alexander et al. 2006; Koo et al. 2010), total gray matter volume is preserved (Wisco et al. 2008). However, MRI and histological studies in both monkeys and humans have reported an age-related loss of white matter volume that correlates with cognitive decline (Albert 1993; Tang et al. 1997; Guttmann et al. 1998; Peters and Rosene 2003; Wisco et al. 2008). Further, total myelinated fiber length decreases by 27%-45% with age (Tang et al. 1997; Marner et al. 2003) and, in addition to a loss of myelinated fibers, there is an increase in myelin damage in both aging and cognitive impairment (Bowley et al. 2010)**.**

The majority of evidence for age-related myelin pathology stems from studies using MRI to detect volumetric changes (Guttmann et al. 1998; Wisco et al. 2008), diffusion tensor imaging to show loss of myelin integrity (Charlton et al. 2006; Makris et al. 2007; Voineskos et al. 2012), electron microscopy to visualize myelin damage and axonal loss (Peters et al. 2000; Sandell and Peters 2002; Sandell and Peters 2003; Bowley et al. 2010) and biochemical analyses (Hinman et al. 2004; Duce et al. 2006; Hinman et al. 2006; Hinman et al. 2008). The imaging techniques require expensive scanning time and equipment and electron microscopy relies on specific fixation criteria making none of these

techniques useful for archived tissue. However, studying myelination at the light level has been met with challenges. Traditional and adapted versions of histological myelin stains are effective in measuring areas of total myelin loss (such as seen in models of multiple sclerosis), but do not provide the resolution to measure the deep white matter affected by normal aging (for examples, see Pistorio et al. 2006; Savaskan et al. 2009). These methods are not sensitive enough to measure an approximate 10% myelinated axon loss seen in normal aging (Bowley et al. 2010). Spectral Confocal Reflectance (SCoRe) imaging detects myelinated axons in fixed tissue using a confocal microscope (Schain et al. 2014) and may be useful as a label-free method of visualizing age-related myelination changes in the deep white matter.

Little is known about the influence of aging on molecular and transcriptional changes to the major myelin protein, myelin basic protein (MBP). MBP mRNA is synthesized and transported down the peripheral extensions of the oligodendrocyte for translation on-site (Ainger et al. 1993; Baron and Hoekstra 2010; Müller et al. 2013). As a protein, MBP is found between the intracellular compartments of the myelin sheath, acting as an adhesive between the two layers. Without MBP, the intracellular myelin layers pull apart and swell (Min et al. 2009). Disrupting MBP, as seen in the shiverer mouse model, leads to hypomyelination (Kimura et al. 1989). In MS, myelin basic protein (MBP) can be found in the cerebrospinal fluid (CSF; Cohen et al. 1976) and the levels of MBP in the CSF correlate with severity of symptoms and lesions diagnosed via MRI (Lamers et al. 1998). Finally, treating patients with an immunosuppressant decreases CSF MBP (Romme Christensen et al. 2013).

We hypothesized that age-related myelin damage would lead to alterations to MBP transcription and clearance. First, we sought to determine the effectiveness of SCoRe imaging in measuring of demyelination across the lifespan of the rhesus monkey. Next, we investigated gene expression changes of MBP from the dorsal prefrontal cortex. Finally, with age-related myelin damage, we hypothesized that MBP would be cleared to the CSF. To test this, we measured MBP concentrations in the CSF of monkeys across the lifespan using ELISA.

Methods

Subjects

Tissue and cerebrospinal fluid (CSF) were used from 36 rhesus monkeys taken as part of an NIA funded Program Project ("Neural Substrates of Cognitive Decline in Aging Monkeys", P01-AG000001) and a Research Project ("Histopathology, Neuroimaging and Mechanisms of Myelin Damage in Aging Monkey Brain", R01-AG043640). Of the monkeys used in this study, 30 were originally obtained from the Yerkes National Primate Research Center at Emory University in Atlanta, while 6 animals came from other research centers. Prior to selection, health records were screened with strict health criteria to exclude any possible confounding clinical diseases or experimental manipulations that could impact normal aging by affecting the brain or behavior.

Behavioral testing

Upon entering the study, all monkeys received a battery of behavioral tests that assess cognitive functions and have been described in detail elsewhere. The major domains and tasks were a test of rule learning using acquisition of the Delayed Non-Match to Sample

(DNMS) task, extended delays on DNMS (120 sec and 600 sec) to test recognition memory, the Delayed Recognition Span Test (DRST) in both spatial and object modes to assess working memory capacity, and the Category Set Shifting Task (CSST) to test executive function (Herndon et al. 1997; Moore et al. 2005). Based on a principal components analysis (Herndon et al., 1997), a subset of the DNMS and DRST scores were identified as the best predictors of cognitive aging and were compiled into a z-score and designated the cognitive impairment index (CII). This has proven useful in comparing cognitive status with neurobiological endpoints (e.g. Peters, Sethares, & Moss, 1998).

Brain perfusion for fresh and fixed tissue

To harvest fresh tissue for RNA isolation still obtain well-fixed tissue for immunohistochemistry, tissue from 10 of the animals was first perfused with 4 liters of Krebs buffer at 4°C and is followed by 8 liters of 4% paraformaldehyde at 37°C. With the monkey deeply anesthetized, a craniotomy was performed to expose the dura over one hemisphere. At the start of Krebs perfusion, the dura was opened and fresh, unfixed biopsy samples were removed from area 46 and immediately placed on dry ice and then frozen at -80°C for RNA isolation. Once fresh tissue was removed, the perfusate was switched to 4% paraformaldehyde for 10 minutes.

After perfusion, the brain was cryoprotected in buffered glycerol (10% and then 20%) with 2% DMSO, and flash frozen at -75°C and stored at -80°C until cut. This method completely eliminates freezing artifact as well as the shrinkage produced by sucrose cryoprotection (Rosene et al. 1986). One hemisphere was cut in its entirety in the coronal plane into 10 interrupted series of 30-micron thick frozen sections so that sections in a

series are spaced at 300 micron intervals and collected in buffer with 15% glycerol as cryoprotectant and stored frozen at -80°C. Archived tissue was selected for analysis to optimize overlap with available fresh-frozen pieces of area 46 and cerebrospinal fluid. Once selected, vials of sections are removed from the -80°C freezer, thawed in a 20°C water bath and rinsed three times in buffer to remove glycerol cryoprotectant. They are then all "batch processed" together as free-floating sections for IHC to ensure that sections from all cases are processed in identical reagents under identical conditions and for the same time (Giannaris and Rosene 2012; Estrada et al. 2017; Shobin et al. 2017).

Spectral Confocal Reflectance (SCoRe) imaging

SCoRe imaging was used to evaluate age-related changes in myelinated axons (Schain et al. 2014). For this, 4% paraformaldehyde fixed, 30µm thick brain sections from 25 animals were slide mounted and air-dried for 1 hour, coverslipped with Aqua-Mount (Thermo Scientific, Waltham, MA) and imaged on a Leica TCS SP8 MP with a 40X/1.3 oil immersion objective and excited by 488nm, 552nm, and 638nm lasers. Emissions were collected at 486nm – 490nm, 559nm – 563nm, and 631nm – 635nm, respectively and the genu of the corpus callosum was imaged in 10 z-stacked 0.68 micron images per animal. Each image was thresholded and measurements taken for percent area using FIJI software (Schindelin et al. 2012).

Immunohistochemistry

Select sections were processed for immunohistochemistry to verify co-labeling of SCoRe imaging with axons. Tissue was thoroughly washed and blocked with SuperBlock (Thermo Scientific, Waltham, MA) for 1 hour. Next, sections were incubated in primary

antibody solution containing mouse anti-hypophosphorylated neurofilament H (NFH; Abcam) diluted to 1:1000 with 0.5% SuperBlock and 0.3% Triton X. Sections were incubated in primary antibody solution for at 4°C overnight. Tissue was washed very thoroughly and placed into secondary antibody solution containing donkey anti-mouse Alexa Fluor 647 (Life Technologies, Carlsbad, CA) diluted to 1:500 with 0.5% SuperBlock, and 0.3% Triton X for 2 hours. Samples were thoroughly washed, mounted, and coverslipped using Aqua-Mount (Thermo Scientific, Waltham, MA). Slides were imaged on a confocal microscope at 40X and colabeling with SCoRe was verified by visual assessment.

RNA isolation and qPCR

Archived samples from six old (ages 18+) and four young animals (ages 6-9) were used for this study. Tissue was removed from the freezer, placed on dry ice, and 100mg pieces were excised. On ice, sections were passed through progressively smaller gauged needles from 18 to 24 gauge in TRIzol. RNA was extracted according to manufacturer's protocol and resuspended in 40µl RNAse-free water. Samples were measured for RNA concentration and optical density values at 260/280 using NanoDrop (Thermo Fisher, Waltham, MA). RNA was then reverse transcribed (RT) to cDNA using a High Capacity RNA-to-cDNA kit (Thermo Scientific, Waltham, MA). Briefly, 2µg of RNA was added to 10µl RT Buffer Mix 2X, 1µl 20X Enzyme Mix and filled to 20µl with nuclease-free water (negative RT controls were created by withholding 20X Enzyme Mix from the sample). The reaction mixture was centrifuged briefly to remove any bubbles and incubated in a

CFX96 Thermo Cycler (Bio-Rad, Hercules, CA) at 37°C for 1 hour. The reaction was then be heated to 95°C for 5 minutes and then held at 4°C.

Quantitative Polymerase Chain Reaction (qPCR) was performed using PowerUp SYBR Green Master Mix (Thermo Fisher, Waltham, MA). Samples of cDNA (10ng) were added to PCR tubes with 10µL SYBR Green Master Mix in triplicate, RNAse-free water and 0.2nm of primers designed using Primer-BLAST (National Center for Biotechnology Information) for the monkey MBP gene (RefSeq XM_015122215.1):

Forward: CTCTGGCAAGGACTCACACC

Reverse: GGTAATGGGGGCAAATGGGA

These primers amplify a 431-bp fragment of the gene. Primers were also used for the housekeeping gene, GAPDH (Sigma Kicqstart Primers). Thermo cycling settings were optimized for both sets of primers to be run simultaneously. Briefly, tubes were heated to 50°C for 2 minutes then further heated to 95°C for 2 minutes. Next, samples were cycled 40 times through denaturing with heat at 95°C for 15 seconds, annealed at 55°C for 15 seconds, and extended at 72°C for 30 seconds. As controls, cDNA was run in triplicate along with no template controls for each primer. Fluorescent signal was measured at the end of each extension step. Cycle threshold (Ct) values were normalized to GADPH to determine the relative amount of MBP gene expression using the ΔΔCt method to calculate fold change.

Cerebrospinal fluid collection and Myelin Basic Protein ELISA

CSF was collected from the thoracic spine of 23 monkeys prior to euthanasia and gravity settled for up to four hours at 4°C. Clear and colorless liquid was removed from

the tube and stored in aliquots and frozen at -80°C until use. Samples were rapidly thawed immediately prior to use in ELISA assay.

To evaluate MBP contents in the CSF, a sandwich-ELISA was used (Ansh labs, Webster, TX). Two separate plates were used to evaluate correlations of CSF MBP with age and age-related cognitive decline and another plate used to compare CSF MBP and DTI data. Each plate was coated with MBP antibody by the manufacturer. A standard curve was used in duplicate to allow for detection between 0.3ng/mL and 11ng/mL. Additionally, two known MBP controls were also plated in duplicate as positive controls. One hundred microliters of CSF from each animal was added in triplicate to individual wells. The standards, known positive controls, and CSF samples were incubated on the plate for one hour shaking at 800RPM. All liquid was then aspirated and washed with the kit-provided washing buffer five times. Each well was then incubated with 100µL of MBP antibody-biotin conjugate for one hour shaking at 800RPM. The plate was then aspirated and washed five times with buffer and then loaded with 100µL of Streptavidin-Enzyme Conjugate-RTU and incubated for 30 minutes shaking at 800RPM. The plate was again aspirated and washed five times with buffer prior to incubation with 100µL 3,3', 5,5;-tetramethylbenzidine chromogen solution for 10 minutes shaking at 800RPM. The reaction was then stopped with manufacturer provided Stopping Solution and the absorbance of each well was read using a microplate reader set to 450nm.

Statistics

In assessments of SCoRe and CSF concentrations of MBP, age was considered as a continuous variable. Linear regression was used to statistically measure associations with

dependent variables over the lifespan. Elderly animals (ages 20+) were separated into groups of cognitively spared (CII < 2) and cognitive impaired (CII > 2). Differences between groups were assessed using student's t-test. Alpha was set to 0.05 for all analyses.

Results

SCoRe does not effectively reflect age-related myelin damage, but is sensitive to myelin changes in cognitive impairment

To evaluate myelin damage, we sought to use the recently published method of Spectral Confocal Reflectance (SCoRe) imaging (Schain et al. 2014). Example SCoRe images can be seen from a young (Figure 2.1A) and an old (Figure 2.1B) monkey corpus callosum and verification of co-localization with neurofilament H (NFH) seen in Figure 2.2. We found that percent area of SCoRe signal does not significantly correlate with age ($F(1,23) = 0.00852$, $P = 0.9272$, $R^2 = 0.043$, Figure 2.3A). As the three lasers used in this method are thought to reflect based on the thickness of myelin surrounding the axon (Schain et al. 2014), we next separated the signal by laser, but found that there was also no significance in the 488nm laser ($F(1,23) = 0.091$, $P = 0.766$, $R^2 = 0.04$), the 561nm laser ($F(1,23) = 0.366$, $P = 0.551$, $R^2 = 0.0345$), or the 633nm laser ($F(1,23) = 1.583$, $P = 0.221$, $R^2 = 0.024$) alone.

Next, we separated old animals (ages 20+) into groups of cognitively spared (CII < 2, N = 4) and cognitively impaired (CII > 2, N = 9). Cognitively impaired animals had lower percent area SCoRe signal than cognitively spared animals ($t(11) = 2.538$, $P = 0.0276$, Figure 2.3B). This effect was consistent in the 488nm laser ($t(11) = 2.216$, $P = 0.0487$) and

633nm laser ($t(11) = 2.214$, $P = 0.0489$), but there was no statistically significant difference found in the 561nm laser ($t(11) = 0.933$, $P = 0.371$).

MBP gene expression is increased in older animals

We hypothesized that, in an attempt to correct myelin damage, myelin basic protein gene expression would be increased with age. To test this, we used qPCR to compare MBP gene expression (normalized to GAPDH expression) in frontal brain tissue from young (ages 6-9) and old monkeys (ages 18+). First, we verified that GAPDH Ct was not significantly different between young and old animals ($t(8) = 0.885$, $P = 0.201$). We normalized MBP cycle threshold to GAPDH to get a ΔCt then took the average ΔCt of young animals to use as a reference. ΔΔCt was then calculated for each animal in comparison to the reference and converted to fold change (2^-(ΔΔCt)). To compute the average fold change, we normalized the young animals by dividing 1 by the average of the individual fold change values from young animals to get a normalization factor (0.6769). Individual fold change values were normalized, averaged and correlated with age to find that *MBP* gene expression increases with age ($F(1,8) = 15.4$, $P \leq 0.004$, $R^2 = 0.616$). Taking the average fold change for old animals, we found that *MBP* gene expression increased 9.35 fold in old animals compared to young animals.

The concentration of Myelin Basic Protein increases in the CSF is dependent on age and cognitive impairment

To test the hypothesis that age-related myelin breakdown in the brain would result in the clearance of myelin in the CSF, MBP was measured in the CSF of 23 behaviorally tested rhesus monkeys across the age spectrum (7.6 to 27.8 years) using sandwich ELISA.

As expected, increased concentration of MBP in the CSF was predicted by age ($F(2,20) = 7.102$, $p \leq 0.005$). Approximately 28.96% of the variance in the concentration of MBP in the CSF was explained by age (Figure 2.5A). Although young (ages 5-9) and middle-aged animals (ages 10-19) tend to have low variance in their cognitive abilities, old animals (ages 20+) have a wide range of cognitive abilities. Additionally, myelin degeneration increases not only with age, but also cognitive impairment (Bowley et al. 2010). Thus, old animals were stratified based on their cognitive functions into cognitively spared (CII < 2) and cognitively impaired (CII > 2). It was expected that since cognitively impaired animals have the greatest myelin degeneration those animals would have the greatest amount of myelin cleared to the CSF. However, our results indicated that the concentration of MBP in the CSF of old cognitively impaired animals is significantly less than the concentration of MBP in the CSF of old spared animals ($t(10) = -5.064$, $P \leq 0.0005$, Figure 2.5B).

Finally, we correlated SCoRe signal with the concentration of MBP in the CSF in animals that were used in both experiments. Across all animals, there was no correlation between the concentration of CSF MBP and SCoRe signal in the corpus callosum ($F(1,19) = 0.511$, $P = 0.484$, $R^2 = 0.025$, Figure 2.5C). However, when looking at the old animals only (ages 20+), there was a significant direct correlation between the concentration of MBP in the CSF and SCoRe signal ($F(1,9) = 6.803$, $P = 0.0284$, $R^2 = 0.367$, Figure 2.5D).

Discussion

Summary

In this paper, we investigated age-related changes to myelin using multiple methods. First, we used a label-free technique for myelin visualization, spectral confocal reflectance

(SCoRe) imaging. Although SCoRe was not able to detect known age-related changes to myelin, we found significant a significant decrease in the area occupied by SCoRe label in old cognitively impaired animals. Next, we used RT qPCR to find an age-related increase in MBP gene expression. Finally, we investigated clearance of MBP into the CSF using ELISA. We found that the concentration of MBP in the CSF increased with age. Interestingly, in old animals, cognitively impaired animals had a decrease in MBP concentration in the CSF compared to cognitively spared animals.

SCoRe and myelin visualization

A vast amount of research from our lab and others has shown that myelin damage occurs with age, resulting in notable myelin defects (Bowley et al. 2010) and a loss of myelinated axons (Sandell and Peters 2002; Sandell and Peters 2003). Traditionally, age-related changes to myelination have been investigated through overall white matter changes with structural MRI or at the ultrastructural level with electron microscopy. Although these methods often great insight, each has methodological drawbacks that make them unusable in the current study.

While large-scale imaging methods do not directly measure myelin, MRI can be used to give a broad overview of white matter quality and volume that generally decrease with age (Guttmann et al. 1998; Wisco et al. 2008). Outside of a decrease in white matter volume with age, researchers focused on white matter hyperintensities, age-related lesions that could be visualized via MRI and correlated with cognitive decline (De Groot et al. 2000; de Leeuw et al. 2001; Prins and Scheltens 2015). Recent advances in tractography imaging have made white matter study more accessible. Diffusion tensor imaging (DTI) uses a

measure of fractional anisotropy (FA) to measure what is thought to be myelin integrity (Moseley 2002; Sullivan and Pfefferbaum 2006; Chang et al. 2017). With this, DTI measures of FA have been found to decrease in correlation with age in both humans (Charlton et al. 2006; Voineskos et al. 2012) and monkeys (Makris et al. 2007). While these scans would be useful measures of general myelin integrity, they were not obtained for the majority of animals with available tissue for the current studies.

Using electron microscopy (EM), sections can be visualized at the ultrastructural level to quantify changes in the number of myelinated axons as well as visualize defects in myelination that may not be apparent at the light microscopic level (Bowley et al. 2010). However, doing EM requires sections to be fixed in a specific manner as to not disturb the tissue quality that makes the archived monkey tissue available for the current studies unsuitable for EM processing.

Finding an effective measurement technique to visualize myelin in the usable for this study has thus been difficult. In extreme cases of myelin damage, such as models of multiple sclerosis, histological markers of lipid content (luxol fast blue or eriochrome cyanine) are enough to distinguish lesioned regions. However, these stains are not sensitive enough to distinguish the subtle myelin changes in aging and do not allow for direct visualization of myelinated sheaths. In immunohistochemical stains, antibodies raised against MBP are often used to visualize myelination at the light level. In our studies, we found that immunostaining MBP was clear in the superficial white matter, but MBP staining could not penetrate the deep white matter, potentially due to fat content.

Additionally, immunohistochemistry relies on the labeling of a specific protein that may be changed under the conditions of aging.

Therefore, we sought a label-free method that would allow myelin visualization and quantification at the light level, while not being limited to a specific protein or the superficial white matter. This technique was first reported by Schain and colleagues (2014) as a method to visualize myelinated axons. These researchers hypothesized that SCoRe occurred due to thin film interference, where the laser light is reflected off each layer of myelin, causing interference and allowing for visualization.

In this study, we hypothesized that SCoRe would decrease with age in the corpus callosum due to myelin pathology. However, we found no correlation between age and the area occupied by SCoRe signal. Interestingly, there was a significant decrease found the density of SCoRe-imaged myelinated axons in cognitively impaired aged animals compared to cognitively spared aged animals. These findings contradict previous work using electron microscopy and diffusion imaging. Indeed, Bowley et al (2010) reported a 20% decrease in myelinated axons with age. This discrepancy across methods raise the possibilities that 1) SCoRe lacks the sensitivity to identify age-related myelin damage, but can detect structural differences in myelin that occur with cognitive impairment, when myelin damage is known to be more severe (Bowley et al 2010) or 2) SCoRe images only a subset of myelinated axons that are not affected in aging but are affected in cognitive decline, 3) Fiber bundle orientation and clustering, and properties of myelin constituents, which are distinct across white matter regions in the monkey, produce inherent variability in SCoRe imaging. We believe the findings in this paper are a result of a combination of

these factors. Because of the density of myelin in the corpus callosum, it is possible that reflection is interference between reflected light occurs from more than a single myelinated axon. In our study and in Schain et al (2014), corpus callosum visualization is not as clear as in peripheral nerves or less myelinated structures such as the superficial white matter. Because of the inability to consistently and clearly detect individual myelin fibers, rather than general bundles of myelinated axons, SCoRe in the corpus callosum may not be suitable to detect age-related myelin loss.

Therefore, the decrease in SCoRe signal in cognitive impairment is not likely demonstrative of a loss or thinning of myelin, but a change in quality of myelin. Schain and colleagues (2014) showed that Schmidt-Lanterman incisures were detectable by SCoRe, likely due to the differences in reflection caused by the cellular contents. We hypothesize that changes to protein and/or lipid content of myelin in cognitively impaired animals causes the differences seen in SCoRe signal. Although many studies have investigated age-related changes to myelin structure, few have looked at the molecular content of myelin and none have determined differences in age-related cognitive decline. Previous studies have reported that myelin basic protein content decreases with age (Ansari and Loch 1975; Xing et al. 2012) and age-related ubiquitination of 2’3’-cyclic nucleotide 3’-phosphodiesterase (Hinman et al. 2008), suggesting myelin protein content changes occur with age. Therefore, it is not difficult to imagine changes to the lipid protein content of myelin that could result it altered reflection from SCoRe. EM studies or biochemical analysis of myelin content would aid in our understanding of changes to myelination with age and cognitive impairment and provide a better understanding of the SCoRe signal.

Expression of MBP and myelin damage

As previously mentioned, total MBP content was found to decrease with age (Ansari and Loch 1975; Xing et al. 2012) in addition to myelin loss and damage (Bowley et al. 2010). We hypothesized that age-related myelin damage would result in increased coping mechanisms, such as an increase in MBP gene expression. As expected, our results indicated a 9.35 fold increase in MBP gene expression in dorsal prefrontal cortex with age. Besides our proposal of increased MBP expression as a mechanism to repair myelin damage, we propose a few alternatives based on MBP trafficking and myelin formation.

As mentioned earlier, mRNA synthesis of MBP occurs in the oligodendrocyte and is transported in a vesicle for on-site translation (Ainger et al. 1993; Baron and Hoekstra 2010; Müller et al. 2013). In this process, mRNA production, trafficking, or translation could be improperly functioning with age, causing myelin damage. Our results demonstrate that production of MBP mRNA is occurring robustly, and is actually increased with age and therefore unlikely to be the fault in this mechanism. During stress, RNA binding proteins may sequester non-essential RNAs into stress granules to ensure cell survival (Vanderweyde et al. 2013). It is possible that stress on oligodendrocytes causes sequestration of myelin-related mRNA leading to myelin destabilization and damage. In situ studies to determine localization of myelin mRNA and protein studies to ensure proper translation are necessary to determine if the process of myelin damage involves mRNA.

Clearance of myelin throughout aging and cognitive decline

The major pathology of aging and age-related cognitive decline is myelin damage. In multiple sclerosis, myelin debris clearance occurs and MBP is removed into the CSF in a

manner that correlates with myelin damage (Lamers et al. 1998). We hypothesized that increased myelin damage in aging would lead to clearance of myelin proteins to the CSF. In accorance with our hypothesis, we reported a significant age-related increase in the concentration of MBP in the CSF in rhesus monkeys. However, despite cognitive impairment correlating with an increase in myelin damamge (Bowley et al. 2010), the concentration of MBP in the CSF is significantly lower in cognitively impaired compared to cognitively spared aged monkeys. These results suggest a dysfunction of myelin clearance that separates old monkeys based on cognitive abilities.

Two major mechanisms of debris clearance in the brain are phagocytosis via microglia and glymphatic clearance from the interstitial fluid. Myelin debris clearance is imperitive to homeostasis as myelin debris can inhibit oligodendrocyte differentiation and remyelination (Miron et al. 2013; Lampron et al. 2015). Microglia, however, can become overburdened by age-related myelin damage and unable to sufficiently phagocytose the debris (Safaiyan et al. 2016). As myelin damage accrues and microglia are unable to account for debris degradation, myelin fragments may accumulate in the interstitial fluid. Recently described, the glymphatic system is a paravascular pathway that drives flow and debris clearance between the interstitial fluid (ISF) and the CSF (Iliff et al. 2012). As microglia leave more myelin debris to linger in the ISF, fluid exchange between ISF and CSF would clear the debris to the CSF, as we see with normal aging. However, like the phagocytic system, evidence suggests an age-related decrease in efficiency and flow of the glymphatics (Kress et al. 2014). Future studies evaluating glymphatic efficiency in

conjunction with phagocytic assays are needed to determine the role of each system in cognitive decline.

Conclusions

In this paper, we investigated age-related changes to myelin and a major constituent of myelin, myelin basic protein. We propose an age-related failure in both phagocytosis and glymphatic clearance of myelin. In normal aging without cognitive impairment, we hypothesize that a decrease in phagocytic function leads to an over-reliance on the glymphatics for debris clearance resulting in an age-related increase in myelin debris in the CSF. However, in cognitive impairment, the inefficiencies of both systems take their toll, leading to an accumulation of myelin debris in the ISF (and little myelin in the CSF) and inhibition of remyelination. In both situations, the increase in myelin debris causes an unexpected inhibition in new myelination, leaving oligodendrocytes with increased myelin protein mRNA that cannot be readily used, however further research is needed to provide a more concrete causal connection between these mechanisms. Regardless, our research provides novel insight into the dysfunction of clearance mechanisms in aging and cognitive decline. We suggest these systems as potential targets for therapies to prevent age-related cognitive decline and possibly age-related neurodegenerative disease.

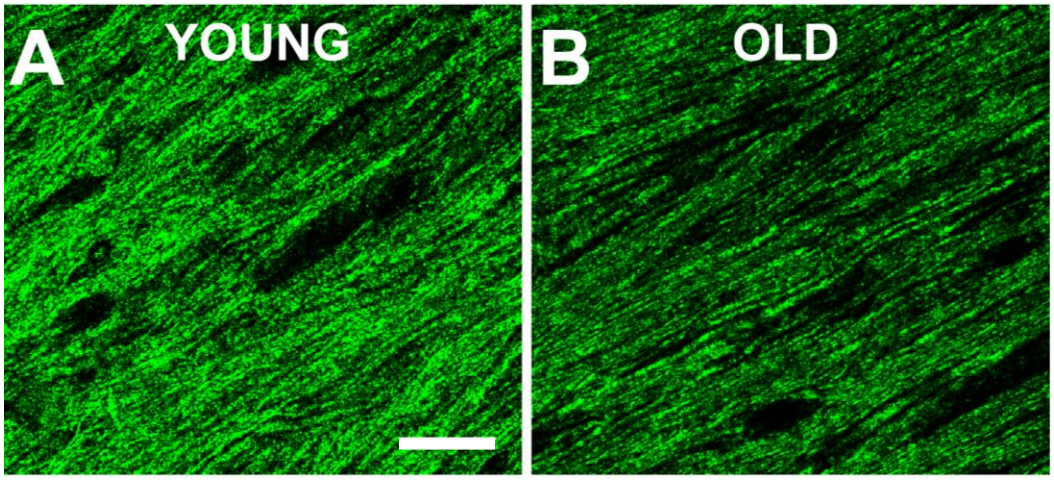

Figure 2.1. Example SCoRe imaging in the corpus callosum. Spectral Confocal Reflectance (SCoRe) imaging is a label free method of collecting reflected light to image myelinated axons using three lasers from a confocal microscope (Schain et al. 2014). We used SCoRe imaging in the corpus callosum of rhesus monkeys to evaluate the ability of this method to detect age-related myelin pathology (Peters and Rosene, 2003). Example images of one optical slice from A) a young monkey (age 9.5) and B) an old monkey (age 25.4). Scale bar = 20µm

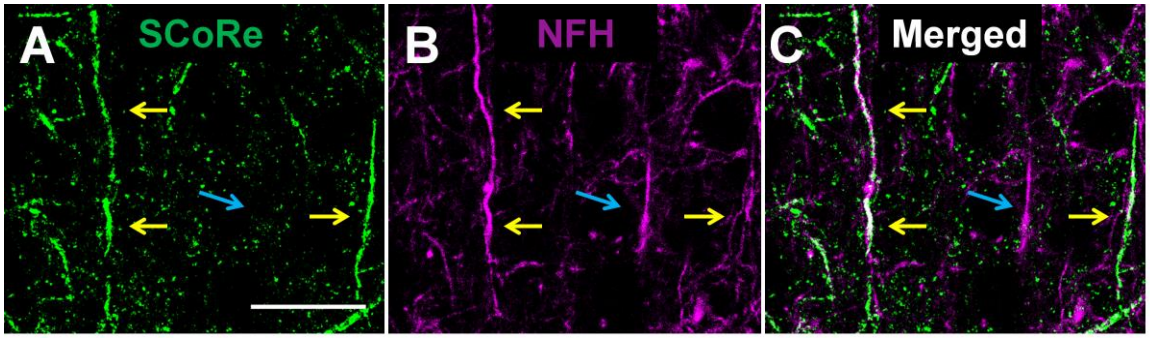

Figure 2.2. SCoRe colocalizes with axons. A) Spectral Confocal Reflectance (SCoRe, green) signal was collected on tissue also immuno-stained with B) neurofilament H (NFH, magenta) in the white/gray boundary of frontal white matter to verify the C) co-localization of SCoRe signal with axons (white). Yellow arrows point out a selection of the double labeled axons and the blue arrow points to an axon with no SCoRe signal. Scale bar = 20um

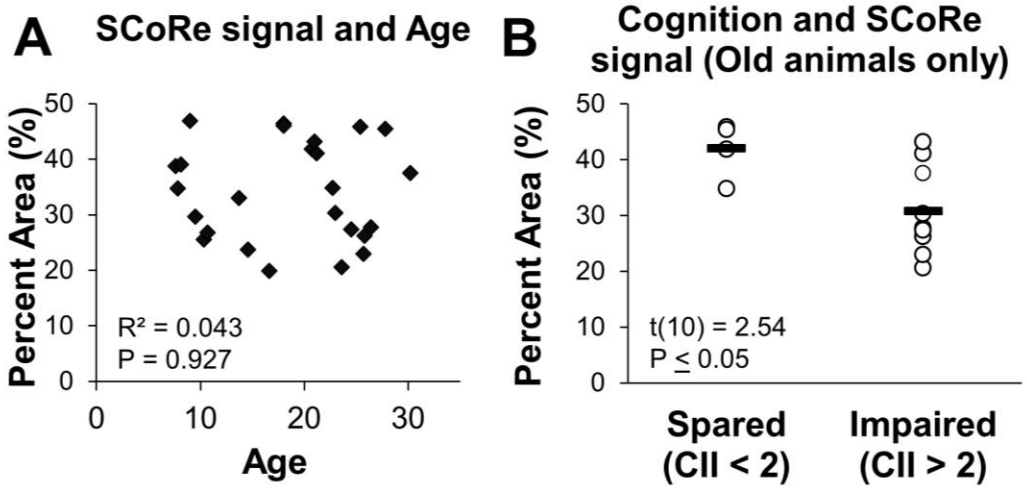

Figure 2.3. SCoRe imaging quantification in aging and cognitive impairment. We tested if Spectral Confocal Reflectance (SCoRe) imaging is able to detect age-related myelin pathology in the rhesus monkey corpus callosum. For each animal, 10 z-stack images were taken from the corpus callosum and quantified for percent area of SCoRe signal collected. A) The percent area of reflectance signal collected by SCoRe did not correlate with rhesus monkey age as shown by scatterplot, where each point represents data from a single monkey. Behavioral data from each monkey was compiled into a z-score known as the Cognitive Impairment Index (CII). To assess if SCoRe could detect myelin pathology in age-related cognitive decline, old monkeys (ages 20+) were separated into groups of cognitively spared (CII < 2) and cognitively impaired (CII > 2). B) Vertical scatter plot showing individual data from each animal (open circles) and mean data (black line). We found that cognitively impaired monkeys had significantly less percent area occupied by SCoRe signal than cognitively spared monkeys, suggesting that SCoRe can detect the myelin pathology separating these groups. *$P \leq 0.05$

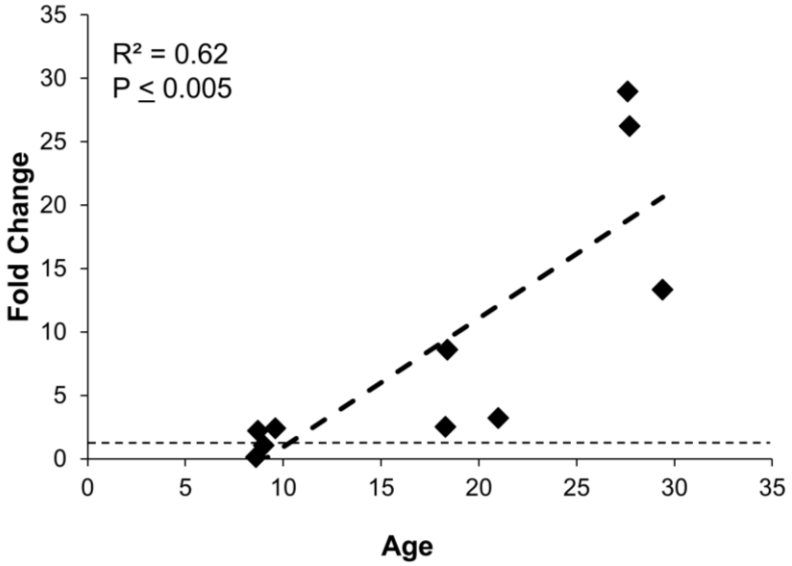

Figure 2.4. Gene expression of MBP in the dorsal prefrontal cortex. RNA was isolated from area 46 of 4 young (ages 6-9) and 6 old monkeys (ages 18+) and reverse transcribed to cDNA. We performed qPCR on MBP and GAPDH and normalized MBP cycle threshold to GAPDH (ΔCt) then took the average ΔCt of young animals to use as a reference. ΔΔCt was calculated for each animal in comparison to the reference and converted to fold change (2^-(ΔΔCt)). To compute the average fold change, we normalized the young animals by dividing 1 by the average of the individual fold change values from young animals to get a normalization factor (0.6769). Individual fold change values were normalized and averaged. As shown above, normalized fold change values are represented as black diamonds and the fold change of 1 (average of the young animals) is presented as a dashed line. We found that *MBP* gene expression increased significantly with age as tested by linear regression ($P \leq 0.005$).

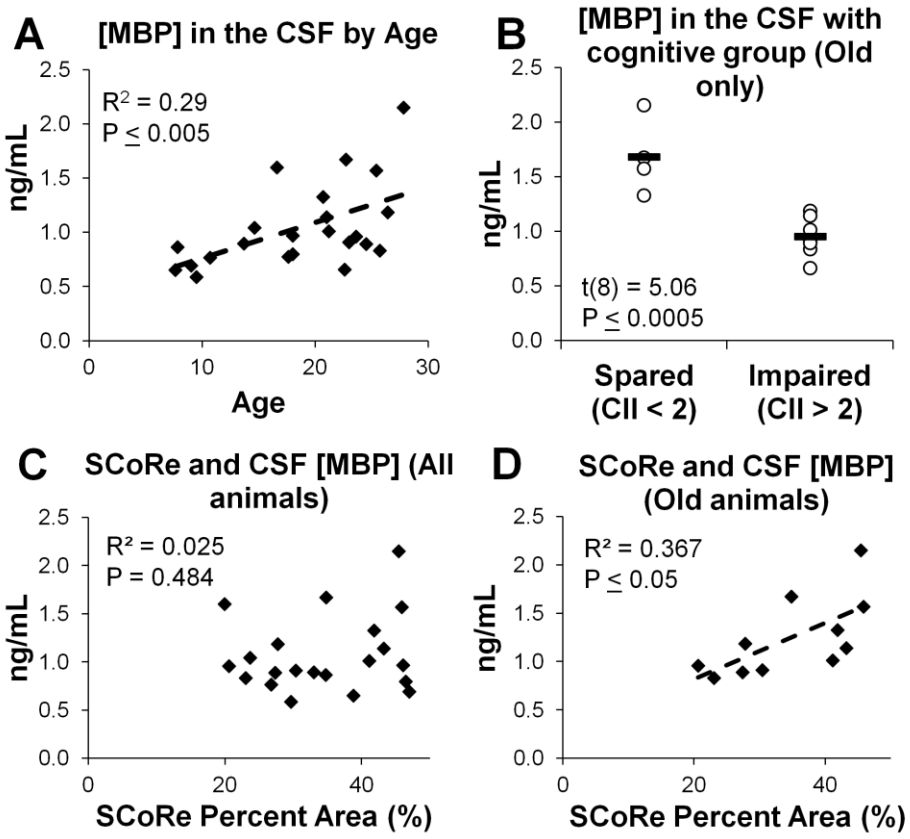

Figure 2.5. The concentration of MBP in the CSF in aging and cognitive decline. We used an ELISA for myelin basic protein (MBP) and cerebrospinal fluid (CSF) taken from monkeys across the rhesus monkey lifespan. A) Scatter plot and linear regression shows that the concentration of MBP in the CSF correlates with age. As myelin pathology increases with age (Bowley et al. 2010), our results suggest that myelin proteins are cleared to the CSF. B) To assess the impact of age-related cognitive impairment on the concentration of MBP in the CSF, old monkeys (ages 20+) were stratified into groups of cognitively spared (CII < 2) and cognitively impaired (CII > 2). Open circles represent individual data from each animal, black bars represent average per group. The concentration of MBP in CSF was significantly greater in the spared animals compared to

the impaired. These results suggest a potential defect in the clearance of myelin proteins to the CSF in cognitively impaired animals. This defect may be hindering remyelination by causing damaged myelin to linger. C) Scatter plots and linear regression of MBP concentration in CSF against SCoRe signal. We found that SCoRe signal did not correlate with monkey age. D) However, in old animals (ages 20+), SCoRe signal percent area was significantly related to the concentration of MBP in the CSF. This suggests that clearance of myelin protein to the CSF is necessary to maintain myelin in old animals.

CHAPTER 3: MICROGLIAL ACTIVATION AND PHAGOCYTOSIS

This chapter has been previously published and has been reproduced here with minor alterations and permission from all authors and appears in:

Shobin et al. (2017) Microglia activation and phagocytosis: relationship with aging and cognitive impairment in the rhesus monkey. Geroscience, 39(2): 199-220

Introduction

Although general changes in microglia activation have been widely studied, the phagocytic capacity of these cells in aging and cognitive decline is not as well understood. Studies on peripheral immunity have shown a loss of phagocytic capacity and function in macrophages with age (Plowden, et al., 2004), although this result is not consistent across all studies (Gardner et al. 1981) and may differ between inflammatory cell types (Linehan et al., 2014). Cultured macrophages from aged humans have a diminished phagocytic capacity for myelin debris (Natrajan et al. 2015) and in vivo studies have shown the rate of remyelination is reduced in aged rodents but can be restored with an infusion of monocytes from young animals (Ruckh et al. 2012). Finally, phagocytic activation of microglia and size of microglial lysosomes increases with age in addition to an increase in microglia adjacent to and contacting myelin (Safaiyan et al. 2016). While these data suggest that phagocytic capacity of old macrophages is impaired, the reason for this functional decline is unknown. Additionally, no study has investigated whether phagocytic activation in the aging brain is related to cognitive decline.

The current study using brain samples from behaviorally characterized rhesus monkeys was designed to assess the relationship between microglial activation and phagocytic phenotype and their associations with age-related cognitive decline. To do so, we use Galectin-3 (Gal-3) antibody as a marker for phagocytic activation. Gal-3 (also known as Mac-2) is a

conserved lectin involved in cell adhesion and phagocytosis in macrophages (Dumic, Dabelic, & Flögel, 2006). Gal-3 is expressed ubiquitously throughout the cell, cell surface, and extracellular space and contains a C-terminal carbohydrate recognition binding domain important for cell adhesion and phagocytosis (Pugliese et al., 2015). Gal-3 is selectively up-regulated in phagocytic macrophages (Elliott et al. 1991) and transgenic mice deficient in Gal-3 have reduced phagocytic ability (Sano et al. 2003). Gal-3 also is necessary for the the microglial response to myelin degeneration (Hoyos et al. 2014). Additionally, we used the LN3 antibody which recognizes the HLA-DR major histocompatability complex class II receptor to mark activated macrophages that could be either pro- or anti-inflammatory (Conde and Streit, 2006). We also used double label immunofluorescence to determine if the phagocytic priming of activated microglia changes with age or is associated with cognitive decline. The overall goal was to test the hypothesis that dysfunctional age-related phagocytic activation in the brain of behaviorally tested rhesus monkeys is related to microglial activation and cognitive impairment.

Materials and Methods

Subjects

Brain tissue from 44 rhesus monkeys was used in this study. This tissue had been collected and stored as part of an NIA funded Program Project ("Neural Substrates of Cognitive Decline in Aging Monkeys", P01-AG000001) and a Research Project ("Histopathology, Neuroimaging and Mechanisms of Myelin Damage in Aging Monkey Brain", R01-AG043640). Of the monkeys used in this study, 38 were originally obtained from the Yerkes National Primate Research Center at Emory University in Atlanta, while

6 animals came from other research centers (see Table 3.X). Prior to selection, health records were screened with strict health criteria to exclude any possible confounding clinical diseases or experimental manipulations that could impact normal aging by affecting the brain or behavior.

Based on tissue availability, monkeys were divided between experiments for activated microglia using LN3 (N=19) and phagocytic microglia using Gal-3 (N=30). Six monkeys overlapped between studies (see Table 3.X). Prior studies of rhesus monkey survival and of cognitive decline suggest that, relative to humans, the rhesus monkey ages at an approximate ratio of 1 year for every 3 human years (Tigges et al., 1988). As such, animals for each experiment were divided into groups of young adult (ages 5.0 - 9.9 at euthanasia), middle-aged (ages 10.0 -19.9 at euthanasia) and old (ages 20+ at euthanasia). While the young and old groups have a relative balance of males and females, there were insufficient males to balance the middle-aged subject group in each experiment. Although stratifying animals by age range allows for easy classification of each animal, in statistical analyses, age was also used as a continuous variable in regression analyses to identify changes that occur across the lifespan.

Behavioral testing

Upon entering the study, all monkeys received a battery of behavioral tests that took place over a three to six month period and was completed approximately one to two months before euthanasia. These tests assess a variety of cognitive domains. Acquisition of the Delayed Non-Match to Sample (DNMS) task is a measure of rule learning. Assessment of extended delays on DNMS (120 sec and 600 sec) test recognition memory. The Delayed

Recognition Span Task (DRST) assesses working memory capacity in both spatial and object modalities. Finally the Category Set Shifting Task (CSST) assesses executive function including set shifting. Details of these tasks can be found elsewhere (Herndon et al. 1997; Moore et al. 2005).

Initial inspection of how these tests compared to our measures of microglial reactivity indicated associations with measures of DNMS and DRST but not with CSST measure. Interestingly, a principal components analysis (Herndon et al., 1997), had demonstrated that a subset of DNMS and DRST measures were the best predictors of cognitive aging. These have been compiled into a z-score which is designated the cognitive impairment index (CII) and has proven useful in comparing cognitive status with a variety of neurobiological endpoints (e.g. Peters, Sethares, & Moss, 1998). To avoid multiple comparison problems the CII was used in all comparisons in this study.

Age and cognitive impairment across experiments

Subjects from each experimental cohort were compared to ensure similarities between groups. As age is normally a predictor for cognitive impairment, the entire cohort (N=44) was first analyzed using regression analysis and results showed that increases in age significantly predicted increases in CII in this cohort ($F(1,41) = 16.19$, $p \leq 0.0005$, $R^2 = 0.266$). As shown in Figure 3.6, linear regression demonstrated a significant direct relationship between age and CII in each of the subsets of subjects used for Gal-3 studies ($F(1,27) = 13.10$, $p \leq 0.001$, $R^2 = 0.320$, Figure 3.6A) and LN3 studies ($F(1,16) = 5.98$, $p \leq 0.05$, $R^2 = 0.227$, Figure 3.6B). As one subject (AM121) with a very large CII appeared to drive the correlation between CII and age in the LN3 cohort, the CII of the LN3 subjects

were tested for outliers using a multiple of 1.5 times the interquartile range to determine a cutoff of CII score 6.32. Thus, AM121 (CII score of 12.37) was removed and the regression still demonstrated that age predicted CII ($F(1,15) = 6.41$, $p \leq 0.05$, $R^2 = 0.253$). As the inclusion of AM121 did not impact the significance of the correlation between age and CII score, this animal was included in all analyses unless otherwise stated.

Brain perfusion and tissue section preparation and storage

Approximately one to two months after the conclusion of behavioral testing, monkeys were deeply anesthetized with sodium pentobarbital and perfused transcardially through the aorta with Krebs Henseleit buffer, pH 7.4 at 4°C for five minutes while fresh tissue samples were harvested. This was followed immediately by perfusion with 4% buffered paraformaldehyde (pH 7.4, 37°C) for 10 minutes. Immediately following perfusion, the brain was blocked, in situ, in the coronal stereotactic plane, removed from the skull and placed in the same paraformaldehyde fixative overnight at 4°C. It was then cryoprotected by successive incubations in 0.1M phosphate buffer containing first 10% glycerol with 2% DMSO and then buffer with 20% glycerol and 2% DMSO until the brain equilibrated (Rosene et al. 1986). It then was flash frozen in isopentane at -75°C after which it was stored at -80°C until it was cut on a freezing microtome into 10 interrupted series of 30 µm thick sections. Sections were collected in buffer with 15% glycerol as a cryoprotectant, equilibrated overnight at 4°C and then frozen and stored at -80°C until removed and thawed for immunohistochemistry.

Immunohistochemistry

To eliminate confounds in processing, sections for all subjects to be stained with an antibody were removed from -80°C storage at the same time, rapidly thawed to room temperature and "batch processed" together in the same reagents for the same time to facilitate quantitative analyses across subjects. For LN3 staining, 6-10 sections per animal were stained at section intervals of approximately 1200 µm. For Gal-3 staining, 4-7 sections per animal were stained at sections intervals of approximately 2400 µm. Once thawed, sections were washed 3 times in 0.05M Tris buffered saline (TBS, pH 7.6) to remove the glycerol. Immunohistochemistry protocols were optimized as described by Hoffman et al. (2008). To break cross-links formed during fixation, antigen retrieval was performed by incubating the sections in 10mM citrate buffer (pH 6.0) in a microwave tissue processor (PELCO Biowave, Ted Pella, Inc., Redding, CA) for 5 minutes at 550W and 40°C followed by incubation in the same buffer at room temperature for 1 hour on a rocking platform. Sections were again washed in TBS (3 x 5 minutes), then incubated with 3% buffered hydrogen peroxide for 30 minutes to quench endogenous peroxidases. Next, tissue was washed with TBS (3 x 5 minutes) and blocked with SuperBlock (Life Technologies, Grand Island, NY) or 10% normal goat serum in TBS (LN3 tissue only) for 1 hour. Primary antibodies were diluted 1:700 (mouse IgG1 anti-Gal-3, Abcam, Cambridge, MA) or 1:10 (mouse IgG2b anti-LN3, MP Biomedicals, Santa Ana, CA) in TBS containing 0.5% SuperBlock (or 2% normal goat serum for LN3 tissue) and 0.3% Triton-X. As a control, a few sections from various animals were placed in carrier solution (TBS containing 0.5% SuperBlock/2% normal goat serum and 0.3% Triton-X) but omitting primary antibody. For tissue in Gal-3 primary antibody, sections were microwaved in primary antibody or carrier

solution for 5 minutes at 250W and 30°C. In both experiments, incubation in primary then proceeded on a rocking platform at 4°C for 40 hours.

After the primary antibody incubation, tissue was washed with TBS (3 x 5 minutes) and incubated for one hour in secondary antibody containing goat anti-mouse (Vector Laboratories, Burlingame, CA) diluted 1:600 in buffer containing 0.5% SuperBlock/2% normal goat serum and 0.3% Triton-X. Tissue labeled with Gal-3 was also microwaved for 5 minutes at 250W and 30°C in secondary antibody. Following the secondary antibody incubation, tissue was washed with TBS (3 x 5 minutes) and incubated with avidin biotin complex using Vectastain ABC kit (Vector Laboratories, Burlingame CA) for 1 hour. Tissue was washed with TBS (3 x 5 minutes), then exposed to a chromogen solution containing 0.5mM 3-3 diaminobenzidine (Sigma-Aldrich, St. Louis, MO) and 0.03% hydrogen peroxide in TBS for 10 minutes. Tissue was then washed with TBS (3 x 3 minutes), mounted on gelatin coated slides, and dried overnight. For Gal-3 stained tissue, slides were lightly counterstained in 0.5% thionin (pH 4.8) for 30 seconds. All slides were then dehydrated through graded alcohols (0%, 50%, 75%, 95%, 100%, 100%, 3 minute each), and cleared in xylenes (2 x 5 minutes). Slides were coverslipped with Permount (Fisher Scientific, Waltham, MA).

Regions of interest

Regions of interest (ROI) were identified using a 2X objective and boundaries outlined according to the criteria illustrated in Figure 3.7.

Cingulum Bundle (Figure 3.7A-D): The cingulum bundle (CGB) was defined as a semi-triangular white matter region within the cingulate gyrus. For the Gal-3 experiments and

the rostral sections in the LN3 experiments, the CGB was bounded ventrally by the CC. The caudal portions of the CGB used in the LN3 experiments are bounded by the cingulate gyrus gray matter and an arbitrary line connecting area 29a-c to the junction of area 31 and the parietal area PE cingulate.

Corpus Callosum (Genu, Figure 3.7A, B): For the genu of corpus callosum (CC), LN3 cell counting was bounded slightly more medially than that of Gal-3 counting, thus the entirety of the CC defined in the LN3 experiment was contained in the CC defined in the Gal-3 experiment. For the LN3 experiment, the anterior edge of the CC was identified in the first serial section containing callosal fibers from the midline. For Gal-3 experiments, the most rostral section was identified as the first section containing both CC and internal capsule. The posterior end of the genu for both experiments was identified when the septum pellucidum first appears as it separates the anterior body from the rostrum. The dorsomedial boundary of the genu is the indusium griseum or the lateral ventricle (once the caudate is present) and the dorsolateral boundary is the anterior cingulate gyrus. For LN3 sampling, the lateral boundary of the genu is defined as a straight line connecting the medial edge of the gray/white boundary of the anterior cingulate to the lateral edge of the indusium griseum or the lateral edge of the lateral ventricle (once the caudate is present). For Gal-3 experiments, the lateral boundary of the CC extended from the lateral edge of the lateral ventricle to the ventrolateral edge of the cingulum bundle as to not overlap with the CGB or the FWM.

Frontal White Matter (Figure 3.7A, B): For both experiments, the frontal white matter (FWM) was defined as the white matter region excluding corpus callosum and cingulum

bundle starting from the lateral most junction of the CC and caudate nucleus, ventral lateral across the putamen, then ventral to the intersection of the putamen and the claustrum and dorsal to the white matter beneath the inferior arcuate sulcus. The FWM then follows the border of the gray matter around to where it began.

Unbiased stereology

Standard unbiased stereology was performed on blind coded sections using a Nikon E600 light microscope equipped with a Q-Imaging digital camera, a motorized stage and Stereo Investigator software (MBF Bioscience, Williston, VT). Gal-3 and LN3 positive cells were identified using the soma as the counting target and numbers estimated using the optical fractionator method as described by West, Slomianka, & Gundersen, 1991. For each ROI and marker, pilot studies were performed to determine appropriately sized sampling grids and counting frames. For Gal-3 stained tissue, 4-7 sections were used for each animal. Sections were blind coded and counted using a 20X/0.50 objective lens within a counting frame of 99.0 X 66.6 X 10 μm^3 with the dissector top and bottom guard volume extending 5 µm below the z extent of the counting brick. For LN3 stained tissue, 6-10 sections were blind coded and counted using a 60X/1.40 oil-immersion objective lens within a counting frame of 60 X 60 X 5 μm^3 with the dissector top and bottom guard volume extending 1 µm below z extent of the counting brick.

The sampling grid was randomly placed over the outlined ROI prior to counting. Cells were considered to be Gal-3 or LN3 positive if they contained dark brown staining of a small cell body and at least one process or an enlarged circular cell body alone. The cell body was used as the counting object for cells that fell within the dissector or across its

inclusion planes. The Cavalieri estimator was used to estimate volumes and the coefficient of errors (CE) was calculated as described by Gundersen et al. (1999). With the counting frame and sampling grid used in the current study, a minimum of 100 cells for each region and animal and were counted and the CE was 0.1 or less to ensure minimal variance due to sampling. Due to the low number of Gal-3 positive cells in young and middle-aged animals, CE values below 0.1 were unattainable making stereological estimations of total cell counts difficult. Therefore, cell density reported in mm^3 was used to compare relative counts between subjects.

Morphology

In old animals (ages 20+), subtypes of Gal-3 positive cells were identified and counted according to the morphological criteria as ramified, hypertrophic, or amoeboid (see Figure 3.8) as defined by Karperien et al. (2013). As shown in Figure 3.8, cells were counted as ramified if they had one or more thin process extending from a small, dense cell body. Amoeboid cells were identified if they had enlarged, semi-circular cell bodies with limited to no processes extending from the soma. Hypertrophic cells were identified if they had any of the following: 1) a semi-circular or rod-like cell body with no processes, 2) an enlarged, non-circular cell body with at least one process, or 3) an enlarged, non-circular cell body with dark, dense, and thicker processes.

Immunofluorescence Co-localization and Quantification

For double label immunofluorescence of activated microglia (LN3+) and the phagocytic phenotype (Gal-3+), two sections containing FWM from each of nineteen animals were stained using mouse IgG2b anti-LN3 and mouse IgG1 anti-Gal-3. Sections

were thawed together and first washed with buffer to remove the glycerol and then incubated in SuperBlock for 1 hour, and placed in 0.5% SuperBlock, 0.3% Triton-X solution containing LN3 (1:62.5) and Gal-3 (1:150) overnight at room temperature. As negative controls, sections were either incubated in carrier solution, carrier solution containing Gal-3, or carrier solution containing LN3. Following primary antibody incubation, tissue was washed with TBS then incubated in secondary antibody solution containing 0.5% SuperBlock, 0.3% Triton X, AlexaFluor 488 goat anti-mouse IgG2b (1:1000, Invitrogen, Carlsbad, CA) and AlexaFluor 568 goat anti-mouse IgG1a (1:1000, Invitrogen, Carlsbad, CA). Sections were then washed and mounted. Once semi-dry, the slides were rehydrated in buffer for 5 minutes, then dehydrated in 70% ethanol for 5 minutes and incubated with Autofluorescence Eliminator Reagent (Millipore, Darmstadt, Germany) for 45 seconds. The slides were cleared with 70% ethanol (3 x 1 minute) and coverslipped using anti-fading mounting medium (PVA-DABCO, Sigma-Aldrich, St. Louis, MO).

Co-localization of Gal-3 and LN3 was determined in the FWM of young and old animals using a Leica TCS SPE laser scanning confocal microscope (Buffalo Grove, IL). AlexaFluor-488 emission was detected using argon laser excitation at 488nm whereas Alexafluor-568 emission was detected using 561nm laser excitation. To ensure equal counting between animals, exhaustive searches were first performed for the less dense Gal-3 labeled cells in young animals. Pre-scanning determined that twenty-five z-stack images could be taken per animal with at least 1 Gal-3 positive cell per image identified with a 40X objective lens. The width of the image was determined by the point where no Gal-3

positive staining was visualized. The number of z-slices were determined using the automated system optimized settings. LN3 was visualized in green and Gal-3 in magenta. Cells in each image were counted as single labeled Gal-3 (magenta only in a cell body with at least one process) or Gal-3 double labeled with LN3 (white image of double-labeled cell body with at least one process). Double labeled cells were further subdivided into two categories: 1) overlapping double label (white staining verified as double labeling by investigation of individual color channels) and balloon double label (magenta "ballooned" white or magenta process extending from a cell body encircled by green label).

Z-stack images contained in .LIF files were counted using FIJI (version 1.49m, National Institutes of Health). Individual channels for green and magenta were opened and contrast was automatically enhanced. The channels were then merged and the z-stack compressed using the z-projection function to flatten all images in the stack to one image. The percentage of each type of Gal-3 labeling was determined by manual counting with the investigator blind to subject conditions.

Statistics

All analyses were performed using the R-project (x64, version 3.10) and RStudio (version 0.98.1102) for statistical computing and an alpha significance level of 0.05. Three factor ANOVA with two between subject factors (age groups (3) X sex (2)) and one repeated measure (region (3)) was performed with subjects stratified by young, middle-age and old. When statistically significant differences were found by ANOVA, a Tukey A (HSD) post-hoc test was used to identify the critical factor while controlling for multiple comparisons. Linear regression analyses (alpha = 0.05) were conducted to assess the

relationship of LN3 cell density, Gal-3 cell density and Gal-3 morphological subtype density to age or cognitive function (in old animals only). A chi-squared test of independence was used to test differences in Gal-3 double labeling with LN3 between young and old animals.

Results

Galectin-3 phagocytic cell density increases with age

Examples of Gal-3 staining are shown in Figure 3.9A and 3.9B and the volume of each ROI and the estimated Gal-3 positive cell density is shown in Table 2 for each animal. To determine if the density Gal-3 positive staining (cells/mm^3) differed by sex or ROI, animals were stratified into age groups (young, middle-aged, old) and ANOVA was used to assess the effects of age group, sex, and ROI. There were no significant differences in density of Gal-3 positive cells between regions ($F(2,64) = 0.085$, $p = 0.919$) or between sexes ($F(1,64) = 0.026$, $p = 0.873$), but Gal-3 cell density did approach significance by age ($F(2,64) = 2.763$, $p = 0.071$, see Figure 3.10A) and there were no significant interaction effects between factors. A Tukey-A post-hoc analysis was performed comparing Gal-3 cell densities across sex, ROIs, and groups. This post-hoc analysis demonstrated that the density of Gal-3+ cells was significantly higher in old animals compared to both young ($p \leq 0.00001$) and middle-aged animals ($p \leq 0.00001$). Middle-aged animals did not significantly differ from young animals ($p = 0.243$). These differences were consistent for all ROIs.

To test the hypothesis that Gal-3 cell density increased with age, linear regression was used with age as a continuous variable. There was a significant age-related increase in the

density of Gal-3 positive cells in the CGB (Fig 5B, ($F(1,26) = 29.9$, $p \leq 0.0001$) with age accounting for approximately 51.7% of the variance in Gal-3 cell density ($R^2 = 0.517$). Similarly in the FWM (Figure 3.10C), the density of Gal-3 positive cells significantly increased with age ($F(1,27) = 31.6$, $p \leq 0.0005$) which accounted for 52.2% of the variance in Gal-3 cell density ($R^2 = 0.522$). Similarly, in the CC (Figure 3.10D), Gal-3 cell density significantly increased with age ($F(1,26) = 17.3$, $p \leq 0.0005$) where it accounted for 37.6% of the variance.

LN3 activated microglial density increases regionally with age

LN3 positive staining can be seen in Figure 3.9C and 3.9D. To determine if there were statistical differences between LN3 cell density (cells/mm^3) a 3-way ANOVA was run with subjects stratified by age, sex, and ROI. There was no significant effect of sex ($F(1,35) = 0.53$, $p = 0.473$), but there were significant effects for region ($F(2,35) = 7.72$, $p \leq 0.005$) and age group ($F(2,35) = 3.97$, $p \leq 0.05$). There were no significant interaction effects. To further investigate the significant differences in age groups, one-way ANOVA analyses were performed between cell density and age group for each of the three regions. There were no significant differences in LN3 cell density between age groups in the CC ($F(2,15) = 1.42$, $p = 0.272$) or in the FWM ($F(2,15) = 2.56$, $p = 0.111$). However, LN3 cell density did differ significantly by group in the CGB ($F(2,15) = 7.70$, $p \leq 0.005$). Tukey post-hoc analysis revealed that old animals had significantly greater LN3 positive cell density compared to both middle-aged ($p \leq 0.05$) and young animals ($p \leq 0.01$, see Figure 3.11A).

Linear regression analysis was used to determine if density of LN3 positive cells in each region was associated with age. As shown in Figure 3.11B, the density of LN3 positive

cells in the CGB significantly increased with age ($F(1,16) = 22.1$, $p \leq 0.0005$), where age accounted for 54.0% of the variance in LN3 cell density ($R^2 = 0.540$). In the FWM (Figure 3.11C), the relationship between age and LN3 cell density approached significance ($F(1,16) = 4.12$, $p = 0.059$) and age explained 15.5% of the variance in LN3 positive cell density ($R^2 = 0.155$). In the CC (Figure 3.11D), the relationship between LN3 cell density and age again approached significance ($F(1,17) = 3.70$, $p = 0.072$) but age accounted for only 13.0% of the variance in LN3 positive cell density ($R^2 = 0.13$).

Gal-3 cells are a subset of LN3 positive microglia

To determine if Gal-3 positive phagocytic cells also expressed the "activated" LN3 phenotype, the percentage of Gal-3 cells double labeled with LN3 was determined in young and old animals using immunofluorescence and confocal microscopy. As shown in Figure 3.12A-C, two different classes of cells were identified: 1) Single labeled: a cell that was Gal-3 positive and LN3 negative and 2) Double labeled: a cell that contained both Gal-3 staining and LN3 staining. Additionally, as shown in Figure 3.12E, some of the double labeled cells had a distinct morphology with the Gal-3 signal contained within an LN3 positive "balloon" within the LN3 positive cell, but without necessarily overlap of both labels. For all subjects, 91.3% of Gal-3 positive cells were double labeled with LN3 and only 8.7% were not. Additionally, of the Gal-3 positive cells 75.5% of Gal-3 staining showed almost complete overlap with LN3 whereas 15.8% of cells the Gal-3 positive signal was surrounded by an LN3 balloon (Figure 3.12D). To determine if the proportion of Gal-3 double labeled with LN3 differed between ages, a chi-square test was performed

and revealed no significant differences between young and old animals ($\chi^2(1, N = 20) = 0.767, p = 0.678$).

Density of hypertrophic and amoeboid Gal-3 cells predicts cognitive decline

To determine if microglial activation or phagocytic phenotype were associated with age-related cognitive impairment, linear regression was used to compare density to CII score of old animals (ages 20+ years) with each marker. CII was not associated with LN3 cell density in the CGB ($F(1,4) = 0.007, p = 0.937, R^2 = 0.248$) or the FWM ($F(1,5) = 1.24, p = 0.317, R^2 = 0.038$), but was significantly predicted by LN3 cell density in the CC ($F(1,4) = 8.37, p \leq 0.05, R^2 = 0.551$). However, this effect was largely driven by one animal (AM121). Using a multiple of 1.5 times the interquartile range, AM121 was identified as an outlier for CII score. When AM121 was removed, the CII score was no longer predicted by LN3 cell density in the CC ($F(1,4) = 0.07, p = 0.799, R^2 = 0.227$).

For Gal-3, there was no relationship between cell density and CII in the CGB ($F(1,11) = 0.27, p = 0.614, R^2 = 0.065$) or the CC ($F(1,11) = 0.010, p = 0.923, R^2 = 0.09$). However, increased Gal-3 cell density in the FWM significantly predicted increased CII ($F(1,12) = 10.8, p \leq 0.01$) accounting for 42.9% of the variance in CII score ($R^2 = 0.429$, Figure 3.13A).

To determine if the significant relationship of Gal-3 cell density in the FWM to CII score was due to phagocytic morphologies, linear regression was used to assess the relationship between the densities of ramified, hypertrophic, and amoeboid Gal-3 positive cells and CII of animals 20 years or older. While the density of ramified Gal-3 cells was not associated with CII ($F(1,11)$ 0.98, $p = 0.343, R^2 = 0.002$, Figure 3.13B), CII was

significantly predicted by the density of amoeboid Gal-3 cells ($F(1,10) = 16.94$, $p \leq 0.005$, $R^2 = 0.592$, Figure 3.13C) and also by the density of hypertrophic Gal-3 cells ($F(1,11) = 0.05$, $p \leq 0.05$, $R^2 = 0.357$, Figure 3.13D).

Discussion

Summary

The current study utilized immunohistochemical labeling with Galectin-3 and LN3 antibodies to identify phagocytic and activated microglial in the brains of cognitively assessed rhesus monkeys. In the cingulum bundle, corpus callosum and frontal white matter, Gal-3 and LN3 cell densities increased significantly with increasing age. Of the Gal-3+ phagocytic microglia, 90% co-localized with LN3 marker for activated microglia. In about 15% of the Gal-3 positive cells, the markers were not fully overlapped but, instead, showed a small Gal-3 positive outgrowth characterized as Gal-3+ phagocytic "balloons." While total numbers of double labeling and Gal-3 balloons increased with age, the percentage of double labeled Gal-3 and ballooned Gal-3 did not differ between age groups. To determine if either phagocytic activation or total microglial activation were related to the degree of age-related cognitive decline, the densities of Gal-3+ and LN3+ microglia were evaluated in behaviorally tested old monkeys ($\geq$20 years of age). In these aged subjects, increased Gal-3+ cell density correlated with increased cognitive decline in the frontal white matter but not in the cingulum or the genu of the corpus callosum. In contrast, LN3+ cell density only correlated with cognitive performance in the corpus callosum although this was mainly driven by one animal that was very impaired. Since microglial morphology may be indicative of function (Karperien et al. 2013), we analyzed

morphological subtypes of Gal-3+ cells in the frontal white matter of the aged animals to determine if the previously identified correlation or Gal-3+ cell density and cognitive impairment was due to microglia with an activated morphology. While the density of Gal-3+ cells with a ramified morphology was not related to cognitive impairment, the density of both hypertrophic and amoeboid subtypes was significantly associated with increased cognitive impairment.

Functional Classification of Microglia by Immunohistochemistry and Morphology

Microglia have been dichotomized as M1/pro-inflammatory which corresponds with the classical notion of activation or as M2/anti-inflammatory which is an alternative activation state. *In vitro*, M1 activation is defined by responsivity to IFN-γ or LPS challenge causing release of pro-inflammatory cytokines such as TNF-α or IL-6, and production of reactive oxygen species. The alternative M2 activation is defined by responsivity to IL-4 leading to the release of anti-inflammatory cytokines such as TGF-β and IL-10 (for review on microglia activation, see Cherry et al., 2014). However, identifying, defining and interpreting activation states *in vivo* has been inconsistent (Gordon and Martinez, 2010; Prinz and Priller, 2014). For example, the current study utilizes LN3, an antibody to the HLA-DR MHC II surface receptor as a marker for microglial activation. Some report that MHC II expression increases with microglial "activation" following pathogen-associated molecular patterns (Town et al. 2005). However, MHC II expression is regulated by toll-like receptor stimulation and the M1 activation pathway via IFN-γ (Ting and Trowsdale 2002) but nevertheless is associated with both pro- and anti-inflammatory phenotypes (Conde and Streit 2006). Hence, MHC

II expression can also be regarded as a marker for identifying the general population of microglia (Conde and Streit, 2006; Mittelbronn et al., 2001). While the Gal-3 literature is more consistent in that it is necessary for phagocytosis (Sano et al. 2003; Dumic et al. 2006), Gal-3 has not been widely utilized in the brain and only recently recognized as a marker for phagocytic activation (Safaiyan et al. 2016).

Thus, immunohistochemical staining with LN3 or Gal-3 may not necessarily indicate the presence of one specific functional state (activation or phagocytosis). Rather Gal-3+ staining may simply indicate that the microglial cell is “primed” for phagocytic activation while the presence of LN3+ staining may indicate the cell is "primed" for inflammatory activation (Norden and Godbout 2013; Perry and Holmes 2014). Double labeling with LN3 and Gal-3 would indicate that both processes are available when necessary. Consistent with this interpretation of microglia priming, Sierra et al. (2007) showed that while aged mice have higher baseline mRNA expression of both M1 cytokines (TNF-α, IL-6, IL-1β) and M2 cytokines (IL-10, TGF-β), when challenged with LPS, older mice have both more robust pro- and anti-inflammatory cytokine responses compared to young mice. This indicates that microglia that appear as “activated” by IHC, may be primed and ready to respond when challenged. Therefore, the current data demonstrate that both phagocytic priming (Gal-3+ cells) and general microglial activation increase with age in frontal white matter regions. Further, as over 90% of Gal-3 cells are co-labeled with LN3, it is clear that the majority of phagocytic primed cells are activated microglia.

Further insight into functional state may be gained by examining the morphological subtypes of labeled microglia. As reviewed by Karperien et al. (2013): ramified microglia

with small, round cell bodies and thin processes are thought to be non-inflammatory, surveilling the neuronal environment for damage (Nimmerjahn et al. 2005). In contrast, hypertrophic microglia are often polarized, with enlarged soma and denser processes representative of “activated” or inflammatory microglia (Lee et al. 2008). Amoeboid microglia with rounded somata and limited processes are indicative of phagocytic microglia (Bohatschek et al. 2001). Although these data suggest that morphology is indicative of function, no study to date has demonstrated exactly what cytokines are being released or what exact functions are occurring in each morphological state. Hence, the traditional M1/M2 dichotomy and division into "activated" and "resting" cells is being re-examined (Ransohoff 2016). In the current study, phagocytic microglia stained for Gal-3 are separated by these morphological subtypes. As expected, the Gal-3 positive cells were primarily hypertrophic (~60%) or amoeboid (~30%). Moreover, only the density of hypertrophic and amoeboid Gal-3+ cells correlated with cognitive impairment. The observation that ramified Gal-3+ cells do not change with age or predict cognitive decline suggests that there is a baseline number of Gal-3+ cells that are primed for phagocytosis but have not developed an inflammatory phenotype. The changes in total Gal-3+ staining likely indicates an increase in the number of cells taking on morphologies indicative of an inflammatory phenotype. This demonstrates that Gal-3 immunoreactivity is a useful marker for inflammation and phagocytosis in the brain.

Microglial activation and phagocytosis throughout the lifespan

One hallmark of brain aging is chronic M1/pro-inflammatory activation of microglia (Cribbs et al., 2012; Holtman et al., 2015, see Norden and Godbout, 2013 for review).

Increased overall microglial activation with age has been reported using different IHC markers in rodents (Rozovsky et al. 1998; Sierra et al. 2007), monkeys (Sheffield and Berman 1998; Sloane et al. 1999), and humans (DiPatre and Gelman, 1997; Rogers et al., 1988; Streit and Sparks, 1997). The current study confirms and expands upon this general finding by demonstrating that the density of LN3 (total activation) and Gal-3 (phagocytic activation) positive microglial increases with age in white matter pathways of the frontal lobe (the cingulum bundle, corpus callosum and frontal white matter). Bowley et al. (2010) and many others (Feldman and Peters, 1998; Peters and Sethares, 2002; Sandell and Peters, 2003) have reported an age-related accumulation of myelin defects and axon loss in forebrain white matter pathways of the rhesus monkey (e.g. the corpus callosum and cingulum bundle, anterior commissure). Additionally, others have shown age-related loss of white matter volume in MRI (Guttmann et al. 1998; Wisco et al. 2008), increases in white matter hyperintensities in MRI (Tullberg et al. 2004; Wakefield et al. 2010) and increased myelin damage inferred by loss of fractional anisotropy from diffusion tensor imaging (DTI; Makris et al., 2007). As myelin defects accumulate with age, it is likely that microglia would be activated and participate in the clearance of damaged white matter and axons. Interestingly, neither LN3 nor Gal-3 antibodies show robust staining in the gray matter in young or old monkeys (data not shown).

Phagocytosis and demyelination

Despite the large body of evidence that myelin is damaged and lost and microglia are activated with age, evidence of myelin removal has been limited. Peters & Sethares (2002), using electron microscopy, described small myelin fragments in astrocytes and less

frequently in microglia. This is in contrast to *in vitro* studies that report macrophages, such as microglia, phagocytose myelin at a greater rate than astrocytes (Williams et al., 1994). Other studies report that myelin phagocytosis is impaired with age (Ruckh et al. 2012; Natrajan et al. 2015) and can be inhibited by pro-inflammatory cytokines (Brück et al. 1992; Liu et al. 2006). Thus, it is possible that the chronically pro-inflammatory microglia of the aging brain could slow the removal and phagocytosis of myelin debris (Rawji et al., 2016).

In a demyelinating model of experimental autoimmune encephalomyelitis (EAE), Gal-3 expression has been shown to increase (Reichert and Rotshenker 1999), but, despite this increase, myelin clearance in this model is insufficient to allow recovery of myelination to normal levels (Neumann et al. 2009). Similarly, studies have shown that if myelin debris is not removed, remyelination is impaired (Lampron et al. 2015). In this regard, it is also known that oligodendrocyte precursor cells are recruited to areas of demyelination, but differentiation into mature myelinating oligodendrocytes is impaired by myelin debris (Kotter et al., 2005; Kotter et al., 2006). These observations suggest that a limiting factor in repair and restoration of myelin may be the phagocytic capacity of the microglia to remove myelin debris.

Phagocytic functionality

The data from the current study suggest that stimulation of phagocytosis increases with age in parallel with myelin damage. The correlation of increased phagocytic phenotype (amoeboid cells) with increased cognitive decline reported here and the age-related increase in myelin damage reported in this same model (see Peters and Kemper, 2012 for

review) likely means that phagocytosis is not sufficient to effectively remove damaged myelin (Ruckh et al. 2012; Natrajan et al. 2015). Hence, the observed increase in Gal-3 positive microglia with age could indicate that microglia have been "primed" for phagocytosis by detection of deteriorating myelin, but are either dysfunctional or the amount/rate of myelin damage is too much for microglia to efficiently phagocytose the debris. As more myelin debris accumulates and is not repaired, a vicious cycle could result in which more microglia are recruited and release pro-inflammatory cytokines, but fail to remove sufficient myelin debris to allow for remyelination and resolution of inflammation (Ruckh et al. 2012; Natrajan et al. 2015).

In our immunofluorescence study of Gal-3 co-localization with LN3, approximately 15% of the cells had a distinct balloon-like formation extending from an otherwise normal looking LN3+ microglial soma. This feature resembles the phagocytic cups previously described *in vitro* (Kay et al., 2006; Leverrier & Ridley, 2001; Murray et al., 2005). These actin-dependent cups form during the initial stages of phagocytosis as a macrophage begins to engulf debris. It would be expected that the percentage of microglia displaying these phagocytic cups would increase with accumulating damage. To the extent that presence of Gal-3+ phagocytic balloons are markers of phagocytic function, the present data showed no difference in the percentage of cells double-labeled cells with phagocytic cups between young and old animals. Since all evidence suggests that white matter in the aged brain likely contains significant myelin damage, the lack of an increase in the percentage of microglia with phagocytic cup suggests an impairment in phagocytic responsivity.

Phagocytic capacity and age-related neurodegenerative diseases

With age, microglia have been described as dystrophic and senescent (Streit et al. 2004), but the functionality and phagocytic capacity of these senescent microglia is unknown. In a recent study in mice, Safaiyan et al. (2016) identified an age-related increase in Gal-3 microglia and an increase in microglia contacting myelin visualized by double label IHC, suggesting that microglia not only have increased phagocytic activation, but also that this increased activation may be related to myelin. Similar inefficient debris clearance has been seen in age-related neurodegenerative diseases such as Alzheimer's, where β-amyloid aggregation is also thought to be related to an impaired phagocytic capacity of microglia (Chung et al. 1999; Lucin et al. 2013; Hickman and El Khoury 2014). These data suggest that age-related impairment of microglial phagocytosis is not limited to myelin. However, the question still remains as to the cause of the impaired microglial function. For example, perhaps age-related accumulations of a variety of protein aggregates like amyloid as well as myelin debris overburden microglia. Alternatively, perhaps microglia functionality simply declines with age, allowing damage to go unresolved? These questions must be considered not only in aging, but also in neurodegenerative diseases where debris clearance could play a key role in disease progression. Further, as the leading risk factor for neurodegenerative diseases is age (Mayeux and Stern 2012), it is possible that the burden of myelin debris may play a role in the ability of microglia to deal with other damage in the brain, such as amyloid plaques, phosphorylated tau oligomers, or α-synuclein aggregates.

Autophagy and aging

While phagocytosis is important for the clearance of cellular debris, autophagy is the process required for normal maintenance of cellular function through breakdown of intracellular debris (Glick et al. 2010). Data indicate that inhibiting autophagy in mice decreases lifespan and increases protein aggregation (Hara et al. 2006; Komatsu et al. 2006). In contrast, increasing autophagy in worms (Hansen et al. 2008) and flies (Simonsen et al. 2008) extends lifespan. Interestingly, calorie restriction without malnutrition increases autophagy in rats (Kume et al. 2010) and extends life span (Weindruch and Walford 1982) and monkeys (Mattison et al. 2017). While the exact mechanism by which calorie restriction enhances autophagy is unclear, it is thought to involve AMPK or Sirtuin 1 stimulation or insulin-like growth factor inhibition (Johnson et al. 2013). Although both autophagy and phagocytosis show age-related functional changes, little is known about possible linkage between these clearance mechanisms. Additionally, it is unknown why these mechanisms for degradation become faulty with age and whether these changes occur in monkeys.

Cognitive decline and phagocytosis

While the density of LN3+ and Gal-3+ microglia increase significantly with age, it is curious that Gal-3+ cell density in the FWM was the only strong correlate with cognitive impairment. While some have reported that cognitive impairment is predicted best by total frontal white matter (Tullberg et al., 2004, Wakefield et al., 2010), others have claimed that regional specificity is important (Bowley et al., 2010, Head, 2004, Mielke et al., 2009). Bowley et al. (2010) showed myelin defects are specifically correlated with cognitive decline in the cingulum, but not the corpus callosum. However, DTI data from Mielke et

al. (2009) and Head (2004) suggest that frontal white matter damage, but not temporal or occipital, correlate with cognitive performance. The specificity of the current finding of a relationship of Gal-3 with cognitive impairment only in FWM could suggest that myelin damage was more severe in this area, leading to more microglia being primed for phagocytosis but ultimately ineffective in allowing remyelination. This is consistent with our additional observation that within the FWM, the density of both hypertrophic (activated) and amoeboid (phagocytic) Gal-3+ cells correlated with cognitive decline while the density of ramified (resting) microglia did not. It further suggests that these microglia are not functioning properly and allow myelin damage to accumulate, leading to an increase in the number of microglia recruited and activated and a continuation of the inflammatory response. The specificity of this finding to the FWM might indicate especially faulty clearance mechanisms in this region, i.e. a particular vulnerability. However, it is possible that Gal-3+ microglia are simply acting as a surrogate marker for the overall white matter damage and general aging dysfunction. Understanding the regional differences in myelin damage and age-related pathologies is essential to determining the relation of inflammation to and the causes of age-related cognitive decline.

Conclusions

During aging, myelin deteriorates and appears to be a strong predictor of the age-related cognitive decline seen in normal aging (Bartzokis 2004; Peters 2009). As the myelin debris accumulates, it likely leads to the increased recruitment of the activated and phagocytic microglia observed in the present study. In a healthy adult, this would trigger an acute inflammatory response supporting microglial phagocytosis and clearance of the debris,

resolving with oligodendrocyte precursor cell differentiation and remyelination. However, with aging, the capacity of microglia to clear the myelin debris likely declines as shown by Plowden et al. 2004 and Safaiyan et al. 2016, leaving microglia unable to effectively respond to the damage and remyelination impeded by inhibition of oligodendrocyte differentiation. Similar phagocytic inefficiencies may also contribute to the vulnerability of the brain to age-related neurodegenerative diseases. Thus therapeutics targeting the phagocytic functionality of aging microglia could prove useful not only in facilitating remyelination, and slowing or even reversing age-related cognitive decline, but might also be valuable in treating age-related neurodegenerative diseases**.**

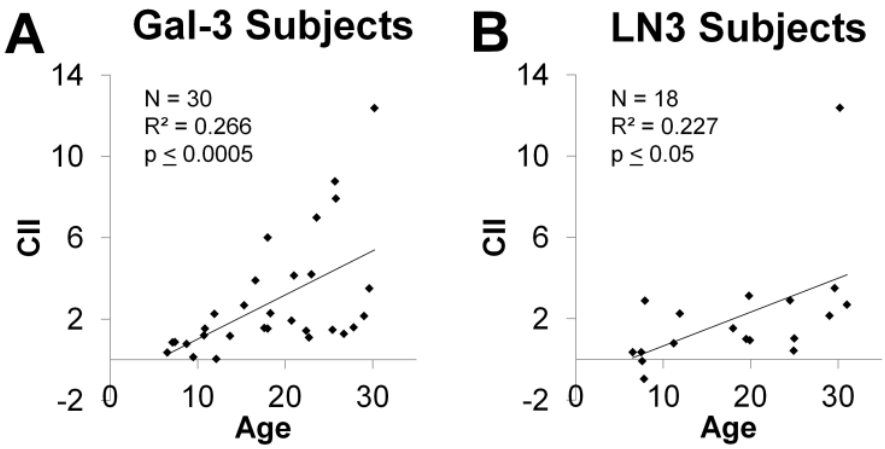

Figure 3.6. Subject comparison between studies. For both the cohort of subjects in the A) Gal-3 analysis and those in B) the LN3 analysis, linear regression analyses show that cognitive impairment index (CII) scores increase significantly with age. There is a statistical outlier with severe impairment that drives the LN3 effect, but, even with this subject removed the increase in CII with age is still significant ($R^{2 =}$ 0.253, $p \leq 0.05$).

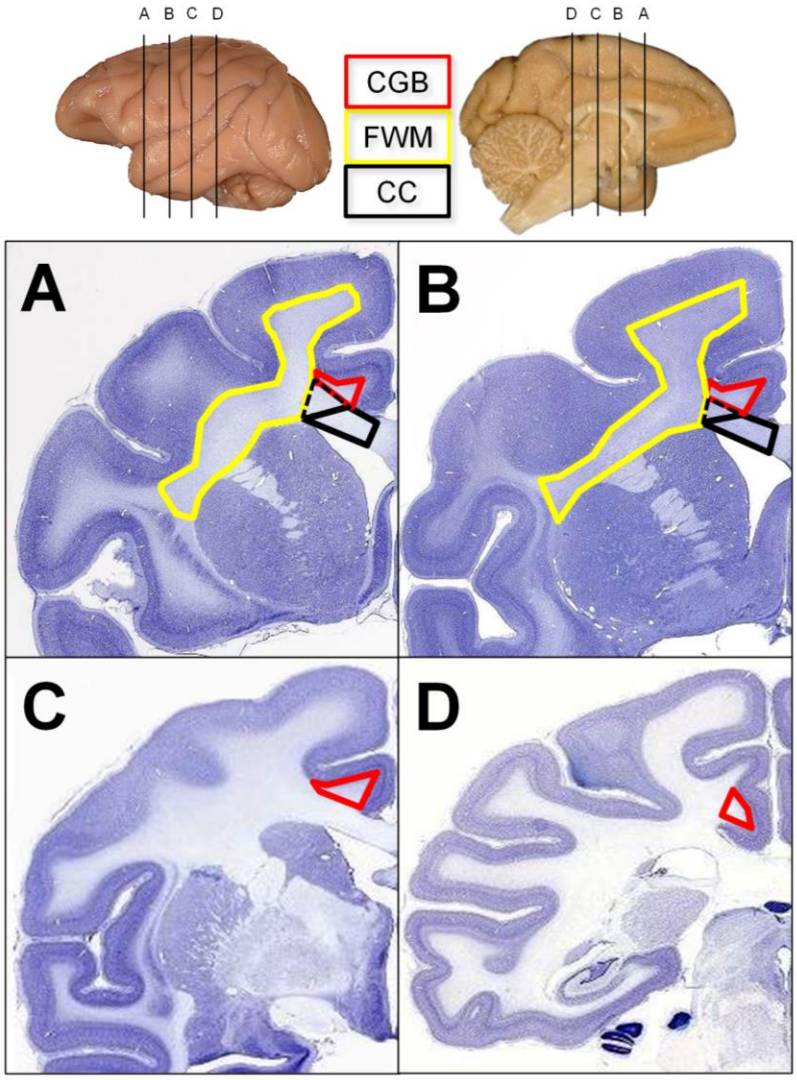

Figure 3.7. Regions of interest. Nissl stained sections from the NIH Blueprint NHP Atlas, (http://www.blueprintnhpatlas.org/static/home) show the approximate rostral and caudal boundaries for each region of interest analyzed: the cingulum bundle (CGB, red), frontal white matter (FWM, yellow) and anterior part of the body of the corpus callosum (CC, black). For the Gal-3 experiment, the CGB was sampled between AP +30.00 (A) and AP +25.50 (B), whereas, for the LN3 experiment, the CGB was sampled between AP +17.45 (C) and AP +0.30 (D). For both Gal-3 and LN3 experiments the FWM was analyzed from AP +30.00 (A) to AP

+25.50 (B). For the LN3 analysis, cells in the CC were counted within the black solid boundary. For the Gal-3 experiment the CC region of interest included the solid black line plus the region within the black dotted line. Interaural measurements estimated from Paxinos, Huang, & Toga (2000).

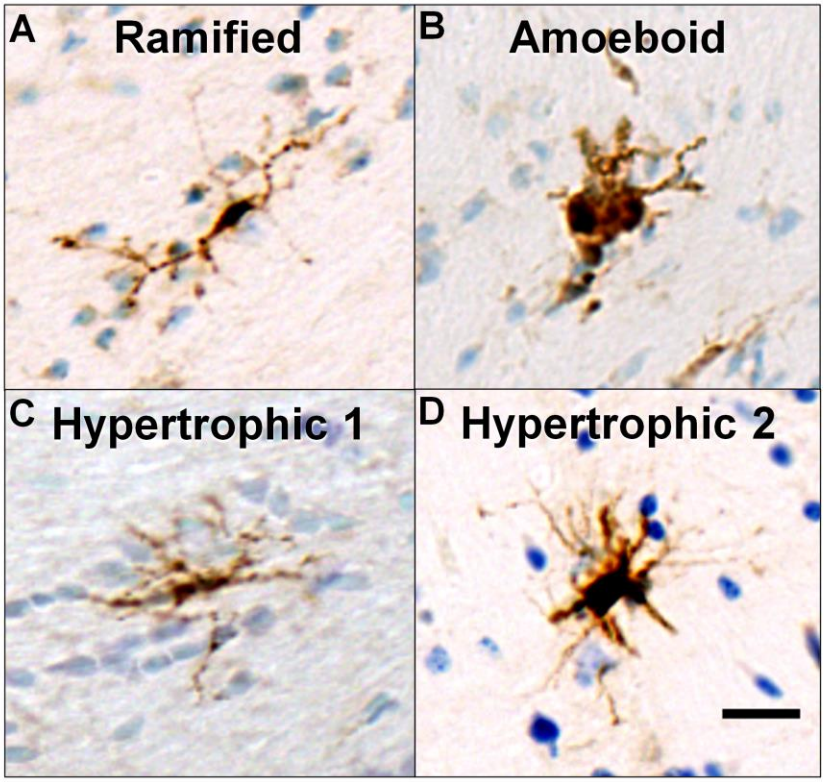

Figure 3.8. Morphological characterization of Gal-3 positive cells. Bright field photomicrograph of Gal-3 immunolabeling (brown) with thionin counterstain (blue) in FWM showing microglial morphology as follows: A) Ramified microglia contain dense cell bodies and thin processes distributed around the cell. B) Amoeboid microglia are characterized by large, round stained cells with only a few, short processes or no processes. C-D) Hypertrophic Gal-3 positive cells are found in a variety of shapes and sizes but range from cells with C) an elongated cell body and short, dense processes to D) cells with a densely stained and curved cell body with short, dense processes or intense cell body staining with thin processes extending outwards. Scale bar = 20µm.

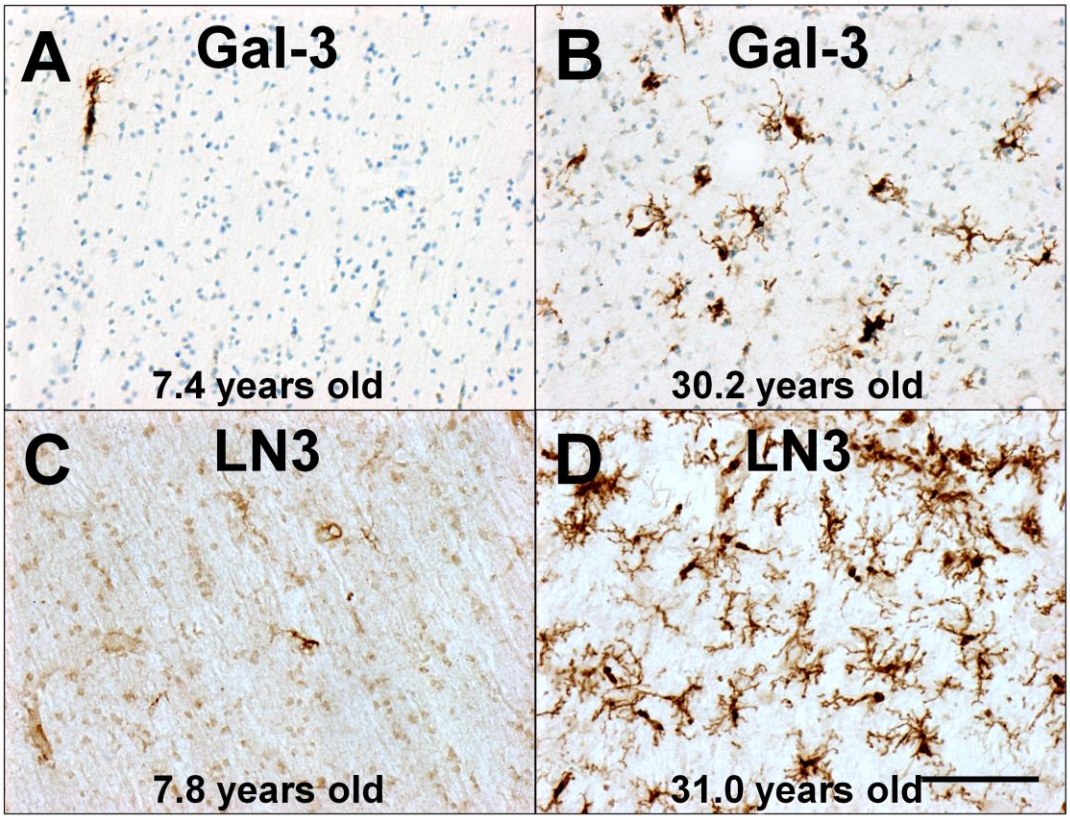

Figure 3.9. Typical staining in the Frontal White Matter for Gal-3 and LN3 positive cells. A) The scarcity of Gal-3 staining in a young subject compared to B) the robust staining for an aged subject. C) Similarly, we see sparse LN3 positive staining in a young subject compared to D) dense staining in an aged subject. A thionin counterstain was used for Gal-3 stained sections, as indicated by blue staining seen in A and B. Scale bar = 0.1mm

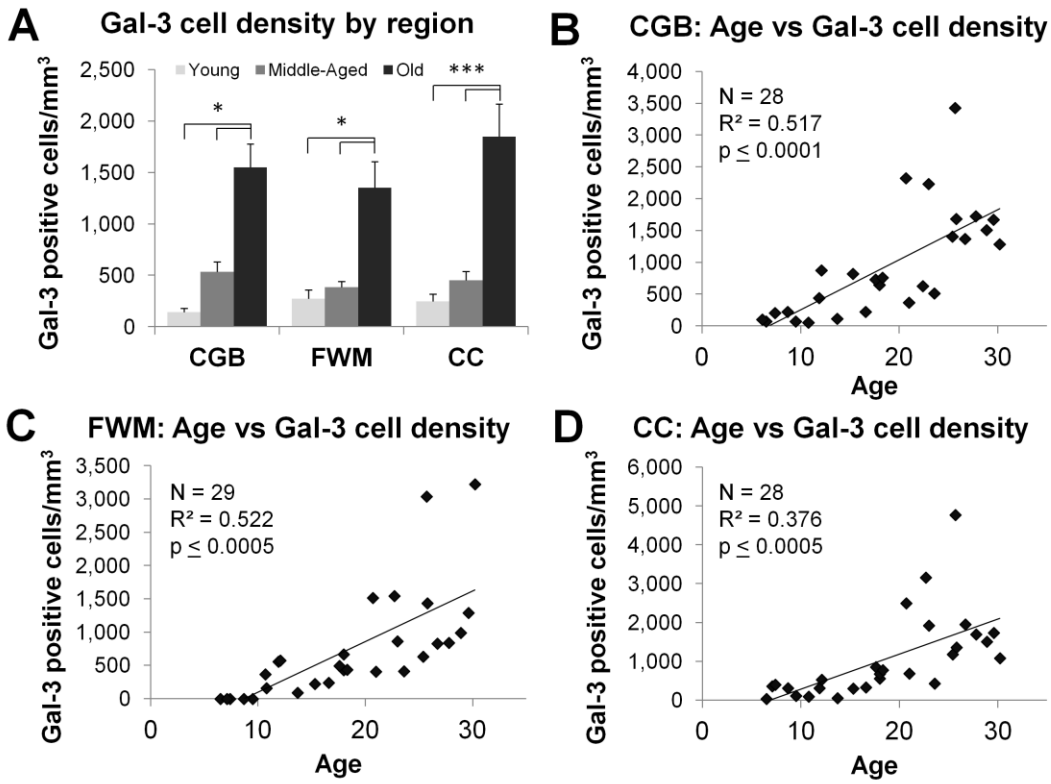

Figure 3.10. Galectin-3 stereological quantification. A) Bar graphs comparing mean Gal-3 cell density for each region stratified by age groups. A 3-way ANOVA demonstrated that while there were no significant effects of sex or regions, there was a significant effect of age groups. Tukey-A post-hoc analysis demonstrated that within each region of interest, Gal-3 cell density was significantly greater in old animals compared to young and middle-aged animals. B-D) Scatterplots of Gal-3 cell density in each region of interest. Linear regression analysis showed that Gal-3 cell density was positively associated with age in all three regions. *$p \leq 0.05$, ***$p \leq 0.0005$

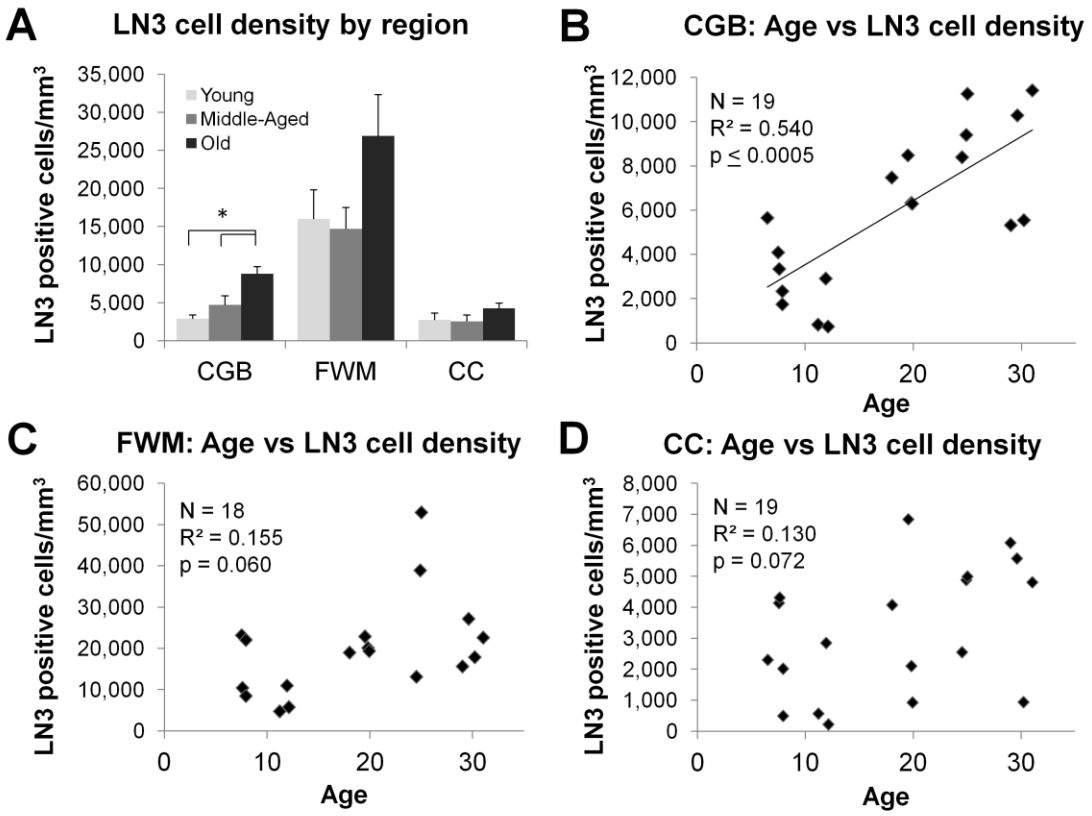

Figure 3.11. Stereological quantification of LN3. A) Bar graphs displaying mean LN3 cell density for each region stratified by age group within each region of interest. A 3-way ANOVA demonstrated that there was no significant effect of sex, but there were significant effects of age groups ($P \leq 0.05$) and within regions ($P \leq 0.005$) with no significant interactions. Tukey-A post-hoc analysis demonstrated that within the CGB, LN3 cell density was significantly greater in aged subjects compared to middle-aged ($P \leq 0.05$) and young ($P \leq 0.01$). B-D) Scatterplots of LN3 cell density in each region of interest. B) Linear regression analysis demonstrated that LN3 cell density was positively associated with age in the CGB and C, D) approached a statistical association in the FWM and the CC. *$P \leq 0.05$

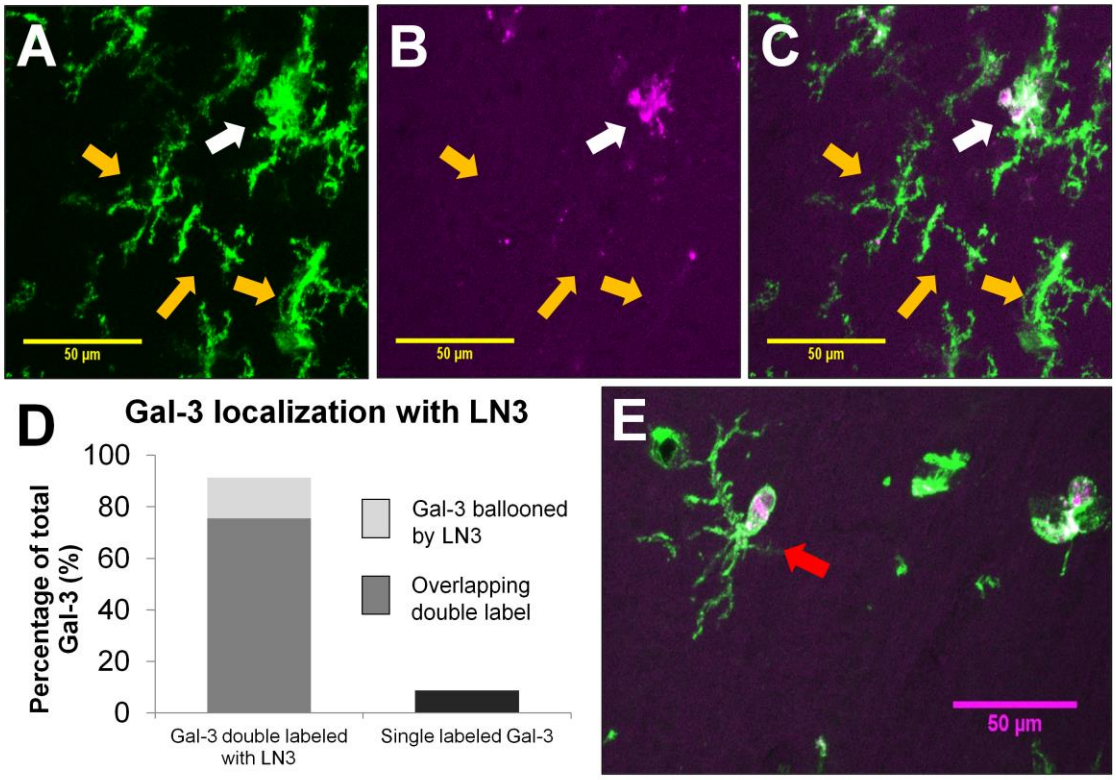

Figure 3.12. Analysis of LN3 and Gal-3 double labeling. Confocal images were taken in a z-stack and z-projected image of standard deviation of mean intensity using FIJI software. Examples for A) LN3 only (green) and B) for Gal-3 only (magenta). C) The merged image and shows one cell with co-localization in white (white arrow) while the other three cells indicated by yellow arrows remain single labeled for LN3. D) Gal-3 is found in 91.3% of LN3 positive cells while 8.7% of Gal-3 cells do not colabel with LN3 positive cells. E) A subset of the Gal-3 and $LN3^{+}$ double labeled cells contained small, round, offshoots of LN3 that surrounded, but did not always colocalize with Gal-3 staining. These offshoots are referred to as "balloons" and one is indicated by the red arrow. Scale bars = 50µm.

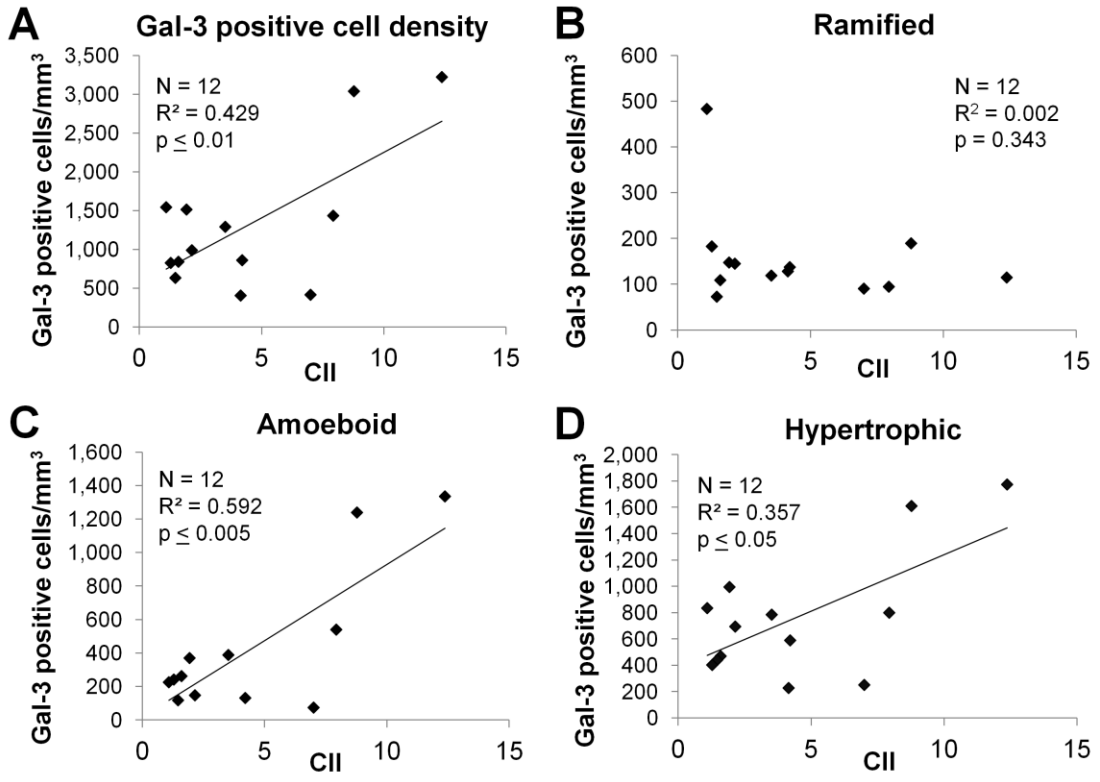

Figure 3.13. Galectin-3 cell quantification in age-related cognitive decline. Scatterplots showing the linear relationship of cognitive impairment (CII) to Gal-3 positive cell density in total and by morphological subtypes in the FWM of old animals (ages 20+). Regression analysis showed that CII is significantly related to A) total Gal-3 cell density, but not B) to the density of ramified Gal-3 cells. However, the density of C) amoeboid Gal-3 cells and D) hypertrophic Gal-3 cells both significantly predicted by CII score. This suggests that only the inflammatory-associated amoeboid and hypertrophic morphologies of Gal-3 cells are associated with increased cognitive impairment.

CHAPTER 4: LIPOFUSIN LOCALIZATION IN WHITE MATTER GLIAL CELLS

Introduction

One of the most long-standing theories of cellular aging and senescence is the "free radical theory of aging" first proposed by Harman in 1956. This continues to be a major hypothesis despite decades of data and debate (see Liochev 2013; Viña et al. 2013; Gladyshev 2014; Reeg and Grune 2015). The theory posits that reactive oxygen species (ROS) increase with age and cause excessive oxidative stress that leads to cellular damage. ROS are primarily produced by mitochondria as a function of metabolism and electron transport (Turrens 2003; Kregel and Zhang 2007). However, ROS can also be induced by intrinsic factors such as cytokines (Yang et al, 2007) and growth factors (Bae et al. 1997). Excess ROS and resulting oxidation can cause severe cellular damage including protein modifications and misfolding as well as damage to lipids and to DNA (Kregel and Zhang 2007). The mitochondrial-lysosomal axis theory of aging stems from the oxidation hypothesis by proposing that ROS-induced dysfunctions to mitochondria create a feed forward loop with increased ROS production and generation of more cellular debris that needs to be degraded by the lysosome (Brunk and Terman 2002a). Lysosomes, either overburdened or dysfunctional themselves, are unable to keep up with the amount of material needing to be degraded leading to accumulation of intracellular debris aggregates and impaired autophagy (Terman 2001).

Proteins are more likely to become oxidized with increased ROS generation, a process that can lead to protein cross-linking (Stadtman and Berlett 1997). Oxidized proteins are

targeted for degradation through the ubiquitin-20S proteosome pathway (Davies 2001; Jung et al. 2014). During degradation, cross-linked proteins can interact with other cellular debris such as lipids, sugars, and metals to undergo a Fenton reaction, creating a non-degradable aggregate called lipofuscin (Terman and Brunk 1998; Höhn et al. 2013). Lipofuscin is formed primarily by proteins (approximately 30-70%) and lipids (20-50%), but also contains trace amount of metals (primarily iron) and carbohydrates (Brunk and Terman 2002a). Due to the heterogeneity of lipofuscin accumulations, there is no standard antigenic target to use for detection. However, the oxidized protein carbonyls and amino groups of lipofuscin undergo reactions that create Schiff bases that autofluoresce (Yin 1996).

It is well documented that lipofuscin increases linearly with age, especially in cells that are long lived or don't turn over (see Brunk and Terman 2002; Höhn et al. 2013; Reeg and Grune 2015). In the brain, some neurons, most notably Betz cells, evidence large amounts of lipofuscin accumulation (Peters and Sethares 1993). while others in the same region do not (Tigges et al. 1990). However, cellular function of neurons does not seem affected by lipofuscin accumulation (Tigges et al. 1990) and neuronal loss does not occur with age (Peters et al. 1998; Merrill et al. 2000). Additionally, many, but not all glial cells in the gray matter also show age-related increases in lipofuscin (Peters et al. 1991).

MRI studies on the aging brain in humans and monkeys show little change in total gray matter volume with age but instead show a loss of white matter volume (Wisco et al. 2008, Guttmann et al. 1998). Light microscopy also supports age-related white matter pathology showing a decrease in the total length of myelinated fibers in the human brain (Tang et al.

1997; Marner et al. 2003) even as neuron numbers are preserved (Terry et al. 1987; Freeman et al. 2008). At the ultrastructural level, there is an age-related increase in myelin pathology along with a loss of myelinated fibers particularly in frontal white matter regions (Bowley et al., 2010, Li et al., 2017). These myelin defects have been observed in the visual cortex (Peters, Moss, & Sethares, 2000), the optic nerve (Sandell and Peters, 2002), fornix (Peters et al., 2010) and the anterior commissure (Sandell & Peters, 2003). In addition, both white matter volume and myelin damage correlate with age-related cognitive decline (Albert 1993; Bowley et al., 2010).

Although there is strong evidence for age-related white matter dysfunction, few studies have investigated lipofuscin accumulation in the white matter. Safaiyan et al (2016) found that the number and volume of lipofuscin clusters increases in white matter microglia with age. Additionally, the size of lipofuscin clusters in microglia was found to be larger than that of those in the gray matter. Finally, myelin debris removal by microglia increased the amount of lipofuscin within the cells.

In this study, we quantified lipofuscin accumulation within the frontal white matter and cingulum bundle of behaviorally tested aging rhesus monkeys to determine if there was an age-related increase in lipofuscin density and size that are also associated with cognitive impairment. Additionally, we investigated the localization of lipofuscin in white matter microglia, astrocytes and oligodendrocytes. Our results demonstrate a relationship between white matter lipofuscin size and cognitive impairment. Through our analysis of glial cells and lipofuscin, we present the framework for understanding how lipofuscin accumulation

in the white matter could be disrupting glial processes of autophagy and myelination, leading to myelin damage and impaired cognition.

Methods

Subjects

Brain tissue from 30 rhesus monkeys was used in this study. This tissue had been collected and stored as part of an NIA funded Program Project ("Neural Substrates of Cognitive Decline in Aging Monkeys", P01-AG000001) and a Research Project ("Histopathology, Neuroimaging and Mechanisms of Myelin Damage in Aging Monkey Brain", R01-AG043640). Of the monkeys used in this study, 28 were obtained from the Yerkes National Primate Research Center at Emory University in Atlanta and 2 animals came from other research centers. Prior to selection, health records were screened with strict health criteria to exclude any possible confounding clinical diseases or experimental manipulations that could impact normal aging by affecting the brain or behavior.

Previous studies of rhesus monkey survival and of cognitive decline suggest that the rhesus monkey ages at an approximate ratio of 1 year for every 3 human years (Tigges et al., 1988). Using this, animals were subdivided into age groups of young adult (ages 8.1 - 13.7), middle-aged (ages 16.0 -19.9) and old (ages 20+). Although stratifying animals by age range allows for easy classification of each animal, in statistical analyses, age was also used as a continuous variable in linear regression to identify changes that occur across the lifespan.

Behavioral testing

All monkeys received a series of behavioral tests that assess cognitive functions. The major tasks used in this study were a test of rule learning using acquisition of the Delayed Non-Match to Sample (DNMS) task, extended delays on DNMS (120 sec and 600 sec) to test recognition memory, the Delayed Recognition Span Test in both spatial and object modes to assess working memory capacity, and the Category Set Shifting Task (CSST) to test executive function (Herndon et al. 1997; Moore et al. 2005). Based on a principal components analysis (Herndon et al., 1997), a subset of the DNMS and DRST scores were identified as the best predictors of cognitive aging and were compiled into a z-score designated the cognitive impairment index (CII). This has proven useful in comparing cognitive status with neurobiological endpoints (e.g. Peters, Sethares, & Moss, 1998). Middle-aged and old animals (ages 16+) were divided into groups of cognitively spared (CII < 2) and cognitively impaired (CII > 2) to investigate factors that exacerbate age-related cognitive decline.

Brain perfusion and tissue section preparation and storage

After behavioral testing was completed, monkeys were deeply anesthetized with sodium pentobarbital and transcardially perfused through the aorta with ice cold Krebs Henseleit buffer (pH 7.4, 4°C) for five minutes during which fresh biopsy samples for in vitro neurophysiology or biochemical analyses were harvested. Subsequently the perfusate was switched to 4 liters of 4% buffered paraformaldehyde (pH 7.4, 37°C) which was perfused over 10 minutes. Immediately after perfusion, the brain was blocked in the coronal stereotactic plane, removed from the skull and placed in the 4% paraformaldehyde fixative overnight at 4°C. The brain was then transferred through successive incubations in 0.1M

phosphate buffer containing first 10% glycerol with 2% DMSO and then buffer with 20% glycerol and 2% DMSO until the brain equilibrated for cryoprotection (Rosene et al. 1986). Finally, the brain was flash frozen in -75°C isopentane after which it was stored at -80°C until it was cut on a freezing microtome into 10 interrupted series of 30 µm thick sections. Brain tissue sections were collected in buffer with 15% glycerol as a cryoprotectant, equilibrated overnight at 4°C and then frozen and stored at -80°C until removed and thawed for immunohistochemistry.

Immunohistochemistry

Six experiments using single immuno-fluorescence labeling methods were employed to label microglia (Iba1), astrocytes (glial fibrillary acidic protein (GFAP), oligodendrocytes (Olig-2), oligodendrocyte precursor cells (platelet derived growth factor α (PDGFRA), mature oligodendrocytes (CC1 clone of the APC protein) and lysosomes (LAMP-1). For each animal, one tissue section containing frontal white matter and cingulum bundle was used for each label and processed individually. Immunofluorescence was performed as described previously (Shobin et al, 2017), with slight changes necessary for optimal staining of each label. Briefly, tissue sections were washed in 0.05M tris buffered saline (TBS). For PDGFRA staining, sections underwent heated antigen retrieval in Citrate Buffer (pH 6.0) using a PELCO Biowave Pro microwave (Ted Pella, Inc., Redding, CA) for 5 minutes at 550W with a maximum temperature of 40°C followed by a one hour incubation at room temperature. All sections were then washed in buffer and blocked with SuperBlock (ThermoFisher Scientific, Waltham, MA) for one hour before overnight incubation in primary antibody at room temperature in carrier solution of 0.5%

SuperBlock and 0.5% Triton X in 0.05M TBS (goat anti-Iba1, 1:1000, Abcam, Cambridge, MA; mouse anti-GFAP, 1:500, Dakocytomation, Glostrup, Denmark; rabbit anti-Olig2, 1:750, Abcam, Cambridge, MA; mouse anti-CC1 (APC), 1:500, Millipore-Sigma, Burlington, MA; rabbit anti-PDGFRα 1:500, Cell Signaling Technologies, Danvers, MA; rabbit anti-LAMP-1, 1:1000, Abcam, Cambridge, MA). For PDGFRA staining, sections were incubated in a 0.05M TBS solution with a pH of 9.0 and left incubating in primary antibody for an additional night at 4°C. Next, tissue sections were washed in buffer and incubated for two hours in secondary antibody solution containing 0.5% SuperBlock, 0.5% Triton X, and an AlexaFluor 488 (or AlexaFluor 647 for LAMP-1) tagged for the appropriate animal at 1:1000 dilution (donkey anti-goat, donkey anti-rabbit, or donkey anti-mouse, Invitrogen, Carlsbad, CA). Sections were then washed in buffer, slide-mounted and coverslipped using anti-fade polyvinyl mounting media containing DABCO (Millipore-Sigma, Burlington, MA). Slides were stored in 4°C before confocal analysis.

Autofluorescence quantification

A Leica TCS SPE laser scanning confocal microscope (Buffalo Grove, IL) was used to visualize fluorescence and acquire images for analysis. Four sections from each animal were used for autofluorescence quantification. Tissue was either immunostained with Iba1, Olig2, or GFAP or the tissue was slide mounted and coverslipped without any processing. Confocal z-stacks of 10 optical slices were taken using a 20X/0.75 objective lens of each animal in the frontal white matter. Unprocessed tissue was excited using the 488nm laser and emission was collected with a 500-700nm bandpass filter. Autofluorescence from sections labeled with Iba1, Olig2, and GFAP was excited with the 561nm laser and

emission was collected with a 570-620nm bandpass filter. To determine the number of optical slices, the z for each image was set by the points where no fluorescence could be seen on either side of the section. Image pixel size was set at 1.76 pixels/ μm and the z step size (and number of z-slices) were determined using the automated system optimized settings based on the diffraction limit of the objective. FIJI software (version 1.51i, National Institutes of Health) was used to open Z-stack images contained in .LIF files and conduct analyses of each stack. Images were split into individual channels and thresholded using the triangle method in the Threshold tool. The percent area of white matter occupied by thresholded fluorescent label was assessed on standard deviation intensity z-projection images of each confocal z-stack using the Analyze Particle tool in FIJI. The size of fluorescent objects was quantified by the Analyze Particle tool (on the z-projection image) and the 3-D Object Counter tool (on the confocal z-stack) in FIJI.

Co-localization of lipofuscin and glial markers.

Sections stained with Iba1, GFAP, Olig2, CC1, and PDGFRA were visualized using a Leica TCS SPE laser scanning confocal microscope (Buffalo Grove, IL). Dual channel confocal imaging was achieved using a multitrack set-up, with sequential excitation, followed by sequential emission of two channels. First, immunofluorescence was excited using the 488nm laser and emission was collected between 500-555nm. Subsequently, lipofuscin autofluorescence was detected using excitation from a 561nm laser and emission collected between 570- 625nm. Confocal z-stack tiff images of 10 optical slices were each taken in the frontal white matter of each tissue section. Channels were separated into two

separate images for co-localization analysis using Coloc2. Correlation between glial immunolabeling and lipofuscin was assessed for degree of overlap using Pearson's R.

Co-localization of lipofuscin and lysosomes

To measure co-localization of lysosomes with lipofuscin, nine animals (3 young, 3 old spared, and 3 old impaired) were stained with LAMP-1 antibody and imaged using a confocal microscope at an optical slice of 0.68μm as described above. FIJI software was used to separate z-stack images into individual slices and then separated by channel into an image containing lipofuscin and an image containing LAMP-1. The lipofuscin image was then thresholded into a binary image used to generate regions of interest (ROIs). These ROIs were then overlaid onto the corresponding LAMP-1 image and the percent area occupied by LAMP-1 was measured.

Microglial morphology

Microglia morphology was adapted from the cluster analysis of Karperien et al (2013) and updated from Shobin et al (2017). Z-stack images of microglia labeled with Iba1 were used from the previous co-localization analysis. Briefly, microglia were identified as either ramified or hypertrophic. Ramified microglia had small, semi-rounded soma with many thin processes extended. Hypertrophic microglia were all other microglia that came in many distinct shapes and sizes including enlarged or elongated cell bodies, dense or thickened processes, or few processes to no processes with an amoeboid shape. Cells were characterized by morphological subtype and whether they contained a lipofuscin cluster. The percentage of ramified cells containing lipofuscin and the percentage of hypertrophic cells containing lipofuscin were quantified and compared across age.

Microglia soma volume quantification

Using the same microglia images, soma volumes were quantified using Neurolucida 360 software (MBF Biosciences). Soma were reconstructed and characterized as single labeled or colocalized with lipofuscin. Cluster analysis was used to determine bins of "small" and "large" microglia based on soma size. Interactions were determined using ANOVA and Chi-square tests for independence.

Autofluorescence spectra analysis

To assess autofluorescence, one section per animal was mounted onto gelatin coated slides, air dried for one hour, and coverslipped using polyvinyl alcohol mounting media containing DABCO (Millipore-Sigma, Burlington, MA). A Carl Zeiss LSM 710 NLO microscope with spectral image lambda stack functionality was used to determine the emission spectral profile of autofluorescence. Tissue was excited with three lasers and emission detected at distinct intervals as follows: an argon laser that excites at 488nm with emissions collected between 490 - 720nm, a 561nm laser with emissions detection between 570 TO 720nm, and a 633nm laser with emission detection between 640 TO 720nm. For each animal, a spectral lambda stack was created at a randomly chosen point in the frontal white matter. Ten autofluorescent objects (presumably lipofuscin) were selected and emission profiles of those ten objects were collected with each laser. After background subtraction, the emission profiles of the ten objects were averaged together to get the average emission profile for each animal at each of the three excitations used.

Statistics

Linear regression was used to compare variables to age whereas one way ANOVA and t-tests were used to determine differences in variables between age and cognitive groups, respectively. For all analyses, alpha was set to 0.05.

Results

Autofluorescence in the white matter increases with age

Images of lipofuscin associated autofluorescence can be seen in Figure 4.14A and B. To evaluate autofluorescence throughout age, particle analysis on standard deviation intensity z-projection images of confocal z-stacks was used to determine the changes in the percent area of autofluorescence. For size analysis of autofluorescent puncta, we used both particle analysis on 2D z-projection images and 3-D object analysis on confocal z-stacks. As expected, there was an age-related increase in the percent area of autofluorescence in the FWM ($F(1,29) = 22.62$, $P = 0.000054$, $R^2 = 0.427$, Figure 4.14C), but not in the CGB ($F(1,28) = 2.58$, $P = 0.119$, $R^2 = 0.051$, Figure 4.14D). We then used 3-D object analysis to determine volume and surface area for autofluorescent objects. There was a significant positive correlation between the average object volume and age in both the FWM ($F(1,29) = 19.74$, $P = 0.00012$, $R^2 = 0.385$, Figure 4.14E) and the CGB ($F(1,28) = 21.7$, $P = 0.00007$, $R^2 = 0.417$, Figure 4.14F).

We next groups animals by age into groups of young (6.2 - 13.7), middle-aged (16-19.8), and old (20.7 - 30.2) to determine differences in object volume distribution by age. For each animal, autofluorescent puncta were separated into three bins based on object volume: objects of under 10 voxels^3, 10 to 49 voxels^3, and over 50 voxels^3 for both the FWM and the CGB ROIs. Performing a MANOVA to assess overall differences in object

size per size bin across age groups and ROI, we found a significant effect of age groups ($F(12,42) = 2.025$, $P = 0.046$), but not statistically significant effects between ROIs with no interactions. To examine this further, we analyzed each bin separately using ANOVA to find differences between age-groups in only the CGB for mean volume of objects under 10 voxels^3 ($F(2,27) = 5.285$, $P = 0.0116$) and objects over 50 voxels^3 ($F(2,27) = 6.684$, $P = 0.004$). In both cases, Tukey post-hoc testing revealed that, compared to old animals, young animals had a greater percentage of objects under 10 voxels^3 ($P = 0.01$). However, old animals had a significantly greater proportion of objects over 50 voxels^3 compared to both young ($P = 0.006$) and middle-aged animals ($P = 0.035$).

The size of autofluorescent objects is increased with greater cognitive impairment

Middle-aged and old animals (ages 16+) were separated into groups of cognitively spared (CII < 2) and cognitively impaired (CII > 2) to compare density and sizes of autofluorescent objects using the same methods as described previously (see Figure 4.15A-B for example images). Interestingly, there was no significant difference based on cognitive impairment in percent area of autofluorescence in either the FWM ($T(21) = 1.43$, $P = 0.084$, Figure 4.15C) or the CGB ($T(20) = 0.43$, $P = 0.366$, Figure 4.15D). The average object volume, however, was significantly greater with cognitive impairment in both the FWM ($t(21) = 2.23$, $P = 0.0184$, Figure 4.15E), and the CGB ($t(20) = 1.72$, $P = 0.05$, Figure 4.15F).

Autofluorescence in the white matter primarily colocalizes with microglia and oligodendrocytes

To determine which glial cells colocalized with lipofuscin associated autofluorescence, we used the Coloc2 plug-in for FIJI to calculate a Co-localization Coefficient (CLC) based on a pixel-by-pixel Pearson's correlation of signal intensity between the two channels for each image stack. The greater the CLC, the higher the degree of signal co-localization between the two channels. For this analysis, one animal was excluded for all stains due to tissue quality after processing. A second animal was excluded from Iba1 analyses due to lack of noticeable staining. Example co-localizations for each marker can be seen in Figure 4.16A-C. We compared the average CLC for each glial marker using a within-subjects ANOVA. Significant differences between lipofuscin co-localization with glial cell types were detected ($F(2,83) = 3.879$, $P = 0.0245$). To further determine differences in co-localization of lipofuscin with distinct glial types, we used paired t-tests to compare CLC (see Figure 4.16D). Lipofuscin co-localization with Iba1 was significantly greater, with a greater average CC, than co-localization with GFAP ($t(28) = 14.79$, $P \leq 0.0001$) and Olig2 ($t(28) = 3.20$, $P = 0.0034$). Additionally, lipofuscin co-localization with Olig2 was significantly greater than co-localization with GFAP ($t(28) = 8.55$, $P \leq 0.0001$).

Next, we looked for age-related changes to lipofuscin co-localization with each glial stain. We found a significant age-related increase in lipofuscin co-localization with Iba1 ($F(1,28) = 8.089$, $P = 0.00839$, $R^2 = 0.202$, Figure 4.17A) and with Olig2 ($F(1,29) = 23.25$, $P = 0.00004$, $R^2 = 0.434$, Figure 4.17C). There was a statistical trend for an age-related increase in lipofuscin co-localization with GFAP ($F(1,29) = 4.11$, $P = 0.052$, $R^2 = 0.100$, Figure 4.17B).

Finally, we separated middle-aged and old animals (ages 16+) into groups of cognitively spared (CII < 2) and cognitively impaired (CII > 2) to determine differences in lipofuscin colabeling with each glial marker. We found no significant difference in colabeling between cognitive groups for any marker.

Hypertrophic microglia containing lipofuscin increase with cognitive impairment

To assess if microglia morphology was related to lipofuscin co-localization, we analyzed an average of 140 iba1 labeled microglia from 29 animals. Cells were classified as either ramified (Figure 4.18A) or hypertrophic (Figure 4.18B-C) based on morphological appearance. To aid in morphological quantification, images were digitally magnified 4X using FIJI with a pixel size of 1.76 pixels/μm (Figure 4.18D-E). Each cell was further identified as either containing no lipofuscin or containing lipofuscin. Previous work has established that microglia inflammation and hypertrophic phenotypes are associated with age (Shobin et al. 2017). We verified this finding by establishing an age-related increase in the percentage of microglia with a hypertrophic morphology ($F(1,27) = 11.46$, $P = 0.000547$, $R^2 = 0.339$, Figure 4.19A). We next hypothesized that a greater percentage of hypertrophic microglia would contain lipofuscin compared to ramified microglia. However, we found that there was no difference in the percentage of ramified cells that contained lipofuscin and the percentage of hypertrophic cells that contained lipofuscin ($t(28) = 0.5466$, $P = 0.589$).

Next, we hypothesized that the percentage of microglia containing lipofuscin would be greater in cognitively impaired animals. Old animals (ages 20+) were stratified into groups of cognitively spared (CII < 2) and cognitively impaired (CII > 2). The percentage

of total microglia that contained lipofuscin was increased in cognitively impaired animals ($t(20) = 2.20$, $P = 0.02$, Figure 4.19B). Next, we separated the colocalized microglia into ramified and hypertrophic to find that the percentage of lipofuscin-containing microglia in ramified microglia was increased in cognitively impaired animals ($t(20) = 3.56$, $P = 0.001$, Figure 4.19C), the percentage of hypertrophic microglia containing lipofuscin was not statistically different between cognitive groups ($t(20) = 1.27$, $P = 0.11$, Figure 4.19D).

To determine if these same results could be detected quantitatively, we used soma size volumes to determine differences in microglial co-localization with lipofuscin. First, we analyzed the volume of individual somas from 4 cognitively spared (CII < 2) and 4 cognitively impaired animals (CII > 2). Using a cluster analysis, soma sizes were categorized as "small" (soma volume $\leq$ 140μm) and "large" (soma volume > 140μm). Using these criteria, we performed a within-subjects ANOVA to determine differences in the percentage of colocalized microglia by size ("small" or "large"), co-localization with lipofuscin (colocalized or not colocalized), and cognitive impairment (Spared: CII < 2, Impaired: CII > 2). There were significant differences in the percentage of microglia based on size ($F(1,22) = 14.0$, $P = 0.001$), co-localization with lipofuscin ($F(1,22) = 10.8$, $P = 0.003$), and interactions between group and soma size ($F(1,22) = 5.93$, $P = 0.023$) and soma size and co-localization with lipofuscin ($F(1,22) = 5.29$, $P = 0.031$). To evaluate the significant interactions, we performed chi-square tests for independence for the percentages of microglia by cognitive impairment and soma size to find a significant relationship between these variables ($\chi^2 = 18.5$, $P \leq 0.01$). Microglia in spared animals were more likely to have small soma volumes than microglia from cognitively impaired animals.

However, we found no significant relationship between microglial morphology and lipofuscin (χ^2 = 9.80, P = 0.22) nor between lipofuscin colocalization with microglia and cognitive impairment (χ^2 = 6.5, P = 0.477).

Lipofuscin colocalizes equally with OPCs and mature oligodendrocytes

To evaluate whether lipofuscin colocalized with oligodendrocyte precursor cells (OPCs, see Figure 4.20A) or mature myelinating oligodendrocytes (see Figure 4.20B), we again used the Coloc2 plug-in for FIJI software to analyze markers for OPCs and mature oligodendrocytes (mOligos). We determined that there was no significant difference in lipofuscin co-localization with CC1 or PDGFRA as assessed by PCC (t(28) = 1.246, P = 0.2267). Both markers demonstrated an age-related increased in correlation with lipofuscin (PDGF: F(1,27) = 6.36, P = 0.018, R^2 = 0.161, Figure 4.20C; CC1: F(1,28) = 9.459, P = 0.005, R^2 = 0.226, Figure 4.20D).

For cognitive impairment, we divided middle-aged and old animals (ages 16+) into groups of cognitively spared (CII < 2) and cognitively impaired (CII > 2). We found no significant differences between groups in the amount of lipofuscin that colocalized with CC1 (t(22) = 0.10603, P = 0.45826) nor with PDGFRA (t(21) = 0.7556, P = 0.229).

Autofluorescent lipofuscin is predominately associated with lysosomes

We hypothesized that autofluorescence was lipofuscin and would therefore be colocalized with lysosomes. We colabeled LAMP-1 (Figure 4.21A) with lipofuscin (Figure 4.21B) to visualize co-localization (Figure 4.21C). Lipofuscin objects were segmented (Figure 4.21D) and applied to a corresponding LAMP-1 image (Figure 4.21E) to determine

the percent area of lipofuscin occupied with LAMP-1 (Figure 4.21F). Our analysis revealed that 96.7% (S.E. = 2.88%) of lipofuscin objects contained LAMP-1 staining.

The emission profile of autofluorescence is primarily stimulated by 488nm lasers and 561nm lasers, not far-red 633nm lasers

To characterize the nature of white matter autofluorescence, we determined the excitation/emission spectra of autofluorescence. We excited the tissue of each animal at 488nm, 561nm, and 633nm and measured the emission profiles (Figure 4.22). At 488nm, the autofluorescence had two emission peaks with maximums at 520nm (Fluorescence Intensity (FI) = 25) and 600nm (FI =23) and minimal emission from 620nm to 730nm (FI = 1.1-7.1). With a 561nm laser, autofluorescence had two emission peaks at 600nm (FI = 70) and 650nm (FI = 38) and declining emission from 660nm to 730nm (FI = 9.4). The 633nm laser showed very little autofluorescence emission with no clear peak, but a maximal emission was recorded at 660nm (FI = 4.5).

Discussion

Summary

In this paper, we evaluated lipofuscin accumulation in frontal lobe white matter throughout the lifespan of the rhesus monkey. We measured lipofuscin accumulation to find an age-related increase in the amount and size of white matter lipofuscin. Interestingly, the cluster size, but not total amount, of lipofuscin increased with cognitive impairment. We next looked at glial cells to find that lipofuscin is primarily found in microglia and oligodendrocytes, but not astrocytes. In microglia, lipofuscin accumulation is not associated with a specific cellular morphology, but lipofuscin does appear to increase in

microglia with cognitive impairment. Lipofuscin is found in both oligodendrocyte precursor cells (OPCs) and mature oligodendrocytes (mOligos), but there is slight preference of lipofuscin for OPCs. Additionally, we characterized the lipofuscin autofluorescence to find that lipofuscin autofluoresces with excitation from a 488nm laser and a 561nm laser with emission spectra that ranged from 490nm to 700nm. A 633nm laser did not excite noticeable autofluorescence. Finally, we verified that autofluorescent lipofuscin was associated with lysosomes.

Lipofuscin accumulation as evidence for lysosomal dysfunction and impaired autophagy

Lipofuscin is well-regarded as an accumulation that ubiquitously occurs with aging and correlates to longevity, giving it the moniker "the age pigment" (Brunk and Terman 2002a). Therefore it was not surprising that we found lipofuscin to increase in density and size with age in the frontal white matter and cingulum bundle. Lipofuscin in the brain has not been as well-studied as other regions of the body, especially the eye, and the white matter has been particularly overlooked. As lipofuscin accumulates in postmitotic cells, neuronal lipofuscin was investigated thoroughly. While lipofuscin was found in neurons, particularly large Betz cells (Tigges et al. 1990), there was no evidence for cellular dysfunction (Tigges et al. 1992) or neuronal loss (Vincent et al. 1989; Peters et al. 1991) suggesting that lipofuscin accumulation was merely a benign indicator of age. In contrast to this view, lipofuscin has been widely studied in the retina where it has been indicated in the progression of macular degeneration (Dorey et al. 1989; Bergmann et al. 2004) due to impaired lysosomal function (Holz et al. 1999), decreased autophagy (Saadat et al. 2014) and decreased phagocytosis (Ambati et al. 2013).

Similar dysfunction has been reported for fibroblasts burdened with lipofuscin (Terman et al. 1999a; Terman et al. 1999b; Stroikin et al. 2007), mesenchymal stem cells (Stolzing and Scutt 2006) and microglia (Safaiyan et al. 2016). Brunk and Terman (2002) suggested that cellular dysfunction arises in cells containing lipofuscin. Lipofuscin-burdened cells direct lysosomal function towards degrading lipofuscin, using an abundance of limited lysosomal resources that leave the cell unable to cope with additional degradative functions required for normal autophagy. This results in further damage to the cell by inhibiting mitochondrial renewal and increasing oxidative damage. In the brain, Safaiyan et al (2016) found that the lipofuscin burden in microglia specifically reduced myelin phagocytosis. Additionally, lipofuscin particles in microglia were commonly associated with myelin basic protein. Based on our current data and our previous work (Chapters 2 and 3; Shobin et al., 2017), we suggest that age-related myelin damage could be directly increasing lipofuscin accumulation in the brain. We suggest a feed-forward mechanism whereby myelin damage leads to increased lipofuscin, thereby impairing phagocytic properties of microglia and inhibiting myelin repair (Kotter et al. 2006). Thus, the increased presence of lipofuscin in the aged monkey white matter likely indicates a decrease cellular functionality.

Lipofuscin burden associated with age-related cognitive impairment

We found that while total lipofuscin density does not change in age-related cognitive impairment, there is an increase in the size of lipofuscin clusters in both the CGB and the FWM. This suggests that in cognitively spared animals, lipofuscin is distributed more evenly between cells, whereas cognitively impaired animals contain single cells that

are burdened with a greater lipofuscin load. Lipofuscin can decrease autophagy and eventually inhibit lysosomal function by demanding a large amount of degradative enzymes (Brunk and Terman, 2002a). In cognitive impairment, it is possible that certain cells vulnerable to lipofuscin accumulation would have a greater degree of functional loss compared with cells that contain little or no lipofuscin.

As more lipofuscin accumulates within a cell and normal autophagy is inhibited, organelles within the cell that would be normally turned over, such as mitochondria are left in place and can become dysfunctional (Bratic and Larsson 2013). Damaged mitochondria can produce more ROS and can contain larger amounts of iron. Byproducts of damaged mitochondria (ROS and iron; see Bratic and Larsson, 2013) can then induce lipofuscin formation by oxidizing and cross-linking proteins, thereby creating a feed-forward loop where cells become more sensitive ROS and accumulate lipofuscin and damaged mitochondria which create more ROS (Brunk and Terman 2002b). Cells in cognitively impaired animals that contain a greater load of lipofuscin would be therefore more susceptible to oxidative damage and eventual cellular dysfunction

Cellular vulnerability to lipofuscin accumulation: microglia and oligodendrocytes

Both microglia and oligodendrocytes are necessary components of remyelination after damage (Kotter et al. 2005; Lampron et al. 2015). As myelin is turned over regularly throughout life (Ando et al. 2003; Yeung et al. 2014), microglia and oligodendrocytes work in close concert to keep the system intact. With semi-regular myelin protein recycling, those proteins within microglia and oligodendrocytes could be easily oxidized and

aggregated as lipofuscin. As lipofuscin can impair normal lysosomal function, the impacts on these cells and the balance of normal myelin turnover could be severely disrupted.

Microglia become increasingly phagocytic with age likely in response to myelin damage (Shobin et al. 2017), but phagocytosing myelin debris increases lipofuscin in microglial cells (Safaiyan et al. 2016), potentially leading to a decrease in phagocytic functionality that could result in the reported increased ROS production and inflammation (Sierra et al. 2007; Norden and Godbout 2013; Vida et al. 2017). These dysfunctions could in turn lead to more myelin damage in a vicious cycle that continuously weakens the functionality of the microglia attempting to resolve the problem.

Like microglia, oligodendrocyte function is thought to decrease with age. Similar to our findings of lipofuscin in oligodendrocytes of the white matter, gray matter oligodendrocytes accumulate age-related dense inclusions resembling lipofuscin (Peters et al. 1991; Peters 1996; Peters and Sethares 2004). that may stress oligodendrocytes and lead to myelin damage seen in normal aging (Peters 2009). This stress may lead to RNA sequestration (Vanderweyde et al. 2013) that would disrupt stable myelin formation (Baron and Hoekstra 2010; Müller et al. 2013). Additionally, oxidation can cause DNA damage in oligodendrocytes that is thought to decrease both myelination remodeling capacity and oligodendrocyte precursor cell differentiation (see Tse and Herrup 2017). Indeed, oligodendrocytes from old animals are less effective at remyelinating than are oligodendrocytes from young animals (Shields et al. 1999). These differences in functionality are thought to arise from impaired precursor recruitment and differentiation

(Sim et al. 2002), suggesting that both mature oligodendrocytes and oligodendrocyte precursor cells are intrinsically affected by aging.

Therapeutic potential

If these suggested mechanisms are correct, reversing lipofuscin accumulation may be an important strategy in improving longevity and reducing cognitive decline. For example, calorie restriction, an effective treatment for improving lifespan in worms, fruit flies, mice, rats (Heilbronn and Ravussin 2003) and monkeys (Mattison et al. 2012) is thought to work by increasing autophagy (Ferreira-Marques et al. 2016) and preserving mitochondrial function (Nisoli et al. 2005; López-Lluch et al. 2006; Lanza et al. 2012). Interestingly, calorie restriction has been shown to reduce lipofuscin accumulation in mice (Moore et al. 1995; Opalach et al. 2010). These results suggest further evidence for the role of lipofuscin in autophagy, but further research into the mechanistic connection is necessary to identify beneficial therapeutic targets.

Conclusions

Myelin defects appear more commonly with age, but the mechanism is still unclear. Our results provide novel data on the glial-specific localization of lipofuscin aggregates in frontal white matter regions vulnerable to myelin damage. We propose a feed-forward mechanism where lipofuscin aggregates may impair autophageal/lysosomal function in microglia and oligodendrocytes. In microglia, this would impair the capacity of the phagocytes to remove and properly degrade myelin debris. In oligodendrocytes, protein oxidation could be impairing proper trafficking of myelin proteins required for proper remyelination. As these cells become less effective, the myelin turnover cycle is

overwhelmed and dysregulated, thus leading to accumulation of myelin damage. This myelin damage signals for increased inflammation, phagocytosis and myelin repair, which is unable to occur as more cells are burdened by lipofuscin. Future research on the mechanistic affects testing the effects of lipofuscin on microglial phagocytosis and myelin formation could provide new therapeutic routes to curb the cognitive effects of aging.

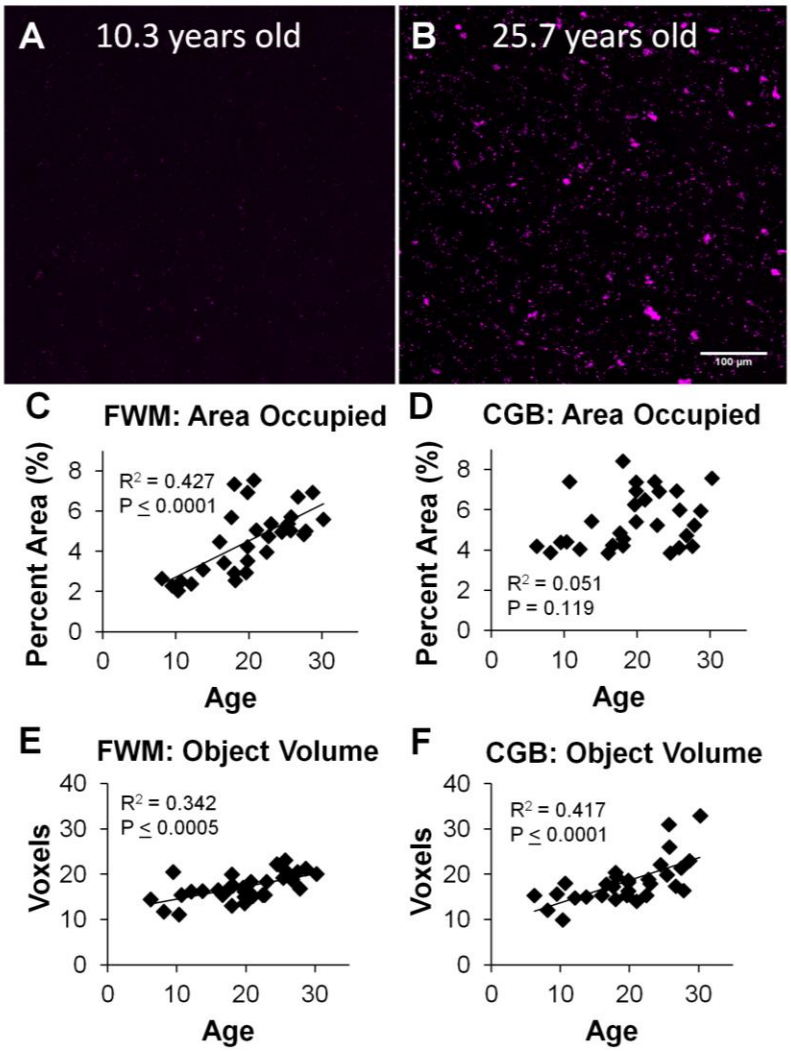

Figure 4.14. Lipofuscin increases with age in the white matter. Example autofluorescence was visualized using confocal microscopy in the frontal white matter (FWM) of A) a young monkey and B) an old monkey. Autofluorescent particles were quantified to determine the density of particle coverage (percent area) as a function of age. Scatter plots and linear regression analyses show that autofluorescence in the brain white matter accumulates with age in C) the FWM, but not the D) cingulum bundle (CGB). Additionally, 3D object analysis was used to evaluate the average volume of individual autofluorescent objects.

Scatter plots and linear regression analyses show that the average object volume increased as a function of age in both E) the FWM and F) the CGB.

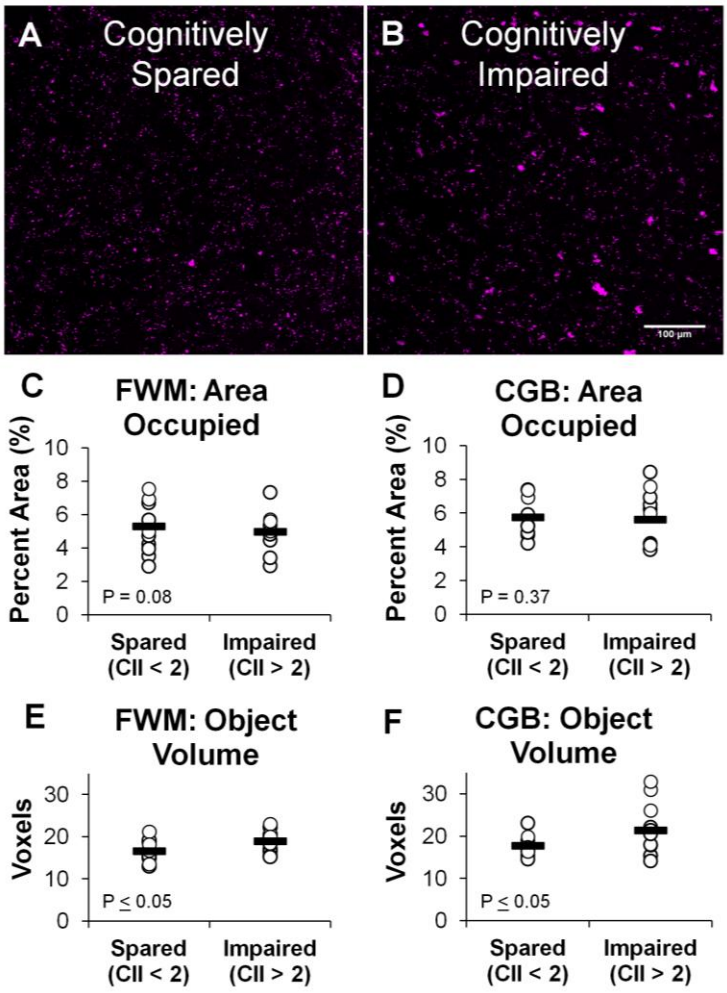

Figure 4.15. Lipofuscin objects increase in volume with cognitive impairment. All monkeys received a battery of behavioral tests used to give a single z-score value called the Cognitive Impairment Index (CII). Middle-aged and old monkeys (ages 16+) were grouped into cognitively spared (CII < 2) and cognitively impaired (CII > 2) subjects. Example images of autofluorescence in FWM of A) a cognitively spared and B) a cognitively impaired animal. C,D) Vertical scatter plot showing individual data from each animal (open circles) and mean data (black line) for autofluorescent particle density, as assessed by percent area and E,F) autofluorescent object size. Autofluorescence percent

area did not differ between cognitive impairment groups in either C) the FWM or D) the CGB. However, compared to cognitively spared animals, cognitively impaired monkeys had significantly larger autofluorescent objects in both E) the FWM and F) the CGB.

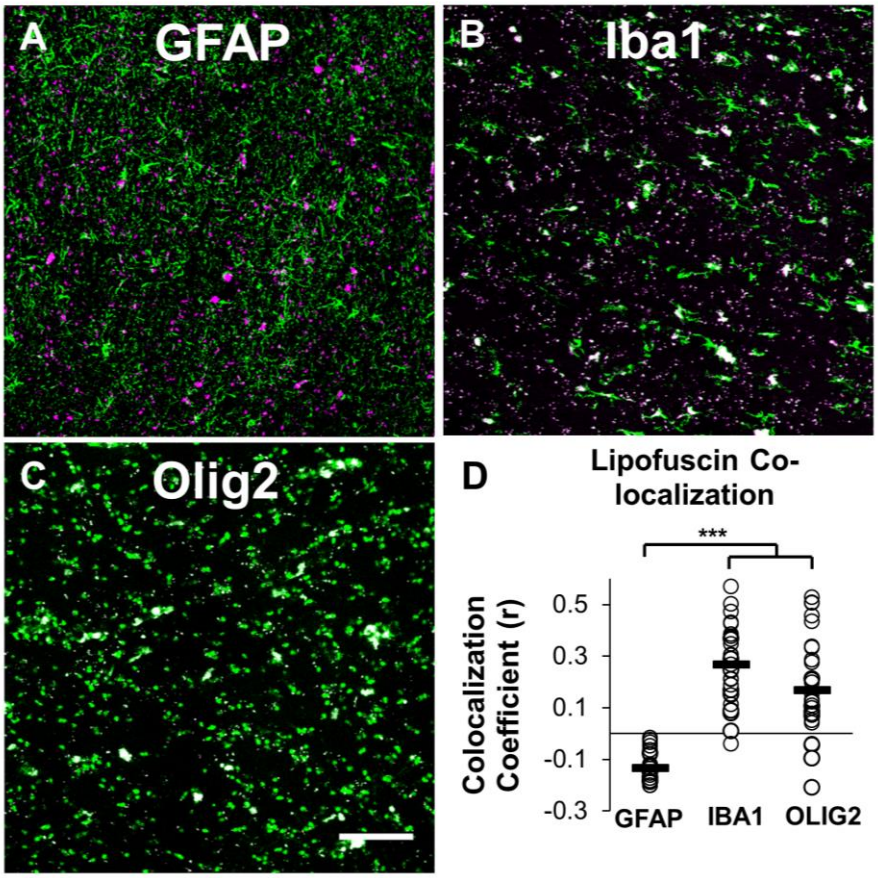

Figure 4.16. Lipofuscin colocalizes with microglia and oligodendrocytes. Autofluorescence was colocalized with three glial markers in brains from 30 monkeys to determine in which cells accumulation was occurring in the white matter. Three glial markers (all labeled in green) were used to colocalize with lipofuscin (colored magenta): A) astrocytes were stained with GFAP, B) microglia were labeled with Iba1 C) and oligodendrocytes were marked with Olig2. Co-localization in all images is seen as a white color. D) Quantification of co-localization of each marker with lipofuscin using a Co-localization Coefficient (CLC) index calculated from a pixel-by-pixel Pearson's Correlation Coefficient of signal intensity between the two channels using coloc2 plug-in from FIJI. Vertical scatter plot shows individual data from each animal (open circles) and

mean data (black line). The average CLC of lipofuscin and Iba1 was significantly greater than the average CLC of lipofuscin and GFAP as well as the average CLC of lipofuscin and Olig2. The CLC of lipofuscin and Olig2 was also significantly greater than the average CLC of lipofuscin and GFAP. Scale Bar = 100um; *** $P \leq 0.005$

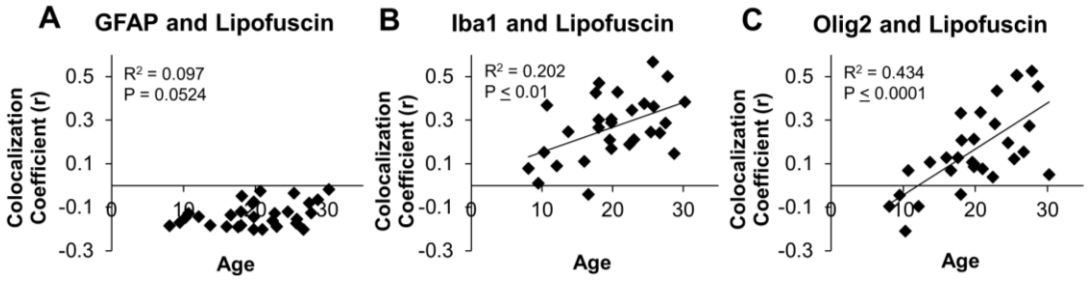

Figure 4.17. Age-related correlations of lipofuscin and glial markers. Scatter plots and linear regression analyses of lipofuscin-glial marker Co-localization Coefficients against age. A) Lipofuscin autofluorescence co-localization with astrocyte staining trended toward a statistically significant linear correlation with age. We found statistically significant age-related increases in lipofuscin co-localization with B) microglial staining and C) oligodendrocyte staining.

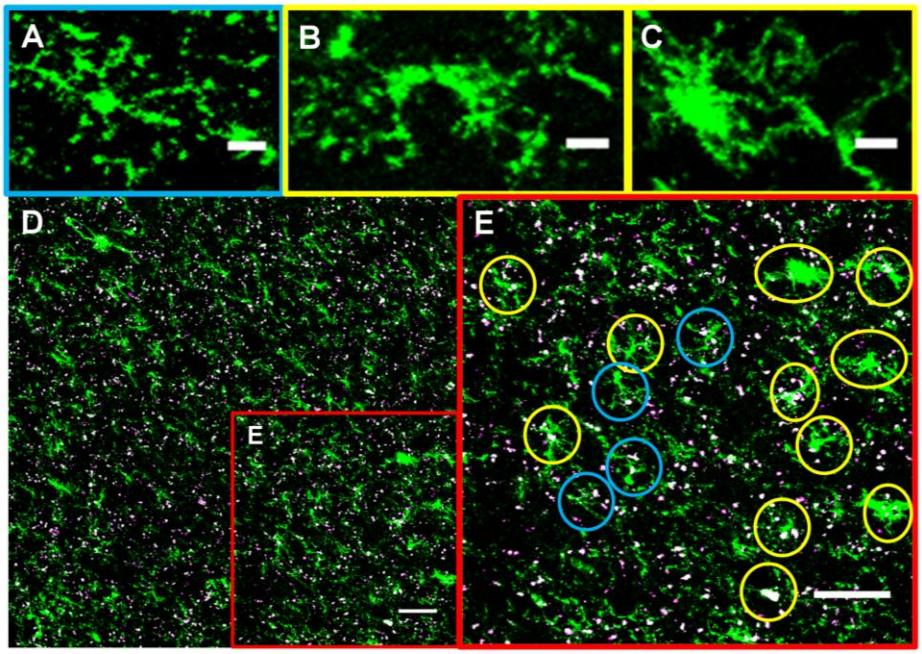

Figure 4.18. Quantification of lipofuscin and microglial morphology. Microglia were stained with Iba1 and imaged with confocal microscopy. Cells were manually counted to determine if microglia morphology related to lipofuscin accumulation. Microglia were characterized as either A) ramified or B,C) hypertrophic, which include both hypertrophic (B) and amoeboid (C) morphologies. D) For each image taken, 1/4th of the image in the bottom right corner was digitally magnified for microglia morphological quantification. E) Microglia were counted as containing lipofuscin or containing no lipofuscin and either ramified (blue circles) or hypertrophic (yellow circles). A-C: Scale bar = 10um; D, E: Scale bar = 50um

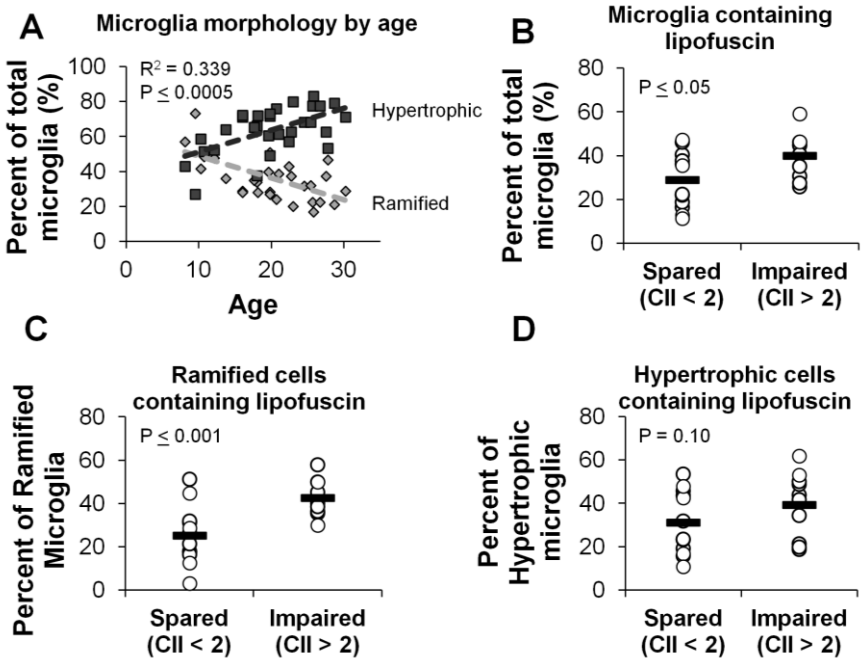

Figure 4.19. Hypertrophic microglia containing lipofuscin increase with CII. A) Scatter plot and linear regressions of percent of lipofuscin-containing microglia by morphological type against age. The percentage of microglia characterized as having a hypertrophic morphology increased with age. B-D) Vertical scatter plots showing individual data from each animal (open circles) and average data (black line): B) The mean percentage of total microglia that contained lipofuscin was greater in cognitively-impaired compared to cognitively-spared middle-aged and elderly animals. When determining differences in lipofuscin correlation by morphology, we found that C) the mean percentage of ramified microglia that contained lipofuscin was significantly greater in cognitively impaired animals, however, D) the mean percentage of hypertrophic microglia that contained lipofuscin did not significantly differ with cognitive impairment.

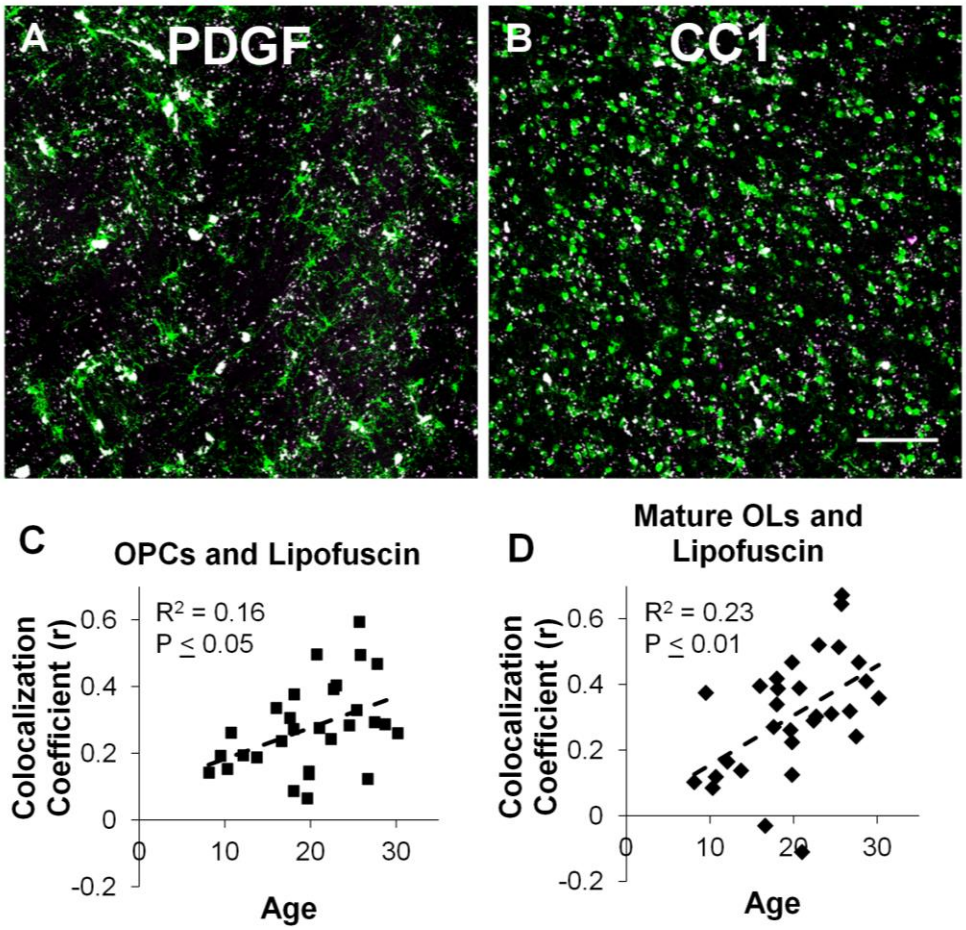

Figure 4.20. Lipofuscin co-localization with oligodendrocyte subtypes A,B) Representative confocal z-projection images showing that lipofuscin was colocalized with A) oligodendrocyte precursor cells (OPCs, PDGF) and B) mature oligodendrocytes (mOligos, CC1). There were no significant differences between the two markers in their extent of co-localization (co-localization coefficients: PGDF/lipofuscin = 0.278; CC1/lipofuscin = 0.305) with lipofuscin. C,D) Scatter plots and linear regressions of co-localization coefficients of each marker with lipofuscin against age. Age was significantly correlated with lipofuscin co-localization for both C) PDGF and D) CC1. Scale Bar = 100um

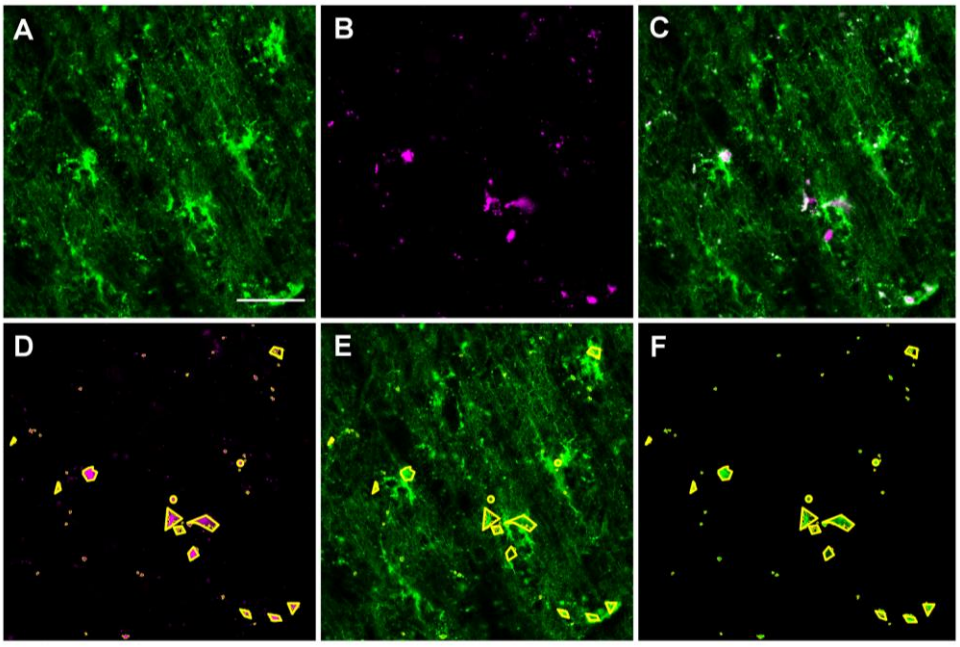

Figure 4.21. Lipofuscin co-localization with lysosomes. To verify that autofluorescent lipofuscin was found lysosomes, we labeled tissue sections from 9 animals with A) LAMP-1 and co-imaged this stain with B) lipofuscin to identify C) co-localization. Z-stacked images were separated by slice and channel. D) The lipofuscin channel was then thresholded to get regions of interest (outlined in yellow). E) These regions of interest were overlaid onto the corresponding LAMP-1 stained image. F) The area stained within the regions of interest could then be analyzed. We found that 96.7% of the lipofuscin regions were stained with LAMP-1, verifying that the autofluorescent lipofuscin was related to lysosomes.

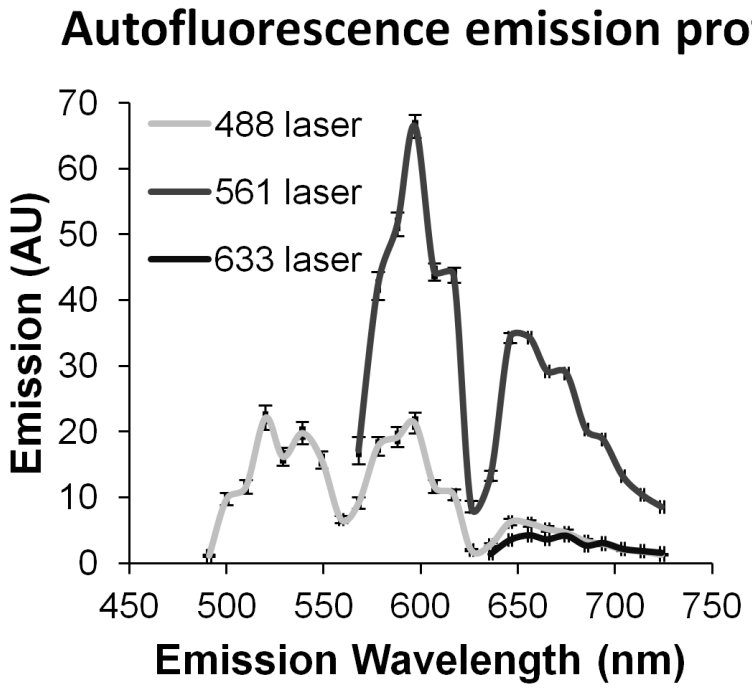

Figure 4.22. Autofluorescence spectra profiles in the white matter. The emission profiles of autofluorescence were recorded using a lambda scan after laser stimulation from one of three lasers (488nm, 561nm, and 633nm). The average fluorescence intensity was taken from 30 animals at each wavelength to determine the emission profile. Stimulation with an argon 488nm laser provides a double-peaked emission spectra with maximums at 520nm and 60nm. Emissions after stimulation with the 561nm laser showed the strongest peaks with maximums at 600nm and 650nm. The 633nm laser showed very little detectable autofluorescence with no clear peak. Standard error is presented at each point.

CHAPTER 5: CONCLUSIONS AND FUTURE DIRECTIONS

Summary of Results

In the previous chapters, we presented evidence for age-related impairment of myelin clearance and the potential processes underlying this dysfunction. First, we looked at a label-free method for myelin detection in the brain, Spectral Confocal Reflectance (SCoRe) imaging. Using SCoRe, we found that the percentage of reflectance did not differ with age, but, in old animals, reflectance was significantly decreased in cognitively impaired animals. Next, we found that myelin basic protein (MBP) in the cerebrospinal fluid (CSF) increased with age. Surprisingly, the concentration of MBP in the CSF was highest in old animals without cognitive impairment and old cognitively impaired animals had significantly less MBP in the CSF. In the old animals, the concentration of MBP in the CSF directly correlated with the amount of SCoRe signal in the brain. We then looked to gene expression to find that MBP expression in lateral prefrontal cortex increased with age. Next, we found that LN3 cells, a marker for microglial "activation", and galectin-3 (Gal-3) cells, a marker of phagocytic activation, increased with age in the frontal white matter regions. Gal-3 cells, but not LN3 cells, increased with cognitive impairment, specifically in the hypertrophic and amoeboid morphologies that are correlated with microglial "activation". To determine any potential cause for cellular functional impairment, we next looked at accumulation of lipofuscin in the frontal white matter. We found that lipofuscin increases in density and size with age, and the size of lipofuscin clusters correlates with cognitive impairment. We determined that lipofuscin was primarily found in microglia and oligodendrocytes. The percentage of microglia that contained lipofuscin increased with

cognitive impairment. Both oligodendrocyte precursor cells (OPCs) and mature myelinating oligodendrocytes contained lipofuscin, with slightly more OPCs containing lipofuscin. Finally, we verified that lipofuscin was found inside lysosomes, with 96% of lipofuscin autofluorescence colocalized with the lysosomal marker LAMP-1.

Looking beyond immunohistochemistry in the aging monkey

In the current work, immunohistochemistry (IHC) has been the predominant method utilized. IHC and histology provide unique information about localization, regionalization, cellular morphology and co-localization between proteins. Indeed, the current studies have made use of these characteristics to give an anatomical overview of the systems involved in age-related cognitive impairment and the myelin pathology in the rhesus monkey. While we have shown that white matter microglial phagocytic activity and lipofuscin accumulation are related to aging and cognitive decline, future work is needed to address the functional changes underlying these correlations.

In the following sections, will propose novel functional experiments to conduct using the rhesus monkey as a model for aging and cognitive impairment. Although both *in vitro* and rodent models are traditionally used for functional assays, each has significant drawbacks to consider in comparison to working with rhesus monkeys. In cell culture, microglia quickly lose their cellular signature (Gosselin et al. 2017) and are known to act in a context dependent manner, with vast gene expression differences throughout the brain (Grabert et al. 2016; Tay et al. 2017). Thus, removing microglia and other glial cells out of the environment of the aging brain is likely to significantly alter gene expression and

function, so every effort must be made to assess the functionality of these cells within the tissue.

In rodents, live imaging has led to a re-evaluation of microglial function outside of immunity, stemming from the seminal paper from Nimmerjahn and colleagues (2005). More recently, tagging the microglial-specific Cx3cr1 gene with green fluorescent protein (GFP) has been widely used as a method of *in vivo* microglial identification and functionality (Butovsky et al. 2014; Bennett et al. 2016). These techniques make the rodent a good model to address cortical function of microglia in health and disease. However, in terms of age-related white matter pathology, the rodent brain lacks a comparible amount of white matter (10%) to the human (37%) (Zhang and Sejnowski 2000). Additionally, mice and human microglial profiles diverge with age, with human microglia having altered gene expression related to neurodegenerative disease, such as those involved in cell adhesion, axonal guidance, and the microglial sensome that are distinct from the gene expression changes seen in the aging mouse (Galatro et al. 2017; Gosselin et al. 2017). Thus, using a monkey (36% white matter, Zhang and Sejnowski 2000) could prove to be a better model in understanding the subtle myelination changes that occur with aging and cognitive decline.

Evaluating complex cellular interactions with RNA-sequencing

Traditionally, macrophage activation has been divided into states of pro-inflammatory (M1) and anti-inflammatory (M2) with a general consensus that M1 activation is increased in the brain with age (Norden and Godbout 2013). However, this dichotomy is too simplistic to represent the dynamic responses of microglia (Ransohoff 2016). While

immunohistochemistry limits our analyses to single proteins, gene expression profiling has begun to uncover the complexity of microglial and macrophage responses to age and disease (Wes et al. 2016). Using RNA sequencing (RNAseq), Hickman et al (2013) found an age-related shift towards transcripts involved in neuroprotection, however others have reported an increase in phagocytic, lysosomal and antigen-presentation transcripts (Holtman et al. 2015). Thus far, most RNAseq studies are limited to mouse brains which consist of 90% gray matter (Zhang and Sejnowski 2000) or human cortical tissue, limiting our knowledge of neuroimmune cells in white matter pathology.

Although the brain was once believed to be an isolated and privileged immune site, recent research has found that communication and recruitment of peripheral innate and adaptive immune cells is highly important in response to damage. Most notably, bone marrow derived macrophages (BMDM) are recruited to the adult brain (Vallieres and Sawchenko 2003; Cogle et al. 2004) and can enhance remyelination (Ruckh et al. 2012). BMDMs have distinct gene expression profiles from microglia (Hickman et al. 2013; Butovsky et al. 2014) and may be more effective phagocytes, but less capable of degrading debris such as myelin (Greenhalgh and David 2014) and potentially more inflammatory than microglia (Simard et al. 2006). Additionally, T-lymphocytes are recruited to the brain in aging and AD (Stichel and Luebbert 2007; Gemechu and Bentivoglio 2012) and may impact disease progression (Dansokho et al. 2016). Yet the role of these cells in influencing myelin pathology and cognitive impairment is unknown.

As macrophages are necessary for OPC maturation (Miron et al. 2013), but macrophages show gene expression and functional changes with age, it is no surprise that

OLs also exhibit age-related changes. Human brains show an age-related decrease in OLs (Pelvig et al. 2008; Fabricius et al. 2013) and impairment of OPC recruitment and differentiation (Sim et al. 2002). Additionally, DNA damage accrues with age in mature OLs, which could further impact myelin gene expression (Tse and Herrup 2017). Together, these data suggest that changes in OL gene expression profiles are likely to be involved in age-related myelin pathology.

We propose to use cognitive tested rhesus monkeys to evaluate gene mRNA expression profiles of microglia, peripheral macrophages, CD3+ lymphocytes, OPC and OLs. Unlike previous studies of aging and neuroimmune cells, this proposed study would utilize RNAseq to evaluate differences in gene expression in the white matter. Using archived frozen tissue from the frontal white matter of behaviorally tested rhesus monkeys from across the age range, gene expression could be correlated with age-related cognitive decline and myelin pathology. A study of this nature would be able to provide an in depth look at the complex gene expression changes in the monkey white matter to compare with what is known from humans and mice. These data could provide a bridge to understand the myelin pathology of aging seen in humans, while highlighting the protections monkeys have from age-related neurodegenerative diseases.

Novel assays to assess connections of aging, lipofuscin and phagocytic capacity using the rhesus monkey

Myelin damage is the major pathology of aging and cognitive impairment (Peters and Rosene 2003). As myelin debris can inhibit remyelination (Kotter et al. 2006), removal of damaged myelin is imperative for restoration. Macrophages are necessary for myelin

phagocytosis (Neumann et al. 2009; Napoli and Neumann 2009; Safaiyan et al. 2016) and remyelination (Lampron et al. 2015). The results presented in this dissertation show that phagocytic priming of microglia in the frontal white matter increases with both age and cognitive impairment (Shobin et al. 2017). However, the phagocytic efficiency of microglia is decreased with age (Natrajan et al. 2015) possibly due to overburdened and inefficient degradative capacity (Safaiyan et al, 2016). Additionally, aged myelin may be less susceptible to phagocytosis (Hendrickx et al. 2014).

To address functionality of the phagocytic response to myelin damage in aging, we propose a novel *ex vivo* phagocytosis assay adapted from Hendrickx et al. 2014. Myelin can be isolated and purified from archived brain tissue of young, old cognitively spared, and old cognitively impaired monkeys and labeled with Alexa Fluor 633. Slices of freshly harvested monkey frontal white matter can then be incubated for separately with myelin from each category of subject. After incubation, slices can be fixed and visualized with immunofluorescence to quantify phagocytosis of myelin within microglia (stained with Iba1 and Gal-3) in relationship to age and cognitive impairment. Additionally, cells could be evaluated for lipofuscin content. Alternatively, tissue could be processed for FACS prior to fixation. Here, cells could be labeled with and gated for microglia (Iba1 or Gal-3), myelin (Alexa Fluor 633), lipofuscin (autofluorescence). The major advantage of using FACS is that cells could be sorted and gene expression differences evaluated using either RNA sequencing or screened using qPCR. Both of these methods would allow for direct quantification of myelin phagocytosis and test the hypotheses that 1) phagocytic functionality is impaired in normal aging, 2) myelin debris is less efficiently cleared in

white matter of aged compared to young monkeys and 3) lipofuscin impairs phagocytic capacity of microglia. These resutls would elucidate the mechanistic connection between microglial phagocytosis and lipofuscin accumulation in age-related myelin pathology.

Functional capacity of OPCs to differentiate and repair myelin in aging

Although the neuroimmune system is imperitive in influencing oligodendrocyte precursor cell (OPC) maturation and differentiation (Miron et al. 2013), it is possible that oligodendrocytes themselves are dysfunctional. Remyelination appears to be slower with in aged rodent models of demyelination (Shields et al. 1999; Ruckh et al. 2012). As expected with increased inflammation, OPC recruitment and differentiation are impaired with age (Sim et al. 2002). Additionally, there may be a decrease in total number of OLs with age in humans (Fabricius et al. 2013; Soreq et al. 2017) as well as decreased expression of OL-specific transcripts (Soreq et al, 2017). Finally, our results demonstrated that both OPCs and mature oligodendrocytes accumulate lipofuscin with age, yet the functional role of lipofuscin in oligodendrocyte function is unknown.

We propose to test whether OPC differentiation is intrinsically impaired with age or extrinsically inhibited by macrophages from elderly monkeys and correlated with cognitive impairment. This can be tested by isolating OPCs from frontal white matter of monkeys from across the lifespan and 1) assaying their ability to differentiate *in vitro* alone, 2) and while co-cultured with microglia isolated from young and old monkey brains, and 3) following transplantation into cultured brain tissue from myelin-lacking shiverer mice. The first experiment will test the hypothesis that OPC differentiation is impaired with age whereas the second experiment tests the hypothesis that age-related microglia alterations

inhibit OPC differentiation. Differentiation can be quantified by measuring relative numbers of OPCs to mature oligodendrocytes after providing differentiation factors. Further, we can assess lipofuscin accumulation within the cells and deteremine whether OPCs containing lipofuscin had altered differentiation. In the third experiment, we can test the hypothesis that the remyelination capacity of oligodendrocytes is imapired with age using a model adapted from Bin et al. 2012. The shiverer mouse is hypomyelinated due to a lack of myelin basic protein gene (Kimura et al. 1989) but can be remyelinated by transplantation of oligodendrocytes that contain the myelin basic protein gene (Bin et al. 2012). Using this model, we can measure the extent of myelination from oligodendrocytes isolated from young and old animals. Together, these results would indicate the effect of age, microglia and lipofuscin on oligodendrocyte function and potentially elucidate novel therapeutic targets to combat aging and age-related cognitive decline.

Conclusions

In the preceding sections, we have demonstrated that damaged myelin clearance may be impaired in aging and cognitive decline, possibly due to the accumulation of lipofuscin. With our results, we have developed the following working model for age-related myelin pathology: normal myelin turnover throughout life aids in the aggregation of lipofuscin clusters and leads to the cellular impairment of microglia and oligodendrocytes. As microglia become dysfunctional with age, they are unable to remove and clear myelin debris from normal myelin turnover as quickly as was once possible. Myelin debris inhibits remyelination (Kotter et al. 2006) and oligodendrocytes and OPCs are halted in their normal function. Oligodendrocytes ready to remyelinate, are instead forced to sequester

their myelin proteins, potentially leading to the formation of oligodendrocyte lipofuscin and further cellular dysfunction. In healthy aging, massive amounts of myelin debris are effectively removed as seen by the presence of MBP in the CSF, whereas cognitively impaired agers are left with lingering myelin debris, causing further damage and improper restoration of functional myelin sheaths. The future studies proposed in this chapter are designed to test this model and to discover novel therapuetic targets to treat the conditions of both normal aging and age-related cognitive decline.

BIBLIOGRAPHY

Abe O, Yamasue H, Aoki S, et al (2008) Aging in the CNS: Comparison of gray/white matter volume and diffusion tensor data. Neurobiology of Aging 29:102–116. doi: 10.1016/j.neurobiolaging.2006.09.003

Ainger K, Avossa D, Morgan F, et al (1993) Transport and localization of exogenous myelin basic protein mRNA microinjected into oligodendrocytes. Journal of Cell Biology 123:431–441. doi: 10.1083/jcb.123.2.431

Albert M (1993) Neuropsychological and neurophysiological changes in healthy adult humans across the age range. Neurobiology of Aging 14:623–625. doi: 10.1016/0197-4580(93)90049-H

Alexander GE, Chen K, Merkley TL, et al (2006) Regional network of magnetic resonance imaging gray matter volume in healthy aging. Neuroreport 17:951–956. doi: 10.1097/01.wnr.0000220135.16844.b6

Alliot F, Godin I, Pessac B (1999) Microglia derive from progenitors, originating from the yolk sac, and which proliferate in the brain. Developmental Brain Research 117:145–152. doi: 10.1016/S0165-3806(99)00113-3

Alzheimer's Association (2013) Alzheimer's disease facts and figures. Alzheimer's Dementia 9:110 –133. doi: 10.1016/j.jalz.2013.02.003

Ambati J, Atkinson JP, Gelfand BD (2013) Immunology of age-related macular degeneration. Nature Reviews Immunology 13:438–451.

Anderson B, Rutledge V (1996) Age and hemisphere effects on dendritic structure. Brain 119:1983–1990. doi: 10.1093/brain/119.6.1983

Ando S, Tanaka Y, Toyoda Y, Kon K (2003) Turnover of myelin lipids in aging brain. Neurochemical Research 28:5–13. doi: 10.1023/A:1021635826032

Ansari KA, Loch J (1975) Decreased myelin basic protein content of the aged human brain. Neurology 25:1045–50.

Bae YS, Kang SW, Seo MS, et al (1997) Epidermal growth factor (EGF)-induced generation of hydrogen peroxide. Role in EGF receptor-mediated tyrosine phosphorylation. The Journal of Biological Chemistry 272:217–221. doi: 10.1074/jbc.272.1.217

Baron W, Hoekstra D (2010) On the biogenesis of myelin membranes: Sorting, trafficking and cell polarity. FEBS Letters. 584:1760–1770.

Barrientos RM, Higgins EA, Biedenkapp JC, et al (2006) Peripheral infection and aging interact to impair hippocampal memory consolidation. Neurobiology of Aging 27:723–732. doi: 10.1016/j.neurobiolaging.2005.03.010

Bartzokis G (2004) Age-related myelin breakdown: A developmental model of cognitive decline and Alzheimer's disease. Neurobiology of Aging 25:5–18.

Bateman RJ, Xiong C, Benzinger TLS, et al (2012) Clinical and Biomarker Changes in Dominantly Inherited Alzheimer's Disease. New England Journal of Medicine 367:795–804. doi: 10.1056/NEJMoa1202753

Bennett ML, Bennett FC, Liddelow SA, et al (2016) New tools for studying microglia in the mouse and human CNS. Proceedings of the National Academy of Sciences 113:E1738–E1746. doi: 10.1073/pnas.1525528113

Bergmann M, Schütt F, Holz FG, Kopitz J (2004) Inhibition of the ATP-driven proton pump in RPE lysosomes by the major lipofuscin fluorophore A2-E may contribute to the pathogenesis of age-related macular degeneration. FASEB Journal 18:562–564. doi: 10.1096/fj.03-0289fje

Bin JM, Leong SY, Bull SJ, et al (2012) Oligodendrocyte precursor cell transplantation into organotypic cerebellar shiverer slices: A model to study myelination and myelin maintenance. PLoS One. doi: 10.1371/journal.pone.0041237

Bohatschek M, Kloss CUA, Kalla R, Raivich G (2001) In vitro model of microglial deramification: Ramified microglia transform into amoeboid phagocytes following addition of brain cell membranes to microglia-astrocyte cocultures. Journal of Neuroscience Researchs 64:508–522. doi: 10.1002/jnr.1103

Bowley MP, Cabral H, Rosene DL, Peters A (2010) Age changes in myelinated nerve fibers of the cingulate bundle and corpus callosum in the rhesus monkey. Journal of Comparative Neurology 518:3046–3064. doi: 10.1002/cne.22379

Bratic A, Larsson NG (2013) The role of mitochondria in aging. Journal of Clinical Investigation. 123:951–957.

Brayne C, Gill C, Paykel ES, et al (1995) Cognitive decline in an elderly population--a two wave study of change. Psychological Medicine 25:673–683. doi: 10.1017/S0033291700034930

Brück W, Brück Y, Friede RL (1992) TNF-alpha suppresses CR3-mediated myelin removal by macrophages. Journal of Neuroimmunology 38:9–17. doi: 10.1016/0165-5728(92)90085-Y

Brunk UT, Terman A (2002a) Lipofuscin: Mechanisms of age-related accumulation and

influence on cell function. Free Radical Biology & Medicine 33:611–619.

Brunk UT, Terman A (2002b) The mitochondrial-lysosomal axis theory of aging. European Journal of Biochemistry 269:1996–2002. doi: 10.1046/j.1432-1033.2002.02869.x

Butovsky O, Jedrychowski MP, Moore CS, et al (2014) Identification of a unique TGF-β-dependent molecular and functional signature in microglia. Nature Neuroscience 17:131–43. doi: 10.1038/nn.3599

Chang EH, Argyelan M, Aggarwal M, et al (2017) Diffusion tensor imaging measures of white matter compared to myelin basic protein immunofluorescence in tissue cleared intact brains. Data in Brief 10:438–443. doi: 10.1016/j.dib.2016.12.018

Charlton RA, Barrick TR, McIntyre DJ, et al (2006) White matter damage on diffusion tensor imaging correlates with age-related cognitive decline. Neurology 66:217–222. doi: 10.1212/01.wnl.0000194256.15247.83

Chaudhari K, Wong JM, Vann PH, Sumien N (2014) Exercise training and antioxidant supplementation independently improve cognitive function in adult male and female GFAP-APOE mice. Journal of Sport and Health Science 3:196–205. doi: 10.1016/j.jshs.2014.04.004

Cherry JD, Olschowka JA, O'Banion MK (2014) Neuroinflammation and M2 microglia: the good, the bad, and the inflamed. Journal of Neuroinflammation 11:98. doi: 10.1186/1742-2094-11-98

Chung H, Brazil MI, Soe TT, Maxfield FR (1999) Uptake, degradation, and release of fibrillar and soluble forms of Alzheimer's amyloid B-peptide by microglial cells. The Journal of Biological Chemistry 274:32301–32308. doi: 10.1074/jbc.274.45.32301

Chung W-S, Welsh CA, Barres BA, Stevens B (2015) Do glia drive synaptic and cognitive impairment in disease? Nature Neuroscience 18:1539–1545. doi: 10.1038/nn.4142

Cogle CR, Yachnis AT, Laywell ED, et al (2004) Bone marrow transdifferentiation in brain after transplantation: A retrospective study. Lancet 363:1432–1437. doi: 10.1016/S0140-6736(04)16102-3

Cohen SR, Herndon RM, McKhann GM (1976) Radioimmunoassay of myelin basic protein in spinal fluid. An index of active demyelination. New England Journal of Medicine 295:1455–1457. doi: 10.1056/NEJM197612232952604

Conde JR, Streit WJ (2006) Microglia in the Aging Brain. Journal of Neuropathology &

Experimental Neurology 65:199–203. doi: 10.1097/01.jnen.0000202887.22082.63

Cotman CW, Head E, Muggenburg BA, et al (2002) Brain aging in the canine: A diet enriched in antioxidants reduces cognitive dysfunction. Neurobiology of Aging 23:809–818. doi: 10.1016/S0197-4580(02)00073-8

Courchesne E, Chisum HJ, Townsend J, et al (2000) Normal brain development and aging: quantitative analysis at in vivo MR imaging in healthy volunteers. Radiology 216:672–82. doi: 10.1148/radiology.216.3.r00au37672

Cribbs DH, Berchtold NC, Perreau V, et al (2012) Extensive innate immune gene activation accompanies brain aging, increasing vulnerability to cognitive decline and neurodegeneration: a microarray study. Journal of Neuroinflammation 9:179. doi: 10.1186/1742-2094-9-179

Crichton GE, Bryan J, Murphy KJ (2013) Dietary Antioxidants, Cognitive Function and Dementia - A Systematic Review. Plant Foods for Human Nutrition 68:279–292. doi: 10.1007/s11130-013-0370-0

Cullum S, Huppert F a, McGee M, et al (2000) Decline across different domains of cognitive function in normal ageing: results of a longitudinal population-based study using CAMCOG. International Journal of Geriatric Pscyhiatry 15:853–862. doi: 10.1002/1099-1166(200009)15:9<853::AID-GPS211>3.0.CO;2-T [pii]

Dansokho C, Ait Ahmed D, Aid S, et al (2016) Regulatory T cells delay disease progression in Alzheimer-like pathology. Brain 139:1237–1251. doi: 10.1093/brain/awv408

Davies KJA (2001) Degradation of oxidized proteins by the 20S proteasome. Biochimie pp 301–310

De Groot JC, De Leeuw FE, Oudkerk M, et al (2000) Cerebral white matter lesions and cognitive function: The Rotterdam scan study. Annals of Neurology 47:145–151. doi: 10.1002/1531-8249(200002)47:2<145::AID-ANA3>3.0.CO;2-P

de Leeuw FE, de Groot JC, Achten E, et al (2001) Prevalence of cerebral white matter lesions in elderly people: a population based magnetic resonance imaging study. The Rotterdam Scan Study. Journal of Neurology, Neurosurgery, and Psychiatry 70:9–14. doi: 10.1136/jnnp.70.1.9

DiPatre PL, Gelman BB (1997) Microglial cell activation in aging and Alzheimer disease: partial linkage with neurofibrillary tangle burden in the hippocampus. Journal of Neuropathology & Experimental Neurology 56:143–149.

Dorey CK, Wu G, Ebenstein D, et al (1989) Cell loss in the aging retina. Relationship to

lipofuscin accumulation and macular degeneration. Investigative Opthalmology & Visual Science 30:1691–1699.

Duce JA, Hollander W, Jaffe R, Abraham CR (2006) Activation of early components of complement targets myelin and oligodendrocytes in the aged rhesus monkey brain. Neurobiology of Aging 27:633–644. doi: 10.1016/j.neurobiolaging.2005.03.027

Dumic J, Dabelic S, Flögel M (2006) Galectin-3: an open-ended story. Biochimica et Biophysica Acta 1760:616–35. doi: 10.1016/j.bbagen.2005.12.020

Edison P, Archer HA, Gerhard A, et al (2008) Microglia, amyloid, and cognition in Alzheimer's disease: An [11C](R)PK11195-PET and [11C]PIB-PET study. Neurobiology of Disease 32:412–419. doi: 10.1016/j.nbd.2008.08.001

Elliott MJ, Strasser A, Metcalf D (1991) Selective up-regulation of macrophage function in granulocyte-macrophage colony-stimulating factor transgenic mice. Journal of Immunology147:2957–63.

Esiri MM (2007) Ageing and the brain. Journal of Pathology 211:181–187.

Estrada LI, Robinson AA, Amaral AC, et al (2017) Evaluation of Long-Term Cryostorage of Brain Tissue Sections for Quantitative Histochemistry. Journal of Histochemistry & Cytochemistry 65:2215541668693. doi: 10.1369/0022155416686934

Fabricius K, Jacobsen JS, Pakkenberg B (2013) Effect of age on neocortical brain cells in 90+ year old human females-a cell counting study. Neurobiology of Aging 34:91–99. doi: 10.1016/j.neurobiolaging.2012.06.009

Feldman ML, Peters A (1998) Ballooning of myelin sheaths in normally aged macaques. Journal of Neurocytology 27:605–614. doi: 10.1023/A:1006926428699

Ferreira-Marques M, Aveleira CA, Carmo-Silva S, et al (2016) Caloric restriction stimulates autophagy in rat cortical neurons through neuropeptide Y and ghrelin receptors activation. Aging (Albany NY) 8:1470–1484. doi: 10.18632/aging.100996

Fjell AM, Amlien IK, Westlye LT, et al (2010) CSF biomarker pathology correlates with a medial temporo-parietal network affected by very mild to moderate Alzheimer's disease but not a fronto-striatal network affected by healthy aging. Neuroimage 49:1820–1830. doi: 10.1016/j.neuroimage.2009.09.029

Fjell AM, Walhovd KB (2010) Structural Brain Changes in Aging: Courses, Causes and Cognitive Consequences. Reviews in Neurosciences doi: 10.1515/REVNEURO.2010.21.3.187

Fjell AM, Westlye LT, Amlien I, et al (2009) High consistency of regional cortical thinning in aging across multiple samples. Cerebral Cortex 19:2001–2012. doi: 10.1093/cercor/bhn232

Freeman SH, Kandel R, Cruz L, et al (2008a) Preservation of neuronal number despite age-related cortical brain atrophy in elderly subjects without alzheimer disease. Journal of Neuropathology & Experimental Neurology 67:1205–1212. doi: 10.1097/NEN.0b013e31818fc72f

Freeman SH, Kandel R, Cruz L, et al (2008b) Preservation of neuronal number despite age-related cortical brain atrophy in elderly subjects without Alzheimer disease. Journal of Neuropathology & Experimental Neurology 67:1205–12. doi: 10.1097/NEN.0b013e31818fc72f

Galatro TF, Holtman IR, Lerario AM, et al (2017) Transcriptomic analysis of purified human cortical microglia reveals age-associated changes. Nature Neuroscience 20:1162–1171. doi: 10.1038/nn.4597

Gardner ID, Lim STK, Lawton JWM (1981) Monocyte function in ageing humans. Mechanisms of Ageing and Development 16:233–239. doi: 10.1016/0047-6374(81)90099-3

Gemechu JM, Bentivoglio M (2012) T Cell Recruitment in the Brain during Normal Aging. Frontiers in Cellular Neuroscience. doi: 10.3389/fncel.2012.00038

Giannaris EL, Rosene DL (2012) A stereological study of the numbers of neurons and glia in the primary visual cortex across the lifespan of male and female rhesus monkeys. Journal of Comparative Neurology 520:3492–3508.

Ginhoux F, Greter M, Leboeuf M, et al (2010) Fate Mapping Analysis Reveals That Adult Microglia Derive from Primitive Macrophages. Science (80) 330:841–845. doi: 10.1126/science.1194637

Gladyshev VN (2014) The Free Radical Theory of Aging Is Dead. Long Live the Damage Theory! Antioxidants & Redox Signaling 20:727–731. doi: 10.1089/ars.2013.5228

Godbout JP, Chen J, Abraham J, et al (2005) Exaggerated neuroinflammation and sickness behavior in aged mice following activation of the peripheral innate immune system. FASEB Journal 19:1329–1331. doi: 10.1096/fj.05-3776fje

Good CD, Johnsrude IS, Ashburner J, et al (2001) A voxel-based morphometric study of ageing in 465 normal adult human brains. Neuroimage 14:21–36. doi: 10.1006/nimg.2001.0786

Gordon S, Martinez FO (2010) Alternative activation of macrophages: Mechanism and functions. Immunity 32:593–604.

Gosselin D, Skola D, Coufal NG, et al (2017) An environment-dependent transcriptional network specifies human microglia identity. Science (80) 356:eaal3222. doi: 10.1126/science.aal3222

Grabert K, Michoel T, Karavolos MH, et al (2016) Microglial brain region-dependent diversity and selective regional sensitivities to aging. Nature Neuroscience 19:504–516. doi: 10.1038/nn.4222

Greenhalgh AD, David S (2014) Differences in the Phagocytic Response of Microglia and Peripheral Macrophages after Spinal Cord Injury and Its Effects on Cell Death. Journal of Neuroscience 34:6316–6322. doi: 10.1523/JNEUROSCI.4912-13.2014

Guerreiro R, Bras J, Brookmeyer R, et al (2015) The age factor in Alzheimer's disease. Genome Medicine 7:106. doi: 10.1186/s13073-015-0232-5

Gundersen HJG, Jensen EB V, Kiêu K, Nielsen J (1999) The efficiency of systematic sampling in stereology - Reconsidered. Journal of Microscopy 193:199–211. doi: 10.1046/j.1365-2818.1999.00457.x

Guttmann CR, Jolesz FA, Kikinis R, et al (1998) White matter changes with normal aging. Neurology 50:972–978. doi: 10.1212/WNL.50.4.972

Hart AD, Wyttenbach A, Hugh Perry V, Teeling JL (2012) Age related changes in microglial phenotype vary between CNS regions: Grey versus white matter differences. Brain, Behavior, and Immunity 26:754–765. doi: 10.1016/j.bbi.2011.11.006

Haug H, Kuhl S, Mecke E, et al (1984) The significance of morphometric procedures in the investigation of age changes in cytoarchitectonic structures of human brain. Journal fur Hirnforschung 25:353–374.

Head D (2004) Differential Vulnerability of Anterior White Matter in Nondemented Aging with Minimal Acceleration in Dementia of the Alzheimer Type: Evidence from Diffusion Tensor Imaging. Cerebral Cortex 14:410–423. doi: 10.1093/cercor/bhh003

Head D, Snyder AZ, Girton LE, et al (2005) Frontal-hippocampal double dissociation between normal aging and Alzheimer's disease. Cerebral Cortex 15:732–739. doi: 10.1093/cercor/bhh174

Heilbronn LK, Ravussin E (2003) Calorie restriction and aging: review of the literature and implications for studies in humans. The American Journal of Clinical Nutrition

78:361–9.

Hendrickx DA, Schuurman KG, van Draanen M, et al (2014) Enhanced uptake of multiple sclerosis-derived myelin by THP-1 macrophages and primary human microglia. Journal of Neuroinflammation 11:64. doi: 10.1186/1742-2094-11-64

Herndon JG, Moss MB, Rosene DL, Killiany RJ (1997) Patterns of cognitive decline in aged rhesus monkeys. Behavioural Brain Research 87:25–34. doi: 10.1016/S0166-4328(96)02256-5

Hickman SE, Allison EK, El Khoury J (2008) Microglial dysfunction and defective beta-amyloid clearance pathways in aging Alzheimer's disease mice. Journal of Neuroscience 28:8354–60. doi: 10.1523/JNEUROSCI.0616-08.2008

Hickman SE, El Khoury J (2014) TREM2 and the neuroimmunology of Alzheimer's disease. Biochemical Pharmacology 88:495–498. doi: 10.1016/j.bcp.2013.11.021

Hickman SE, Kingery ND, Ohsumi TK, et al (2013) The microglial sensome revealed by direct RNA sequencing. Nature Neuroscience 16:1896–905. doi: 10.1038/nn.3554

Hinman JD, Chen C Di, Oh SY, et al (2008) Age-dependent accumulation of ubiquitinated 2′,3′-cyclic nucleotide 3′-phosphodiesterase in myelin lipid rafts. Glia 56:118–133. doi: 10.1002/glia.20595

Hinman JD, Duce JA, Siman RA, et al (2004) Activation of calpain-1 in myelin and microglia in the white matter of the aged rhesus monkey. Journal of Neurochemistry 89:430–441. doi: 10.1046/j.1471-4159.2004.02348.x

Hinman JD, Peters A, Cabral H, et al (2006) Age-related molecular reorganization at the node of Ranvier. Journal of Comparative Neurology 495:351–362. doi: 10.1002/cne.20886

Höhn A, König J, Grune T (2013) Protein oxidation in aging and the removal of oxidized proteins. Journal of Proteomics 92:132–159.

Holtman IR, Raj DD, Miller J a, et al (2015) Induction of a common microglia gene expression signature by aging and neurodegenerative conditions: a co-expression meta-analysis. Acta Neuropathologicaogica Communications 3: doi: 10.1186/s40478-015-0203-5

Holz FG, Schütt F, Kopitz J, et al (1999) Inhibition of lysosomal degradative functions in RPE cells by a retinoid component of lipofuscin. Investigative Opthalmology & Visual Science 40:737–743.

Hoyos HC, Rinaldi M, Mendez-Huergo SP, et al (2014) Galectin-3 controls the response

of microglial cells to limit cuprizone-induced demyelination. Neurobiology of Disease 62:441–455. doi: 10.1016/j.nbd.2013.10.023

Huhn S, Masouleh SK, Villringer A, Witte AV (2015) Components of a Mediterranean diet and their impact on cognitive functions in aging. Frontiers in Aging Neuroscience. doi: 10.3389/fnagi.2015.00132

Iliff JJ, Wang M, Liao Y, et al (2012) A paravascular pathway facilitates CSF flow through the brain parenchyma and the clearance of interstitial solutes, including amyloid β. Science Translational Medicine doi: 10.1126/scitranslmed.3003748

Jacobs B, Driscoll L, Schall M (1997) Life-span dendritic and spine changes in areas 10 and 18 of human cortex: A quantitative golgi study. Journal of Comparative Neurology 386:661–680. doi: 10.1002/(SICI)1096-9861(19971006)386:4<661::AID-CNE11>3.0.CO;2-N

Jernigan TL, Gamst AC (2005) Changes in volume with age - Consistency and interpretation of observed effects. Neurobiology of Aging 26:1271–1274.

Jung T, Höhn A, Grune T (2014) The proteasome and the degradation of oxidized proteins: Part II - protein oxidation and proteasomal degradation. Redox Biology 2:99–104.

Karperien A, Ahammer H, Jelinek HF (2013) Quantitating the subtleties of microglial morphology with fractal analysis. Frontiers in Cellular Neuroscience 7:3. doi: 10.3389/fncel.2013.00003

Kay JG, Murray RZ, Pagan JK, Stow JL (2006) Cytokine secretion via cholesterol-rich lipid raft-associated SNAREs at the phagocytic cup. The Journal of Biological Chemistry 281:11949–11954. doi: 10.1074/jbc.M600857200

Kim CC, Nakamura MC, Hsieh CL (2016) Brain trauma elicits non-canonical macrophage activation states. Journal of Neuroinflammation. doi: 10.1186/s12974-016-0581-z

Kimura M, Sato M, Akatsuka A, et al (1989) Restoration of myelin formation by a single type of myelin basic protein in transgenic shiverer mice. Proceedings of the National Academy of Sciences 86:5661–5

Koo B, Schettler S, Murray D, Lee J (2012) Age-related effects on cortical thickness patterns of the Rhesus monkey brain. Neurobiology of Aging 33(1): e23-31 doi: 10.1016/j.neurobiolaging.2010.07.010

Kotter MR, Li W-W, Zhao C, Franklin RJM (2006) Myelin impairs CNS remyelination by inhibiting oligodendrocyte precursor cell differentiation. Journal of Neuroscience

26:328–332. doi: 10.1523/JNEUROSCI.2615-05.2006

Kotter MR, Zhao C, Van Rooijen N, Franklin RJM (2005) Macrophage-depletion induced impairment of experimental CNS remyelination is associated with a reduced oligodendrocyte progenitor cell response and altered growth factor expression. Neurobiology of Disease 18:166–175. doi: 10.1016/j.nbd.2004.09.019

Krabbe G, Halle A, Matyash V, et al (2013) Functional Impairment of Microglia Coincides with Beta-Amyloid Deposition in Mice with Alzheimer-Like Pathology. PLoS One. doi: 10.1371/journal.pone.0060921

Kregel KC, Zhang HJ (2007a) An integrated view of oxidative stress in aging: basic mechanisms, functional effects, and pathological considerations. American Journal of Physiology Regulatory, Integrative and Comparative Physiology 292:R18-36. doi: 10.1152/ajpregu.00327.2006

Kress BT, Iliff JJ, Xia M, et al (2014) Impairment of paravascular clearance pathways in the aging brain. Annals of Neurology 76:845–861. doi: 10.1002/ana.24271

Lamers KJ, de Reus HP, Jongen PJ (1998) Myelin basic protein in CSF as indicator of disease activity in multiple sclerosis. Multiple Sclerosis 4:124–6. doi: 10.1177/135245859800400306

Lampron A, Larochelle A, Laflamme N, et al (2015) Inefficient clearance of myelin debris by microglia impairs remyelinating processes. Journal of Experimental Medicine 212:481–95. doi: 10.1084/jem.20141656

Lanza IR, Zabielski P, Klaus KA, et al (2012) Chronic caloric restriction preserves mitochondrial function in senescence without increasing mitochondrial biogenesis. Cell Metabolism 16:777–788. doi: 10.1016/j.cmet.2012.11.003

Lee JE, Liang KJ, Fariss RN, Wong WT (2008) Ex vivo dynamic imaging of retinal microglia using time-lapse confocal microscopy. Investigative Opthalmology & Visual Science 49:4169–4176. doi: 10.1167/iovs.08-2076

Leverrier Y, Ridley AJ (2001) Requirement for Rho GTPases and PI 3-kinases during apoptotic cell phagocytosis by macrophages. Current Biology 11:195–199. doi: 10.1016/S0960-9822(01)00047-1

Linehan E, Dombrowski Y, Snoddy R, et al (2014) Aging impairs peritoneal but not bone marrow-derived macrophage phagocytosis. Aging Cell 13:699–708. doi: 10.1111/acel.12223

Liochev SI (2013) Reactive oxygen species and the free radical theory of aging. Free Radical Biology & Medicine 60:1–4.

Liu Y, Hao W, Letiembre M, et al (2006) Suppression of microglial inflammatory activity by myelin phagocytosis: role of p47-PHOX-mediated generation of reactive oxygen species. Journal of Neuroscience 26:12904–12913. doi: 10.1523/JNEUROSCI.2531-06.2006

López-Lluch G, Hunt N, Jones B, et al (2006) Calorie restriction induces mitochondrial biogenesis and bioenergetic efficiency. Proceedings of the National Academy of Sciences 103:1768–1773. doi: 10.1073/pnas.0510452103

Lucin KM, O'Brien CE, Bieri G, et al (2013) Microglial Beclin 1 Regulates Retromer Trafficking and Phagocytosis and Is Impaired in Alzheimer's Disease. Neuron 79:873–886. doi: 10.1016/j.neuron.2013.06.046

Makris N, Papadimitriou GM, van der Kouwe A, et al (2007) Frontal connections and cognitive changes in normal aging rhesus monkeys: A DTI study. Neurobiology of Aging 28:1556–1567. doi: 10.1016/j.neurobiolaging.2006.07.005

Marner L, Nyengaard JR, Tang Y, Pakkenberg B (2003) Marked loss of myelinated nerve fibers in the human brain with age. Journal of Comparative Neurology 462:144–52. doi: 10.1002/cne.10714

Masters CL, Bateman R, Blennow K, et al (2015) Alzheimer's disease. Nature Reviews Disease Primers 15056. doi: 10.1038/nrdp.2015.56

Mattison J a., Roth GS, Beasley TM, et al (2012) Impact of caloric restriction on health and survival in rhesus monkeys from the NIA study. Nature 489:318–321. doi: 10.1038/nature11432

Mayeux R, Stern Y (2012) Epidemiology of Alzheimer disease. Cold Spring Harbor Perspectives in Medicine 2:137–152. doi: 10.1101/cshperspect.a006239

McKhann GM, Knopman DS, Chertkow H, et al (2011) The diagnosis of dementia due to Alzheimer's disease: Recommendations from the National Institute on Aging-Alzheimer's Association workgroups on diagnostic guidelines for Alzheimer's disease. Alzheimer's Dementia 7:263–269. doi: 10.1016/j.jalz.2011.03.005

Merrill DA, Roberts JA, Tuszynski MH (2000) Conservation of neuron number and size in entorhinal cortex layers II, III, and V/VI of aged primates. Journal of Comparative Neurology 422:396–401. doi: 10.1002/1096-9861(20000703)422:3<396::AID-CNE6>3.0.CO;2-R

Mielke MM, Kozauer NA, Chan KCG, et al (2009) Regionally-specific diffusion tensor imaging in mild cognitive impairment and Alzheimer's disease. Neuroimage 46:47–55. doi: 10.1016/j.neuroimage.2009.01.054

Min Y, Kristiansen K, Boggs JM, et al (2009) Interaction forces and adhesion of supported myelin lipid bilayers modulated by myelin basic protein. Proceedings of the National Academy of Sciences 106:3154–3159. doi: 10.1073/pnas.0813110106

Miron VE, Boyd A, Zhao J-W, et al (2013) M2 microglia and macrophages drive oligodendrocyte differentiation during CNS remyelination. Nature Neuroscience 16:1211–1218. doi: 10.1038/nn.3469

Mittelbronn M, Dietz K, Schluesener HJ, Meyermann R (2001) Local distribution of microglia in the normal adult human central nervous system differs by up to one order of magnitude. Acta Neuropathologica 101:249–255.

Moore TL, Schettler SP, Killiany RJ, et al (2005) Cognitive impairment in aged rhesus monkeys associated with monoamine receptors in the prefrontal cortex. Behavioural Brain Research 160:208–221. doi: 10.1016/j.bbr.2004.12.003

Moore WAL, Weindruch R, Walford R, Ivy GO (1995) The effect of caloric restriction on lipofuscin accumulation in mouse brain with age. Gerontology 41:173–186.

Moseley M (2002) Diffusion tensor imaging and aging - A review. NMR in Biomedicine 15:553–560.

Müller C, Bauer NM, Schäfer I, White R (2013) Making myelin basic protein -from mRNA transport to localized translation. Frontiers in Cellular Neuroscience. doi: 10.3389/fncel.2013.00169

Murray RZ, Kay JG, Sangermani DG, Stow JL (2005) A role for the phagosome in cytokine secretion. Science 310:1492–1495. doi: 10.1126/science.1120225

Napoli I, Neumann H (2009) Microglial clearance function in health and disease. Neuroscience 158:1030–8. doi: 10.1016/j.neuroscience.2008.06.046

Natrajan MS, De La Fuente AG, Crawford AH, et al (2015) Retinoid X receptor activation reverses age-related deficiencies in myelin debris phagocytosis and remyelination. Brain 138:3581–3597. doi: 10.1093/brain/awv289

Neumann H, Kotter MR, Franklin RJM (2009) Debris clearance by microglia: An essential link between degeneration and regeneration. Brain 132:288–295.

Nimmerjahn A, Kirchhoff F, Helmchen F (2005) Resting microglial cells are highly dynamic surveillants of brain parenchyma in vivo. Neuroforum 11:95–96. doi: 10.1126/science.1110647

Nisoli E, Tonello C, Cardile A, et al (2005) Calorie restriction promotes mitochondrial biogenesis by inducing the expression of eNOS. Science (80-) 310:314–317. doi:

10.1126/science.1117728

Njie e. MG, Boelen E, Stassen FR, et al (2012) Ex vivo cultures of microglia from young and aged rodent brain reveal age-related changes in microglial function. Neurobiology of Aging. doi: 10.1016/j.neurobiolaging.2010.05.008

Norden DM, Godbout JP (2013) Review: Microglia of the aged brain: Primed to be activated and resistant to regulation. Neuropathology of Applied Neurobiology 39:19–34 doi: 10.1111/j.1365-2990.2012.01306.x

Opalach K, Rangaraju S, Madorsky I, et al (2010) Lifelong Calorie Restriction Alleviates Age-Related Oxidative Damage in Peripheral Nerves. Rejuvenation Research13:65–74. doi: 10.1089/rej.2009.0892

Parkhurst CN, Yang G, Ninan I, et al (2013) Microglia promote learning-dependent synapse formation through brain-derived neurotrophic factor. Cell 155:1596–1609. doi: 10.1016/j.cell.2013.11.030

Patterson SL (2015) Immune dysregulation and cognitive vulnerability in the aging brain: Interactions of microglia, IL-1β, BDNF and synaptic plasticity. Neuropharmacology 96:11–18. doi: 10.1016/j.neuropharm.2014.12.020

Pelvig DP, Pakkenberg H, Stark AK, Pakkenberg B (2008) Neocortical glial cell numbers in human brains. Neurobiology of Aging 29:1754–1762. doi: 10.1016/j.neurobiolaging.2007.04.013

Perry VH, Holmes C (2014) Microglial priming in neurodegenerative disease. Nature Reviews Neurology 10:217–24. doi: 10.1038/nrneurol.2014.38

Peters A (2009) The effects of normal aging on myelinated nerve fibers in monkey central nervous system. Frontiers in Neuroanatomy 3:11. doi: 10.3389/neuro.05.011.2009

Peters A (1996) Age-related changes in oligodendrocytes in monkey cerebral cortex. Journal of Comparative Neurology 371:153–163. doi: 10.1002/(SICI)1096-9861(19960715)371:1<153::AID-CNE9>3.0.CO;2-2

Peters A, Josephson K, Vincent SL (1991) Effects of aging on the neuroglial cells and pericytes within area 17 of the rhesus monkey cerebral cortex. The Anatomical Record 229:384–398. doi: 10.1002/ar.1092290311

Peters A, Kemper T (2012) A review of the structural alterations in the cerebral hemispheres of the aging rhesus monkey. Neurobiology of Aging 33:2357–2372.

Peters A, Morrison JH, Rosene DL, Hyman BT (1998) Are neurons lost from the primate

cerebral cortex during normal aging? Cerebral Cortex 8:295–300.

Peters A, Moss MB, Sethares C (2000) Effects of aging on myelinated nerve fibers in monkey primary visual cortex. Journal of Comparative Neurology 419:364–376.

Peters A, Rosene DL (2003) In aging, is it gray or white? Journal of Comparative Neurology 462:139–143. doi: 10.1002/cne.10715

Peters A, Sethares C (2002) Aging and the myelinated fibers in prefrontal cortex and corpus callosum of the monkey. Journal of Comparative Neurology 442:277–291. doi: 10.1002/cne.10099

Peters A, Sethares C (1993) Aging and the Meynert cells in rhesus monkey primary visual cortex. The Anatomical Record 236:721–729. doi: 10.1002/ar.1092360416

Peters A, Sethares C (2004) Oligodendrocytes, their progenitors and other neuroglial cells in the aging primate cerebral cortex. Cerebral Cortex 14:995–1007. doi: 10.1093/cercor/bhh060

Peters A, Sethares C, Moss MB (2010) How the primate fornix is affected by age. Journal of Comparative Neurology 518:3962–3980. doi: 10.1002/cne.22434

Pistorio AL, Hendry SH, Wang X (2006) A modified technique for high-resolution staining of myelin. Journal of Neuroscience Methods 153:135–146. doi: 10.1016/j.jneumeth.2005.10.014

Plowden J, Renshaw-Hoelscher M, Engleman C, et al (2004) Innate immunity in aging: impact on macrophage function. Aging Cell 3:161–7. doi: 10.1111/j.1474-9728.2004.00102.x

Prins ND, Scheltens P (2015) White matter hyperintensities, cognitive impairment and dementia: an update. Nature Reviews Neurology 11:157–165. doi: 10.1038/nrneurol.2015.10

Prinz M, Priller J (2014) Microglia and brain macrophages in the molecular age: from origin to neuropsychiatric disease. Nature Reviews Neuroscience 15:300–12. doi: 10.1038/nrn3722

Pugliese G, Iacobini C, Pesce CM, Menini S (2015) Galectin-3: an emerging all-out player in metabolic disorders and their complications. Glycobiology 25:136–150. doi: 10.1093/glycob/cwu111

Raj D, Yin Z, Breur M, et al (2017) Increased White Matter Inflammation in Aging- and Alzheimer's Disease Brain.Frontiers in Molecular Neuroscience doi: 10.3389/fnmol.2017.00206

Raji CA, Lopez OL, Kuller LH, et al (2009) Age, Alzheimer disease, and brain structure. Neurology 73:1899–1905. doi: 10.1212/WNL.0b013e3181c3f293

Ransohoff RM (2016) A polarizing question: do M1 and M2 microglia exist? Nature Neuroscience 19:987–991. doi: 10.1038/nn.4338

Reeg S, Grune T (2015) Protein Oxidation in Aging: Does It Play a Role in Aging Progression? Antioxidants & Redox Signaling 23:239–55. doi: 10.1089/ars.2014.6062

Reichert F, Rotshenker S (1999) Galectin-3/MAC-2 in experimental allergic encephalomyelitis. Experimental Neurology 160:508–514. doi: 10.1006/exnr.1999.7229

Ringman JM, Younkin SG, Pratico D, et al (2008) Biochemical markers in persons with preclinical familial Alzheimer disease. Neurology 71:85–92. doi: 10.1212/01.wnl.0000303973.71803.81

Rogers J, Luber-Narod J, Styren SD, Civin WH (1988) Expression of immune system-associated antigens by cells of the human central nervous system: relationship to the pathology of Alzheimer's disease. Neurobiology of Aging 9:339–349. doi: 10.1016/S0197-4580(88)80079-4

Romme Christensen J, Börnsen L, Khademi M, et al (2013) CSF inflammation and axonal damage are increased and correlate in progressive multiple sclerosis. Multiple Sclerosis J 19:877–884. doi: 10.1177/1352458512466929

Rosene DL, Roy NJ, Davis BJ (1986) A cryoprotection method that facilitates cutting frozen sections of whole monkey brains for histological and histochemical processing without freezing artifact. Journal of Histochemistry & Cytochemistry 34:1301–1315. doi: 10.1177/34.10.3745909

Rozovsky I, Finch CE, Morgan TE (1998) Age-related activation of microglia and astrocytes: in vitro studies show persistent phenotypes of aging, increased proliferation, and resistance to down-regulation. Neurobiology of Aging 19:97–103.

Ruckh JM, Zhao JW, Shadrach JL, et al (2012) Rejuvenation of regeneration in the aging central nervous system. Cell Stem Cell 10:96–103. doi: 10.1016/j.stem.2011.11.019

Saadat KASM, Murakami Y, Tan X, et al (2014) Inhibition of autophagy induces retinal pigment epithelial cell damage by the lipofuscin fluorophore A2E. FEBS Open Bio 4:1007–1014. doi: 10.1016/j.fob.2014.11.003

Safaiyan S, Kannaiyan N, Snaidero N, et al (2016a) Age-related myelin degradation burdens the clearance function of microglia during aging. Nature Neuroscience

19:995–998. doi: 10.1038/nn.4325

Safaiyan S, Kannaiyan N, Snaidero N, et al (2016b) Age-related myelin degradation burdens the clearance function of microglia during aging. Nature Neuroscience 1–7. doi: 10.1038/nn.4325

Salat DH, Buckner RL, Snyder AZ, et al (2004) Thinning of the cerebral cortex in aging. Cerebral Cortex 14:721–730. doi: 10.1093/cercor/bhh032

Salthouse T (2010) Selective review of cognitive aging. Journal of International Neuropsychological Society 16:754–760. doi: 10.1017/S1355617710000706.Selective

Sandell JH, Peters A (2003) Disrupted myelin and axon loss in the anterior commissure of the aged rhesus monkey. Journal of Comparative Neurology 466:14–30. doi: 10.1002/cne.10859

Sandell JH, Peters A (2002) Effects of age on the glial cells in the rhesus monkey optic nerve. Journal of Comparative Neurology 445:13–28. doi: 10.1002/cne.10162

Sano H, Hsu DK, Apgar JR, et al (2003) Critical role of galectin-3 in phagocytosis by macrophages. Journal of Clincal Investigation 112:389–397. doi: 10.1172/JCI200317592.

Savaskan NE, Weinmann O, Heimrich B, Eyupoglu IY (2009) High resolution neurochemical gold staining method for myelin in peripheral and central nervous system at the light- and electron-microscopic level. Cell Tissue Research 337:213–221. doi: 10.1007/s00441-009-0815-9

Schafer DP, Lehrman EK, Kautzman AG, et al (2012) Microglia sculpt postnatal neural circuits in an activity and complement-dependent manner. Neuron 74:691–705. doi: 10.1016/j.neuron.2012.03.026

Schain AJ, Hill RA, Grutzendler J (2014) Label-free in vivo imaging of myelinated axons in health and disease with spectral confocal reflectance microscopy. Nature Medicine 20:443–449. doi: 10.1038/nm.3495

Schindelin J, Arganda-Carreras I, Frise E, et al (2012) Fiji: An open-source platform for biological-image analysis. Nature Methods 9:676–682.

Sheffield LG, Berman NE (1998) Microglial expression of MHC class II increases in normal aging of nonhuman primates. Neurobiology of Aging 19:47–55.

Shields SA, Gilson JM, Blakemore WF, Franklin RJM (1999) Remyelination occurs as extensively but more slowly in old rats compared to young rats following gliotoxin-

induced CNS demyelination. Glia 28:77–83. doi: 10.1002/(SICI)1098-1136(199910)28:1<77::AID-GLIA9>3.0.CO;2-F

Shobin E, Bowley MP, Estrada LI, et al (2017) Microglia activation and phagocytosis: relationship with aging and cognitive impairment in the rhesus monkey. GeroScience 199–220. doi: 10.1007/s11357-017-9965-y

Sierra A, Gottfried-blackmore AC, Mcewen BS (2007) Microglia Derived from Aging Mice Exhibit an Altered Inflammatory Profile. Glia 424:412–424. doi: 10.1002/glia

Sim FJ, Zhao C, Penderis J, Franklin RJM (2002) The age-related decrease in CNS remyelination efficiency is attributable to an impairment of both oligodendrocyte progenitor recruitment and differentiation. Journal of Neuroscience 22:2451–9. doi: 20026217

Simard AR, Soulet D, Gowing G, et al (2006) Bone marrow-derived microglia play a critical role in restricting senile plaque formation in Alzheimer's disease. Neuron 49:489–502. doi: 10.1016/j.neuron.2006.01.022

Singh-Manoux A, Kivimaki M, Glymour MM, et al (2012) Timing of onset of cognitive decline: results from Whitehall II prospective cohort study. BMJ 344:d7622. doi: 10.1136/bmj.d7622

Sloane J a, Hollander W, Moss MB, et al (1999) Increased microglial activation and protein nitration in white matter of the aging monkey. Neurobiology of Aging 20:395–405.

Sloane JA, Pietropaolo MF, Rosene DL, et al (1997) Lack of correlation between plaque burden and cognition in the aged monkey. Acta Neuropathologica 94:471–478. doi: 10.1007/s004010050735

Soreq L, Rose J, Soreq E, et al (2017) Major Shifts in Glial Regional Identity Are a Transcriptional Hallmark of Human Brain Aging. Cell Reports 18:557–570. doi: 10.1016/j.celrep.2016.12.011

Stadtman ER, Berlett BS (1997) Reactive oxygen-mediated protein oxidation in aging and disease. Chemical Research in Toxicology 10:485–494.

Stephan AH, Barres BA, Stevens B (2012) The Complement System : An Unexpected Role in Synaptic Pruning During Development and Disease. Annual Review of Neuroscience 35: 369-89 doi: 10.1146/annurev-neuro-061010

Stevens B, Allen NJ, Vazquez LE, et al (2007) The classical complement cascade mediates CNS synapse elimination. Cell 131:1164–78. doi: 10.1016/j.cell.2007.10.036

Stichel CC, Luebbert H (2007) Inflammatory processes in the aging mouse brain: participation of dendritic cells and T-cells. Neurobiology of Aging 28:1507–21. doi: 10.1016/j.neurobiolaging.2006.07.022

Stolzing A, Scutt A (2006) Age-related impairment of mesenchymal progenitor cell function. Aging Cell 5:213–224. doi: 10.1111/j.1474-9726.2006.00213.x

Storsve AB, Fjell AM, Tamnes CK, et al (2014) Differential longitudinal changes in cortical thickness, surface area and volume across the adult life span: regions of accelerating and decelerating change. Journal of Neuroscience 34:8488–98. doi: 10.1523/JNEUROSCI.0391-14.2014

Streit WJ, Sammons NW, Kuhns AJ, Sparks DL (2004) Dystrophic microglia in the aging human brain. Glia 45:208–12. doi: 10.1002/glia.10319

Streit WJ, Sparks DL (1997) Activation of microglia in the brains of humans with heart disease and hypercholesterolemic rabbits. Journal of Molecular Medicine 75:130–138. doi: 10.1007/s001090050097

Stroikin Y, Johansson U, Asplund S, Öllinger K (2007) Increased resistance of lipofuscin-loaded prematurely senescent fibroblasts to starvation-induced programmed cell death. Biogerontology 8:43–53. doi: 10.1007/s10522-006-9029-7

Sullivan E V., Pfefferbaum A (2006) Diffusion tensor imaging and aging. Neuroscience & Biobehavioral Reviews 30:749–761.

Tang Y, Nyengaard JR, Pakkenberg B, Gundersen HJ (1997) Age-induced white matter changes in the human brain: a stereological investigation. Neurobiology of Aging 18:609–15. doi: 10.1016/S0197-4580(97)00155-3

Tay TL, Mai D, Dautzenberg J, et al (2017) A new fate mapping system reveals context-dependent random or clonal expansion of microglia. Nature Neuroscience 20:793–803. doi: 10.1038/nn.4547

Teipel SJ, Lerche M, Kilimann I, et al (2014) Decline of fiber tract integrity over the adult age range: A diffusion spectrum imaging study. Journal of Magnetic Resonance Imaging 40:348–359. doi: 10.1002/jmri.24420

Terman A (2001) Garbage catastrophe theory of aging: imperfect removal of oxidative damage? Redox Report 6:15–26. doi: 10.1179/135100001101535996

Terman A, Abrahamsson N, Brunk UT (1999a) Ceroid/Lipofuscin-loaded human fibroblasts show increased susceptibility to oxidative stress. Experimental Gerontology 34:755–770. doi: 10.1016/S0531-5565(99)00045-5

Terman A, Brunk UT (1998) Lipofuscin: mechanisms of formation and increase with age. APMIS 106:265–276. doi: 10.1111/j.1699-0463.1998.tb01346.x

Terman A, Dalen H, Brunk UT (1999b) Ceroid/lipofuscin-loaded human fibroblasts show decreased survival time and diminished autophagocytosis during amino acid starvation. Experimental Gerontology 34:943–957. doi: 10.1016/S0531-5565(99)00070-4

Terry RD, DeTeresa R, Hansen LA (1987) Neocortical cell counts in normal human adult aging. Annals of Neurology 21:530–539. doi: 10.1002/ana.410210603

Tigges J, Herndon JG, Peters A (1990) Neuronal population of area 4 during the life span of the rhesus monkey. Neurobiology of Aging 11:201–208. doi: 10.1016/0197-4580(90)90546-C

Tigges J, Herndon JG, Peters A (1992) Axon terminals on betz cell somata of area 4 in rhesus monkey throughout adulthood. The Anatomical Record 232:305–315. doi: 10.1002/ar.1092320216

Ting JP-Y, Trowsdale J (2002) Genetic control of MHC class II expression. Cell 109 Suppl:S21–S33. doi: 10.1016/S0092-8674(02)00696-7

Town T, Nikolic V, Tan J (2005) The microglial "activation" continuum: from innate to adaptive responses. Journal of Neuroinflammation 2:24. doi: 10.1186/1742-2094-2-24

Tse KH, Herrup K (2017) DNA damage in the oligodendrocyte lineage and its role in brain aging. Mechanisms of Ageing and Development 161:37–50. doi: 10.1016/j.mad.2016.05.006

Tullberg M, Fletcher E, DeCarli C, et al (2004) White matter lesions impair frontal lobe function regardless of their location. Neurology 63:246–253. doi: 10.1212/01.WNL.0000130530.55104.B5

Turrens JF (2003) Mitochondrial formation of reactive oxygen species. Journal of Physiology 552:335–344. doi: 10.1111/j.1469-7793.2003.00335.x

Vallieres L, Sawchenko PE (2003) Bone marrow-derived cells that populate the adult mouse brain preserve their hematopoietic identity. Journal of Neuroscience 23:5197–5207. doi: 23/12/5197 [pii]

Vanderweyde T, Youmans K, Liu-Yesucevitz L, Wolozin B (2013) Role of stress granules and RNA-binding proteins in neurodegeneration: A mini-review. Gerontology 59:524–533.

Vida C, de Toda IM, Cruces J, et al (2017) Role of macrophages in age-related oxidative stress and lipofuscin accumulation in mice. Redox Biology 12:423–437. doi: 10.1016/j.redox.2017.03.005

Viña J, Borras C, Abdelaziz KM, et al (2013) The Free Radical Theory of Aging Revisited: The Cell Signaling Disruption Theory of Aging. Antioxidants & Redox Signaling 19:779–787. doi: 10.1089/ars.2012.5111

Vincent SL, Peters A, Tigges J (1989) Effects of aging on the neurons within area 17 of rhesus monkey cerebral cortex. The Anatomical Record 223:329–341. doi: 10.1002/ar.1092230312

Voineskos AN, Rajji TK, Lobaugh NJ, et al (2012) Age-related decline in white matter tract integrity and cognitive performance: A DTI tractography and structural equation modeling study. Neurobiology of Aging 33:21–34. doi: 10.1016/j.neurobiolaging.2010.02.009

Wakefield DB, Moscufo N, Guttmann CR, et al (2010) White matter hyperintensities predict functional decline in voiding, mobility, and cognition in older adults. Journal of the American Geriatric Society 58:275–281. doi: 10.1111/j.1532-5415.2009.02699.x

Wes PD, Holtman IR, Boddeke EWGM, et al (2016) Next generation transcriptomics and genomics elucidate biological complexity of microglia in health and disease. Glia 64:197–213. doi: 10.1002/glia.22866

West MJ, Slomianka L, Gundersen HJ (1991) Unbiased stereological estimation of the total number of neurons in thesubdivisions of the rat hippocampus using the optical fractionator. The Anatomical Record 231:482–497. doi: 10.1002/ar.1092310411

Williams K, Ulvestad E, Waage A, et al (1994) Activation of adult human derived microglia by myelin phagocytosis in vitro. Journal of Neuroscience Researchs 38:433–443. doi: 10.1002/jnr.490380409

Wisco JJ, Killiany RJ, Guttmann CRG, et al (2008) An MRI study of age-related white and gray matter volume changes in the rhesus monkey. Neurobiology of Aging 29:1563–1575. doi: 10.1016/j.neurobiolaging.2007.03.022

Xing Y, Samuvel DJ, Stevens SM, et al (2012) Age-related changes of myelin basic protein in mouse and human auditory nerve. PLoS One 7:e34500. doi: 10.1371/journal.pone.0034500

Yeung MSY, Zdunek S, Bergmann O, et al (2014) Dynamics of oligodendrocyte generation and myelination in the human brain. Cell 159:766–774. doi: 10.1016/j.cell.2014.10.011

Yin D (1996) Biochemical basis of lipofuscin, ceroid, and age pigment-like fluorophores. Free Radical Biology & Medicine 21:871–888.

Yuan L, Liu J, Ma W, et al (2016) Dietary pattern and antioxidants in plasma and erythrocyte in patients with mild cognitive impairment from China. Nutrition 32:193–198. doi: 10.1016/j.nut.2015.08.004

Zhang K, Sejnowski TJ (2000) A universal scaling law between gray matter and white matter of cerebral cortex. Proceedings of the National Academy of Sciences 97:5621–6. doi: 10.1073/pnas.090504197

CURRICULUM VITAE